JANUARY 2021

Ph.D. in Chemistry

KHATTAB AL-KHAFAJI

REPUBLIC OF TURKEY

GAZİANTEP UNIVERSITY

GRADUATE SCHOOL OF NATURAL & APPLIED SCIENCES

MOLECULAR MECHANISMS OF AMYGDALIN AS MULTIFUNCTIONAL ANTI-CANCER DRUG: COMPUTATIONAL ASSESSMENT

Ph.D. THESIS

IN

CHEMISTRY

BY

KHATTAB AL-KHAFAJI

JANUARY 2021

MOLECULAR MECHANISMS OF AMYGDALIN AS MULTIFUNCTIONAL ANTI-CANCER DRUG: COMPUTATIONAL ASSESSMENT

Ph.D. Thesis

in

Chemistry

Gaziantep University

Supervisor

Assoc. Prof. Dr. Tuğba TAŞKIN TOK

by

Khattab AL-KHAFAJI

January 2021

REPUBLIC OF TURKEY
GAZİANTEP UNIVERSITY
GRADUATE SCHOOL OF NATURAL AND APPLIED SCIENCES
CHEMISTRY

Name of the Thesis : Molecular Mechanisms of Amygdalin as Multifunctional Anti-cancer Drug: Computational Assessment

Name of the Student : Khattab AL-KHAFAJI

Exam Date : 12.01.2021

Approval of the Graduate School of Natural and Applied Sciences

Assoc. Prof. Dr. Mehmet İshak YÜCE
Director

I certify that this thesis satisfies all the requirements as a thesis for the degree of Doctor of Philosophy.

Prof. Dr. Hüseyin ZENGİN
Head of Department

This is to certify that we have read this thesis and that in our consensus opinion it is fully adequate, in scope and quality, as a thesis for the degree of Doctor of Philosophy.

Assoc. Prof. Dr. Tuğba TAŞKIN TOK
Supervisor

Examining Committee Members:	Signature
Prof. Dr. Emine. Elçin EMRE	…….
Prof. Dr. Hüseyin ZENGİN	…….
Assoc. Prof. Dr. Tuğba TAŞKIN TOK	…….
Assoc. Prof. Dr. Necla BENLİER	…….

Asst. Prof. Dr. Tuba DENKÇEKEN …….

I hereby declare that all information in this document has been obtained and presented in accordance with academic rules and ethical conduct. I also declare that, as required by these rules and conduct, I have fully cited and referenced all material and results that are not original to this work.

Khattab AL-KHAFAJI

ABSTRACT

MOLECULAR MECHANISMS OF AMYGDALIN AS MULTIFUNCTIONAL ANTI-CANCER DRUG: COMPUTATIONAL ASSESSMENT

AL-KHAFAJI, Khattab
Ph.D. in Chemistry
Supervisor: Assoc. Prof. Dr. Tuğba TAŞKIN TOK
January 2021
130 Pages

The 'cancer' is a group of biological diseases. Cancer cell switches off the apoptosis signaling, proliferate uncontrollably, resist to anticancer therapies and spread into distant organs. Therefore, controlling these three main properties by targeting key proteins can give promising strategy as anticancer. Double docking, molecular dynamics (MD) simulation, principal component analysis (PCA), free energy landscape (FEL) and binding free energy estimations (MM/PBSA) are implemented to explore the molecular basis of the biological activities of amygdalin. Amygdalin as apoptosis inducer: the docking clarifies that amygdalin binds to the interface of Bcl-2/BAX complex. The MD simulation exhibited that amygdalin causes disruption between Bcl-2/BAX. Further, FEL and PCA revealed that the Bcl-2/amygdalin is more stable than Bcl-2/BAX. In the case of caspase-3 the matter is different where amygdalin activates caspase-3 through increasing the dynamics of caspase-3. For PARP-1, amygdalin blocked PARP-1 binding pocket. Inhibition of CDK1/Cyclin B, CDK 2/Cyclin A and CDK 4/Cyclin D1 as targets for cell cycle division by amygdalin. The obtained results showed that amygdalin inhibits CDK1/Cyclin B, CDK 2/Cyclin A effectively. Targeting the metastasis, the obtained results revealed that amygdalin shows an inhibitory-metastasis activity against AKT1, FAK1 and ILK proteins. Amygdalin disclosed a clarification of the mystery amygdalin's experimental actions.

Key Words: Amygdalin, Multifunctional, Computational Studies, Apoptosis, Cell Division and Metastasis.

ÖZET

ÇOK FONKSİYONEL ANTİ-KANSER İLAÇ OLARAK AMİGDALİNİN MOLEKÜLER MEKANİZMALARI: BİLGİSAYARLI DEĞERLENDİRME

AL-KHAFAJI, Khattab
Doktora Tezi, Kimya
Danışman: Doç. Dr. Tuğba TAŞKIN TOK
Ocak 2021
130 Sayfa

‘Kanser' bir biyolojik hastalıklar grubudur. Kanser hücresi apoptoz sinyalini kapatır, kontrolsüz bir şekilde çoğalır, antikanser tedavilere direnir ve uzak organlara yayılır. Bu nedenle, anahtar proteinleri hedefleyerek bu üç ana özelliği kontrol etmek, antikanser olarak umut verici bir strateji sağlayabilir. Çift kenetlenme, moleküler dinamik (MD) simülasyonu, temel bileşen analizi (PCA), serbest enerji manzarası (FEL) ve bağlanma serbest enerji tahmini (MM/PBSA), amigdalinin biyolojik aktivitelerinin moleküler temelini keşfetmek için uygulanmaktadır. Apoptoz indükleyicisi olarak amigdalin: kenetlenme, amigdalinin Bcl-2/BAX kompleksinin arayüzüne bağlandığını açıklığa kavuşturur. MD simülasyonu, amigdalinin Bcl-2 / BAX arasında bozulmaya neden olduğunu gösterdi. Ayrıca FEL ve PCA, Bcl-2 / amigdalinin Bcl-2/BAX'tan daha stabil olduğunu ortaya çıkardı. Kaspaz-3 durumunda, mesele, amigdalinin kaspaz-3'ün dinamiklerini artırarak kaspaz-3'ü aktive ettiği durumda farklıdır. PARP-1 için, amigdalin PARP-1 bağlanma cebini bloke etti. Amigdalin ile hücre döngüsü bölünmesi için hedefler olarak CDK1 / Siklin B, CDK 2 / Siklin A ve CDK 4 / Siklin D1 inhibisyonu. Elde edilen sonuçlar, amigdalinin CDK1 / Cyclin B, CDK 2 / Cyclin A'yı etkili bir şekilde inhibe ettiğini gösterdi. Metastazı hedefleyen elde edilen sonuçlar, amigdalinin AKT1, FAK1 ve ILK proteinlerine karşı inhibe edici metastaz aktivitesi gösterdiğini ortaya çıkarmıştır. Amygdalin, Amygdalin'in deneysel eylemlerinin gizemini açıkladı.

Anahtar Kelimeler: Amygdalin, Çok Fonksiyonlu, Hesaplamalı Çalışmalar, Apoptoz, Hücre Bölünmesi ve Metastaz.

DEDICATION

To the soul of my great father who taught me the meaning of working hard and ask Allah to have his mercy upon him.

To my mother the origin of my success.
To my brothers and sister, may Allah bless them.
To my whole (Adnan) family.

ACKNOWLEDGEMENTS

Praise be to Allah who gave me health, strength and patience to conduct this work. I am so grateful to my supervisor, Assoc. Prof. Dr. Tuğba TAŞKIN TOK for her guidance and support throughout the study.

I would like to express my love and gratitude to my family for their support, always best wishes.

TABLE OF CONTENTS

LIST OF TABLES

Page

LIST OF FIGURES

Pages

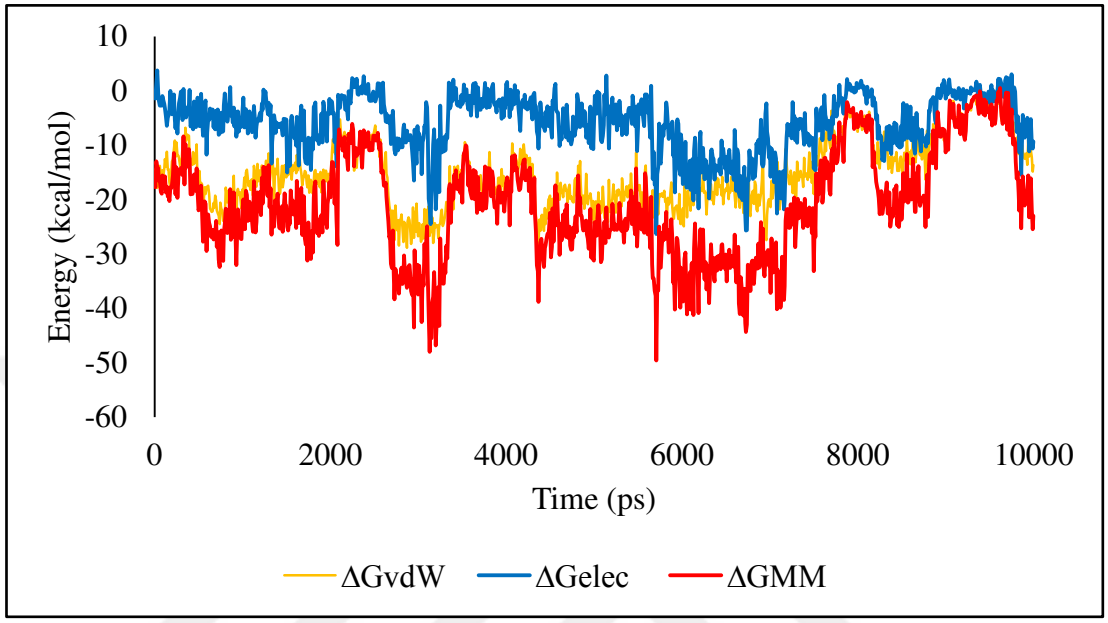

LIST OF ABBREVIATIONS

CDK	Cell-division protein kinase
ILK	Integrin Linked Kinase
FAK1	Focal Adhesion Kinase 1
MD	Molecular Dynamics
2D	Two-Dimensional
3D	Three-Dimensional
PDB	Protein Data Bank
PDBQT	Partial Charge & Atom Type
ADT	AutoDock Tools
ADFR	Autodock Flexible Residue
AGFR	AutoGrid Flexible Residue
LGA	Lamarckian Genetic Algorithm
DLG	Digital Line Graph
GA	Genetic Algorithm
RMSD	Root Mean Square Deviation
TIP3P	Three-Point Transferable Intermolecular Potential
EM	Energy Minimization
RMSF	Root Mean Square Fluctuation
PCA	Principal Component Analysis
GROMACS	GROningen MAchine for Chemical Simulations
CHARMM	Chemistry at HARvard Macromolecular Mechanics
PARP-1	Poly (ADP-ribose) polymerase-1
MFD	Multi-functional Drug
FEL	Free energy landscape analysis
MM/PBSA	Macromolecular Mechanics/Poisson-Boltzmann Surface Area
NVT	Amount of substance (N), volume (V) and temperature (T) are conserved
NPT	Isothermal-Isobaric ensemble, moles (N), pressure (P)

	and temperature (T) are conserved
PBC	Periodic boundary condition

CHAPTER I

INTRODUCTION

1.1 Cancer

Tumor is an extensive group of various diseases that all contain unmanageable growth of irregular cells in the body, producing a cancerous site. Cancerous tissues can migrate to remote locations through the lymphatic system or blood flow. Every year, 9.6 million souls are dying due to cancer worldwide. And around 18 million of new cancer cases are detected. By 2030, the expected annually deaths number caused by cancer reaches more than 13.2 million. One in three individuals will start cancer during their lives (Bray et al., 2018).

Hanahan and Weinberg distinctly explained their purpose: to define ‘a few basic assumptions’ of tumor that were interpreted as ‘acquired powers distributed by most and perhaps all kinds of individual malignancies’. These peculiarities would have to be got ‘for being cancerous’. The approaches they illustrated obviously relate to the established neoplasm cells and. The molecular biologists believe that neoplasm cells are working homogeneous societies also have captured the distinctive hallmarks. Consisted of work was a symbol on ‘the arising course of tumor cell’ which specifies the hypothesized signaling routes that are playing vital roles in the progress of hallmarks. Notwithstanding that there are not reports talking about the idea of the approach of hallmarks is generally considered in the literature to appeal to all tumor cells but the hallmarks of malignancy cells appear in all tumor cells most of the time (Hanahan and Weinberg, 2000).

1.2 Hallmarks of cancer

The malignancy hallmarks framework was established to organize the multiplex character of tumor. Tumors are intricate and generally not returning to healthy status through curative interference. For shaping this intricating, the framework of malignancy hallmarks was established (Hanahan and Weinberg, 2000; Hanahan and Weinberg, 2011) (Figure 1.1). The hallmarks include that first is a genomic instability and mutation, second is a tumour promoting inflam-mation, third is a sustaining proliferative signalling, forth is evading growth suppressors, fifth is a

preventing cell death, sixth is a replicative immortality, seventh is a promoting angiogenesis, eighth is an invasion and metastasis, ninth is a deregulating cellular energetics and finally tenth is an avoiding immune elimination. These hallmarks are practical within the text of the tumour micro-environment. In the beginning of carcinoma can gain a series of variations that promote one or more of the hallmarks, providing them an ambitious improvement over its adjoining cells. With every newly gained advantage, a subclone exceeds the alternative tumour cells and en-ables the hallmark competences to be collected by a sequence of clonal growth.

Malignancy hallmarks framework can be employed to clarify the adaptations that observed in several types of tumor. Thus, it anticipates the oncogenicity of tissue located in a distinct kind of malignancy coinciding the distinct hallmarks of cancer. The melanoma is chosen to demonstrate this proposition of cancer. The assumption is accordingly: oncogenic variations, which are anticipated by the hallmarks of malignancy theoretical scheme, can be identified in melanoma. The objective is not the to provide a complete analysis of all oncogenic variances but it is to test the predictive value of the hallmarks. Based on this, one oncogenic amendment, described for melanoma, is reviewed for all characters of hallmarks (Broertjes, 2015).

Figure 1.1 The distinct hallmarks of tumor that required for normal cells to turn into cancer cells (Broertjes, 2015).

1 Genomic Mutability and Instability

The major hallmark to the progress of cancerous neoplasms is genomic mutability that facilitates an extended amount at which metastable sites are promoted. Genomic mutability allows other hallmarks to be promoted and initiates the development of cancer. For normal cells, it is requisite to preserve the genome stabilized, then they have derived an arsenal of proteins avoiding and correcting errors and eliminates mutation signals. As DNA deterioration is observed, the cell cycle is broken off until it recovers the impairment. If the DNA destruction is beyond tumor improvement, suppressor proteins like p53 stimulates the apoptosis (Hanahan and Weinberg, 2011). In spite of all these secure processes, cells of cancer can be started at specific site and then spread into another parts.

2 Cancer-Promoting Inflammation

The system of immunity system has improved over thousands of centuries to secure the individuals against infecting microbes or viruses. The immune system scours the somatic-illusionist cells that are immolated to assure the continuity of the living thing as an entity. The immune system critically participates in regulating tumor expansion and is a potential remedial machine to strengthen the anti-tumor action. However, inflammation, however, acts as double-edged sword. Chronic inflammation authorizes carcinoma headway in miscellaneous aspects. Cells of immune system excrete a horde of enzymes, signaling molecules and reactive oxygen species (ROS) into the microenvironment of cancer. These molecules stimulate the proliferative signaling resistance to apoptosis and assist to genomic sensitivity, thence activate angiogenesis to facilitate the tumor growth (Hanahan and Weinberg, 2011).

3 Sustaining Proliferative Signaling

Sustained proliferative signaling is an eminent hallmark of cancer. Sustained proliferative signaling magnifies the outcomes of genomic sensitivity. Further, the time for DNA damage repairs is less (Broertjes, 2015).

4 Evading Growth Suppressors

The uncurbed outgrowth of cells of cancer is rise by both sustained proliferative signaling and evading growth suppressors. The p53 and retinoblastoma protein (pRB) are two major suppressors. These proteins restrain the cell cycle, and motivate cell death (Hanahan and Weinberg, 2011).

5.Resisting Cell Death

Apoptosis, programmed death, is a prerequisite in the multicellular organisms especially in fetal expansion of disordered generated cells. For instance, the differentiation between tissues occurs through apoptosis of connected cells (Broertjes, 2015).

6 Enabling Replicative Immortality

Enabling replicative immortality is a vital trait of cancer advancement. Replicative immortality is achieved through telomerase hyperactivation. Telomeres have main role: it is to preserve the chromosomes' ends from degeneration and repair it (Alberts, 2008). The telomeres are further degenerated in each replication, this leads to reducing the productivity of normal cells. The moment that cells can afford proliferative signaling, they start to divide quickly and consume the telomeres. As a result of telomeres consuming, cells enter a state of deterioration (Broertjes, 2015).

7 Inducing Angiogenesis

Tissue compressing which developed in tumors tissues through faster dividing cancer can squeeze on another tissues. This causes to lessen the perfusion of blood. In the lack of sufficient blood stream, the tumor microenvironment is famished of nutrients and oxygen. Besides, it is saturated with carbon dioxide and metabolic wastes. Thereby, angiogenesis can be stimulated (Broertjes, 2015).

8 Activating Invasion and Metastasis

Ninety percent of declared deaths of cancer stemmed from metastatic, which is the ability to spread into distant organs (Chaffer and Weinberg, 2011). Figure 1.2 represents the operation of metastasis, starting by "foraying" the neighbouring organs or tissues. In the subsequent step, tumour cells penetrate lymphatic or blood flows through a process called intravasation. Next, extravasation of tumour cells from lymphatic or blood streams invade to the remote organ (Chaffer and Weinberg, 2011).

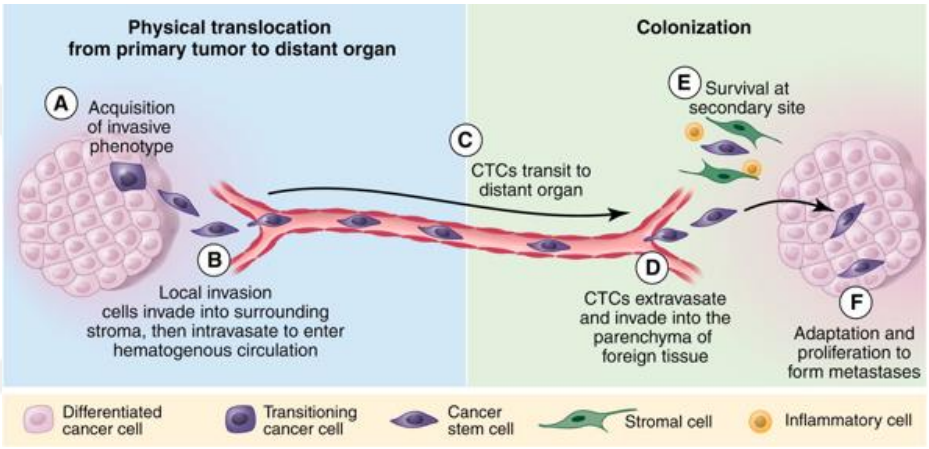

Figure 1.2 The metastatic spread (Broertjes, 2015)

9 Deregulating cellular energetics

In natural physiographic situations the metabolism's energy of the cell is cautiously controlled. The blood is pervading the tissues via the capillaries, and supplying oxygen, nutrients and excretes metabolic wastes. In cancer cells the unregulated cell division engenders an increase number of cells and mass of tissue. These cells pressure on each other leading to high tissue pressure which causes hypoperfusion. Accordingly, it creates in a scantiness of nutrients, hypoxic and metabolic waste aggregation conditions which establishes to aerobic glycolysis. This pathway is much powerless in transmuting glucose to energy; therefore, the cells upregulate glucose receptors (Broertjes, 2015).

10 Avoiding immune destruction

The microenvironment of cancer represents a somatic evolutionary selection. Naturally, in normal environment immune cells surveil and there is surveillance and devour abnormal cells (Merlo et al., 2006). But Cancer cells have the ability to weed out from detecting or downregulating which is considered as a vital selective advantage (Broertjes, 2015).

1.3 The Need for Integrating Approaches of Cancer Therapy

Notwithstanding the recent advances, till now we could not triumph over cancer as a disease like smallpox (Variola major). The real challenges in cancer treatment are many. First, the challenges of cancer treatment are countless. In the cancer the invading pathogenicity does not come from external source, unlike smallpox. This property of cancer complicates the differentiation process of malignant tissues from normal tissues, thereby the enucleating of cancer cells without hurting normal cells is far-fetched action. Second, genomic mutability hallmark of cancer increases the dynamics and the cells to be a very active and adaptiveness extremely. Third, targeting a particular single pathway is stymied through activating an alternative signaling pathways targeted drug. Fourth, the unlimited growth of cancer gives rise to spatially heterogeneous pattern in the tumor cells. As a particular medicine is capable to ravage cells, an imperviable part to this medicine can continue to live and grow again.

The integral strategy is needed for overcoming the tumor resistance by attacking all of the ten hallmarks. Based on this the continuous work to reveal the complexities of different types of cancer is vital through the increasing the knowledge of molecular mechanisms of cancer. Hanahan and Weinberg have been systematized the hallmarks which is considered an elegant framework in comprehension the complexity nature of cancer. hallmarks framework may assist to identify integrated therapies (Broertjes, 2015).

1.4 Current Challenges in Cancer Treatment

Notwithstanding extensive progresses of cancer research is still ongoing but the cancer treatment is compatible with a weakly reductionistic perspective. It's always been Targeting single pathway of cancer that has modestly effect on inhibiting

cancer progress. Nevertheless, consider a node in the targeting of single hallmark cannot drive to effective treatment of cancer. Comparing with what we did for treating HIV treatment, the theoretical predictions at cancer treatments, using drug combinations can be one a favorable curative strategy to stop cancer. Drug combinations have already been proved successful for immunotherapy where blockage of PD-1/L1 represents requisite prop of drug combinations. One of the disadvantages of drug combinations implementation in the clinic is the toxicity. Therefore, it has been soon realized that it is availing to strive for a summary that evokes the spirit of one medicine can targeting many pathways or hallmarks that specifically drive each patients' tumor biology (Zugazagoitia et al., 2016).

1.5 History of Old-Fashioned and New Approach of Drug Discovery

Miscellaneous research papers have re-examined the preliminaries on cancer drug development (Strebhardt and Ullrich, 2008). At the massive acceptance of observation about the exposure to nitrogen mustards diminish the proliferative nature of rapidly dividing lymphoid cells (Hirsch, 2006). By reasoning of Goodman and Gilman that this could act as a curative to cure the patients whose have non-Hodgkin's lymphoma (Goodman et al., 1946). Simultaneous to that time, and based on the watching, vitamin folic acid spurred the acute lymphoblastic leukaemia (ALL) cells. Farber applied aminopterin and amethopterin (folate analogues) for treating ALL, which is considered as the first applying of concept of rational drug development (Frei, 1984). This concept was used again to estimate the 6-mercaptopurine (purine analogues) by Burchenal, Hitchings and Elion (Hitchings and Elion, 1954). Later where found that the nitrogen mustards, and folate analogues and purine analogues that they intervened with DNA replication, as a part of their anticancer activities. In contrast, vincristine (Madagascar periwinkle alkaloids) determined in the 1950s through seeking for anti-diabetic drugs. Vincristine was also found inhibiting the cancer cell division, subsequently inhibiting proliferation through microtubule polymerization mechanism (Johnson et al., 1963). The using of these therapies is continued till now for treating cancer.

Significant advances in the discovery of chemotherapeutics have been started in the 1960s by applying the conception of combining remedies. The rationale behind this

remarkable treatment is the tuberculosis treatment, where each one of them has different mechanism of action. Therefore, the combination was more effective. For cancer, when considering a cancer resistance is developed, we also consider the development of resistance is lesser when using combination of drugs. For treating children with ALL, Holland, Freireich and Frei introduced a 6-mercaptopurine and methotrexate combination as a figure of drug combination approach (Frei et al., 1958).

With the spectacular result obtained at Anti-hormone therapy for treating breast cancer has become an applicable approach. The successful pattern of Anti-hormone therapy is Tamoxifen, according to clinical results which revealed that it is selective estrogen receptor inhibitor. Walpole's group developed the Tamoxifen initially as a contraceptive but showed its anticancer activity when it has been examined for breast tumour in 1971 (Cole et al., 1971). Following clinical investigations have asserted the potentiality of this medicine as estrogen receptor alpha-positive breast cancer reducer. Nowadays tamoxifen is administrated to many hundred thousand of women.

The effect of biology on development drug on cancer at this stage was limited; most therapies had been established either by serendipity or had been elected primarily on the basis that they could limit cell division. However, in the from 1970s to 1980s, the arrival of gene manipulation and molecular genetic analysis transformed the quality of biological research permanently and with it the drug discovery and development process. Molecularly targeted therapies could now be contemplated, that is, drugs that were intelligently designed or selected to inhibit the activity of specific molecules (Table 1.1 and Table 1.2). If operated in the right patient population - on tumours with specific molecular lesions - these therapies promised significant tumour selectivity. One of the most remarkable examples of the development of such a targeted therapy, to which biological research made a critical contribution, is that of imatinib.

Table 1.1 List of available drugs for treating cancer (Lord and Ashworth, 2010).

Drug	**Drug target**	**Cancer types**

Bevacizumab	Vascular endothelial growth factor	Colorectal cancer, non-small cell lung cancer, breast cancer, renal cancer
Bortezomib	Proteasome	Myeloma, lymphoma
Celecoxib	Cyclooxygenase II	Familial adenomatous polyposis
Erlotinib	Epidermal growth factor receptor	Non-small cell lung cancer, colorectal cancer, head and neck cancer
Gefitinib	Epidermal growth factor receptor	
Cetuximab	Epidermal growth factor receptor	Non-small cell lung cancer, colorectal cancer, head and neck cancer
Panitumumab	Epidermal growth factor receptor	
Imatinib	BCR-ABL gene, cKIT gene, Platelet-derived growth factor	Leukemia, gastrointestinal cancer
Dasatinib	BCR-ABL gene, cKIT gene, Platelet-derived growth factor	
Nilotinib	BCR-ABL gene, cKIT gene, Platelet-derived growth factor	
Methotrexate	Dihydrofolate reductase	Multiple cancer types
RAD001	Mammalian target of rapamycin	Renal cancer
Temirolimus	Mammalian target of rapamycin	
Sorafenib	Vascular endothelial growth factor receptor, RAF gene, cKIT gene, Platelet-derived growth factor	Renal cancer, hepatic cancer
Sunitinib	Vascular endothelial growth factor receptor, RAF gene, cKIT gene, Platelet-derived growth factor	
Topotecan	Topoisomerase I	Multiple cancer types
Irinotecan	Topoisomerase I	
Trastuzumab	epidermal growth factor receptor II	Breast cancer
Lapatinib	epidermal growth factor receptor II	Breast cancer

Tamoxifen	Estrogen receptor α	Breast cancer
Exemestane	Aromatase cytochrome P450	
Anastrozole	Aromatase cytochrome P450	
Letrozole	Aromatase cytochrome P450	
Rituximab	CD20	Lymphoma
Tositumomab	CD20	

Table 1.2 List of under clinical investigation compounds for cancer treatment (Lord and Ashworth, 2010).

Drug	**Drug Target**
17AAG	Heat shock protein 90
ABT-737, ABT-263, Obatoclax	B-cell lymphoma-extra-large, B-cell lymphoma 2
Alvocidib	Cyclin-dependent kinases
Olaparib, AG014699	Poly (ADP-Ribose) Polymerase I Poly (ADP-Ribose) Polymerase II
BEZ235	Phosphoinositide 3-kinase
GRN163L	Human telomerase reverse transcriptase
Mapatumumab	TNF-related apoptosis-inducing ligand Receptor
Nutlin-3	Mouse double minute 2 homolog
PLX4032	BRAF gene
GDC-0449	SMO gene
PF-0477736	Checkpoint kinase 1

1.6 The Complementary and Alternative Medicine

The successes of complementary and alternative medicine (CAM) have raised in recent decades. The question whether the statistical properties of spectra are universal. Still this CAM comprises many important nonconventional therapies such

as vitamin therapy, Phyto medicine, homeopathy and traditional Chinese medicine (Fischer et al., 2014). Ingesting natural derived compounds is probably the highest spread in CAM. Fifty to eighty percent of cancer patients combine CAM together with conventional therapy (Huebner et al., 2014; Saghatchian et al., 2014). However, the main discontent with conventional treatment is related to the fact chemotherapeutic side effects that leads to transfer to CAM (Citrin et al., 2012; Gillett et al., 2012).

Thus, knowledge about CAM is majorly obtained through sharing the experiences of patients who suffered from cancer (Huebner et al., 2014). Physicians do not discuss CAM with their patients and also have little information about CAM (Parker et al., 2013). The studies regarding the therapeutic efficacy of particular compounds taken from CAM are scattered and well thought out, but clinical results are still limited. Discrepancies between the using of a natural products and knowledge about an anti-tumour property can only been noticed at the amygdalin. Amygdalin (Figure 1.3) is a naturally occurring in the dextrorotatory configuration (active form) (Milazzo et al., 2007).

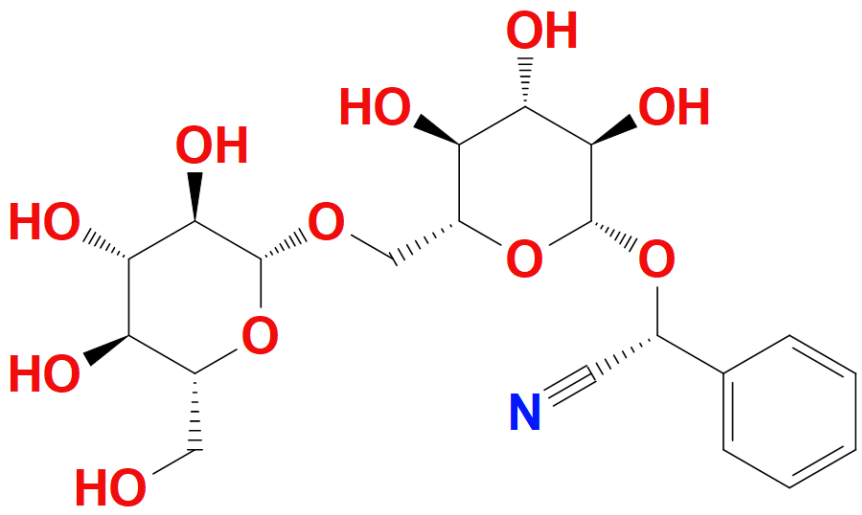

Figure 1.3 The two-dimensional structure (2D) of amygdalin.

1.7 History of Amygdalin and Its Mechanism of Actions

Amygdalin was extracted by Boutron-Charlard and Robiquet from bitter almonds in 1830s (Prunus dulcis) (Blaheta et al., 2016). Based on the obtained results from

Widtmann and Denk's publication mentioned that amygdalin was nontoxic and important for general use (Blaheta et al., 2016). Even earlier than 1848, amygdalin was applied as an anti-cancer in Russia (Petersen and Markle, 1984), while first use of amygdalin in in the United States backs to 1920s (Curt, 1990). Ernst T. Krebs got a patent in 1950s for develop an injectable form of semi-synthetic amygdalin called Laetrile as shown in Figure 1.4 (Dorr and Paxinos, 1978). Although the term "laetrile" is used as second name but, laetrile is D-mandelonitrile-β-glucuronide and is diverse from the natural product amygdalin as shown in Figure 1.3. Amygdalin soon became one of the most popular non-conventional anticancer in the 1970s, where 70,000 patient used it in united states (Moss, 2005). But the real action of amygdalin is still riddle.

The anticancer mechanisms of amygdalin anticancer have been hypothesized several proposed routes. The first hypothesis involves beta-glucosidase (β-glucosidase) activity where β-Glucosidases are enzymes, they are important for removal of nonreducing terminal glucosyl residues from saccharides and glycosides. The fact demonstrates that β-glucosidase is overexpressed and also the activity increases in different types of solid tumours. Amygdalin is metabolized in the by cancer cells because amygdalin contains two glucose molecules, producing yielding hydrocyanic acid and benzaldehyde. Thus, detoxication of free cyanide molecules from body can be done through rendering them into harmless thiocyanate by rhodanese. Then thiocyanate is easily excreted through the urine without harmful effects (Newmark et al., 1981). The researchers attempt to criticise this mechanism because both neoplastic and normal cells include only traces of β-glucosidases and similar amounts of rhodanese. Another hypothesis has suggested that orally consumed amygdalin is metabolized to a mandelonitrile, which is then entirely transported to liver to turn into a beta-glucuronide compound. Beta-glucuronide is then being transmitted to cancer cells and in turn is undergoing catabolizing by β-glucuronidases to release mandelonitrile and subsequently hydrogen cyanide. A third hypothesis proposed that amygdalin deficiency may lead to activate a cancerous condition, where is believed that amygdalin is essential for normal physiological function. That B-17 is an essential compound from plants necessary. This hypothesis emphasizes that regular administration of foods that contain amygdalin can reduce the probability of cancer incidence. No satisfactory explanation has been found for these

discrepancies. Therefore, the need for using other approaches to stop the conflicts between these discrepancies.

1.8 Objective of the Study

Growing evidence showed amygdalin has anticancer activities (Juengel et al., 2016; Makarević, Rutz, Juengel, Kaulfuss, Reiter, et al., 2014; Makarević, Rutz, Juengel, Kaulfuss, Tsaur, et al., 2014; Park et al., 2005; Qian et al., 2015). Several researches have demonstrated the efficiency of amygdalin to control apoptosis in vitro examinations. They proved that amygdalin regulates the apoptosis by inhibiting Bcl-2 and activating the BAX (Chang et al., 2006; Chen et al., 2013), upregulating caspase-

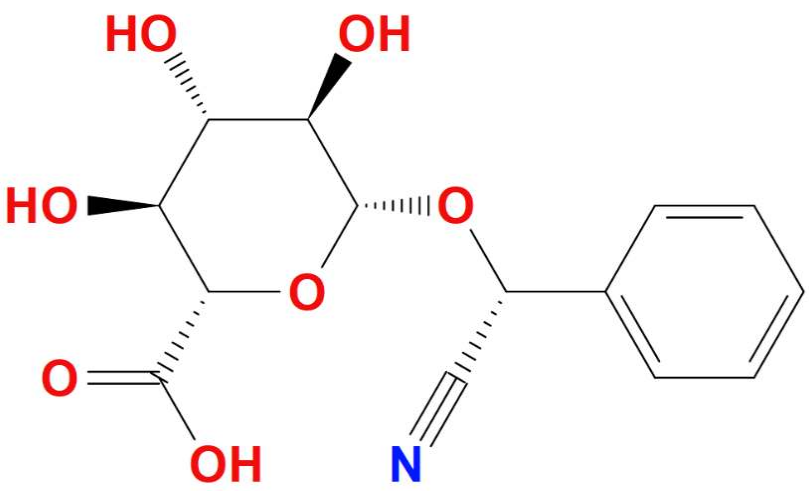

Figure 1.4 The two-dimensional (2D) structure of laetrile.

3 and blocking PARP-1 (Lee and Moon, 2016). And besides, the experimental researches reported that amygdalin blocks the adhesion and invasion of different kinds of cancers (Makarević, Rutz, Juengel, Kaulfuss, Tsaur, et al., 2014; Qian et al., 2015) cells by inhibiting AKT, FAK1, and ILK proteins. Further, the preceding observations of amygdalin exhibited that amygdalin suppresses the cell division of cancer cells through blocking the Cyclin-dependent kinase 1/Cyclin B, Cyclin-dependent kinase 2/Cyclin A and Cyclin-dependent kinase 4/Cyclin D1 (Juengel et al., 2016; Makarević, Rutz, Juengel, Kaulfuss, Reiter, et al., 2014). In spite all the outcomes of investigational results, but the anticancer mechanism of function can be one of the confounding enigmas of how amygdalin acts oppose to malignancy. The

widespread opinion in the community of medical field that the anticancer influences of amygdalin that come out from the hydrogen cyanide (Bhatnagar et al., 2017; Song and Xu, 2014). But the intense comprehension of molecular mechanisms about function of amygdalin is still unexplored. Therefore, in this dissertation we are going to explore the different mechanisms through using the computational approaches. This study was programed to scrutinize the multifunctional activities of amygdalin: regulation of apoptosis, inhibition of cell division and inhibition of the metastasis and invasion.

1.8.1 Regulation of Apoptosis

Normal cells, consequently, are fostering the apoptosis to expel the senescent or deteriorated cells (Pfeffer and Singh, 2018). To minimize the inflammations upshot from anticancer drugs administrations, boosting apoptosis gained more attentiveness through developing anticancer drug (Jan, 2019). However, in cancer, the cells are not only salvation from apoptosis by blocking the signals that lead to apoptosis but also drive to full propagation and this makes tumor cells be survived and be less sensitive for anticancer treatments. Resistance can broadly be defined as a complicated phenomenon that engenders from the interactions of diverse molecules with different signaling pathways. Subsequently, in order to defeat the resistance toward apoptosis,(Mohammad et al., 2015) we have to attack predominant pathways in the apoptosis via inhibit some pathways and activate another pathways. Based on the experimental data, we here have selected the main important pathways are: first, *extrinsic pathway*, Caspases consistently exemplify the nerve network in the apoptotic pathways and by their role in apoptotic process; second, *intrinsic pathway*, in this pathway cytochrome c is excreting from the intermembrane of mitochondria into the cytosol, is effectuated by inserting the BAX/BAK inside mitochondrial membrane, whilst Bcl-2 and Bcl-xL play an opposite functions;(Jan, 2019) and third, *execution Pathway*, in which many of proteins that are required for cleaving caspases proteins. Poly (ADP-ribose) polymerase-1 (PARP-1) is an example of cleaving caspas-3 into a ~25 kDa and a ~85 kD. Inactivation of PARP-1 is indispensable to fragmentating DNA, saving the cells from ATP consumption and following necrotic death, and preventing futile attempts of DNA repair. To effectuate the cells to enter to apoptosis, where cleavage of PARP-1 is fundamental for starting this action

(Diamantopoulos et al., 2014). Depending of on pathways the effective treatment should take in consideration the activation and inactivation can be done by single molecule called as a Multi-functional Drug MFD (Al-Khafaji and Taskin Tok, 2020c).

Bcl-2/BAX complex

Bcl-2 binds to the BAX (Figure 1.5) and leads to oligomerizing the Bcl-2/BAX complex, as a result this oligomerization stops the apoptosis (Verma et al., 2015). Thus the idea of discovering drugs that break this protein/protein interface is an efficient concept to activate the apoptosis of cancer cells (Croce and Reed, 2016). A number of studies were conducting the mutations upon the Bcl-2/BAX, suggest the association of BH3 region of BAX with BH1–3 regions of Bcl-2, the BH1–3 regions which are critically required for Bcl-2/BAX interactions. Where hydrophobic groove of Bcl-2-like protein binds to hydrophobic region of BAX, α2, α 3, α 4, and α 5 helices form the binding groove (Ding et al., 2010; Verma et al., 2015). Thus, the imitating the drug-like small molecules have conditioned to have the action of BH3 peptide, it was arduous work to successfully functioning but required an innovational technology and idiosyncratic strategy. Based on this notation, several research groups commenced to implement the high-throughput screening to identify molecules as inhibitor. One of these molecules was obatoclax, but it has no ability to disrupt Bcl-2/BAX complex (Samuel et al., 2010; Verma et al., 2015) while the *in silico* study of Verma (2013) showed that taxifolin and quercetin have disruption effect (Verma et al., 2015).

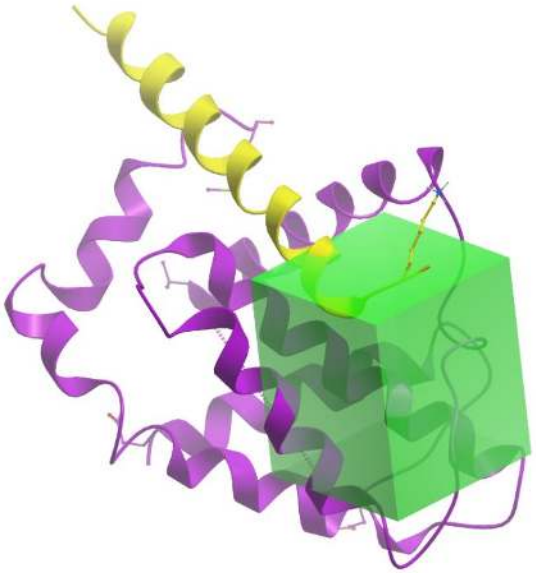

Figure 1.5 3D of Bcl-2/BAX complex (PDB: 2XA0) and green box represents the binding site.

Caspase-3

As drug developers of cancer, promoting the activity of apoptosis through activation caspase-3 can be considered as determinant (Porter and Jänicke, 1999). Furthermore, the caspase-3 (active form of caspase-3) commands to the of cleavage of cellular substrates such as Poly (ADP-ribose) Polymerase (PARP), DNA Fragmentation Factor and finally disassembling of the cell (Kumar, 1995; Liu et al., 1997; Węsierska- Gądek et al., 2004). By nature, caspase-3 is expressed as two chains of inactive proenzymes of conserved sequences (Figure 1.6): a large subunit is 20 kDa, and a small C-terminal subunit is 10 kDa (Thornberry et al., 1997). The transformation from inactive form to active caspase-3 is achieved by the disrupting the interface between these two subunits. But in different types of cancer cells, the caspase-3 is inactive in normal conditions, therefore activating caspas-3 can be done through targeting the interface between two units (Walters et al., 2009).

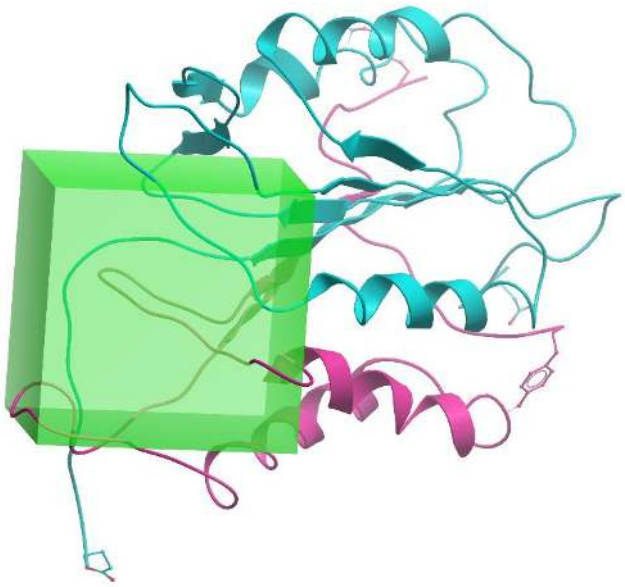

Figure 1.6 3D structure of Caspase-3 complex (PDB: 1RHQ) and green box represents the binding site.

PARP-1

PARP-1 introduces two discrepant roles: it firstly catalyzes the synthesis of poly (ADP-ribose), secondly PARP-1 is inhibited by caspases. PARP-1 proteolyzes into a C-terminal fragment and N-terminal fragment containing the DNA-binding domain (DBD) (Soldani and Scovassi, 2002). PARP-1 is a crucial constituent of the enzyme superfamily. After DNA damage, PARP1 can rapidly attaches to single-strand breaks. The base deletion repair pathway maintains the single-strand breaks. Several strategies have been implemented for developing a PARP1 inhibitors. several mimic the nicotinamide moiety of NAD+ at the NI binding site (Virág and Szabó, 2002). Additional-action mechanisms revealed that some inhibitors can induces cytotoxic PARP/DNA complexes or also even can cause alteration in the phosphorylation signaling pathways (Bellocchi et al., 2005). But, several of these molecules overwhelmingly exhibit a toxic side effects whist the rest cancer cells show resistance against them. Consequently, finding new inhibitors for PARP1 is important. In this concern, *in silico* investigation is an indispensable machine for in-depth comprehension of the binding mechanism of protein-ligand interactions (Mitra et al., 2019).

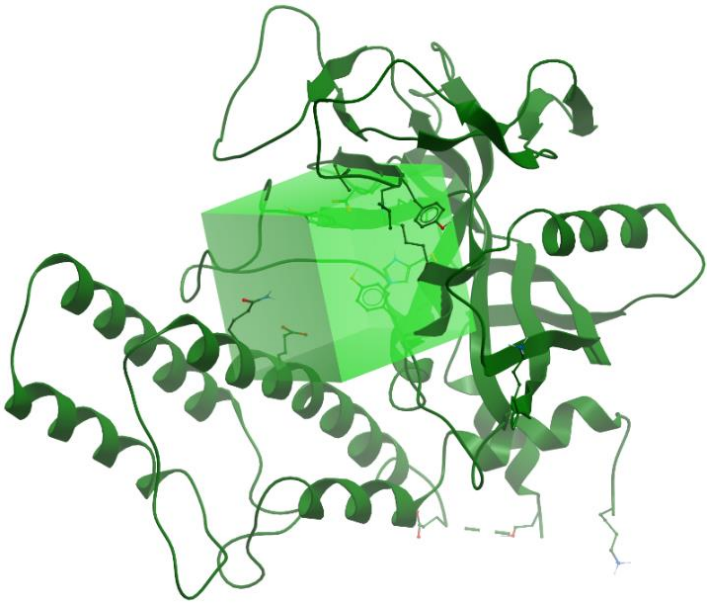

Figure 1.7 3D structure of PARP-1 complex (PDB: 4RV6) and green box represents the binding site.

1.8.2 Inhibition of Cell Division

Proteins kinases are functioning the transfer the phosphate group from ATP into specific amino acid. Protein kinases (Qian et al., 2015). The human genome encodes about 500 putative kinases proteins, which are playing functional roles in cellular signal transduction (Cohen and Alessi, 2013). These kinases are divided into a hierarchy of 134 families and 201 subfamilies (Manning et al., 2002). One of these subfamilies are the cyclin-dependent kinases (CDKs) or cell division cycle protein that regulate the cell division cycle, ordinarily, under the proper control of cyclin partners. Specifically, CDK/cyclin systems guide the orderly cell division by inducing the cell cycle phases which are G0--G1--S--G2--M. (Satyanarayana and Kaldis, 2009; Senderowicz, 2003).

CDKs are basically proline-directed kinases, and the phosphorylation occurs on the serine or threonine residues. CDKs are activated when they are associated with cyclins to form activated CDK/Cyclin complexes (Morgan, 1997). As yet, only 20 member CDK proteins and 20 type cyclins have been documented in natural cells (Malumbres and Barbacid, 2005). But only, CDK1, CDK2, CDK4, and CDK6 were monitored as regulator of cell-cycle division (Obaya and Sedivy, 2002), the other are

involved in non-cell-cycle functions (Lim and Kaldis, 2013). Some proteins of this group of kinases often have been reported as deregulated in human tumors (Malumbres and Barbacid, 2009).

CDK1/cyclin B

CDK1/cyclin B appears to assemble in S-phase (Pines and Hunter, 1989). CDK1/cyclin B activation, firstly recognized at centrosomes, signalizes the commencement of cell division, and CDK1/cyclin B is needed to insure the felicitous completion of cell division (Brown et al., 2015). During G2 and early mitosis, a vast number of substrates were phosphorylated by CDK1/cyclin B, Which initiates the spindle assembly, centrosome duplication, chromosome condensation and so forth (Chashoo and Saxena, 2014; Holt et al., 2009). Yet, however, CDK1 life is diminished by the setup of anaphase as a result of cyclin A and cyclin B ubiquitination and consequent deterioration through the various tasks of the APC/C E3 ubiquitin ligase and the proteasome (Barford, 2011; Clute and Pines, 1999; Peters, 2006).

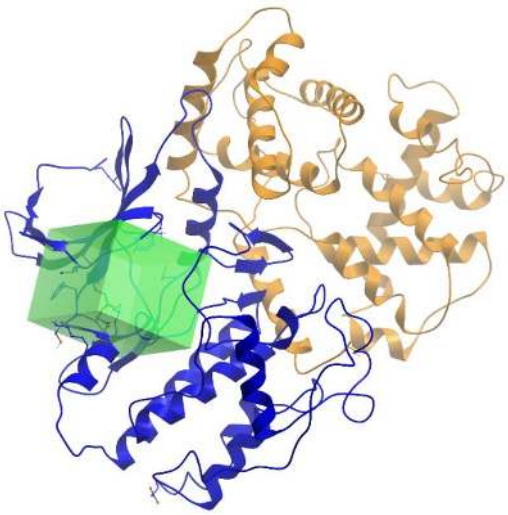

Figure 1.8 3D structure of CDK1 (Blue)/Cyclin B complex (PDB: 4Y72) and green box represents the binding site.

CDK2/cyclin A

During the early stage of S-phase, CDK2/cyclin A is activated. CDK2/cyclin stimulates the phosphorylation of numerous endogenous substrates. Phosphorylation

of these substrates allows to replication of DNA and inactivates the G1 transcription factor E2F. E2F inactivation is necessary for S-phase completing whereas the presence of E2F and in the lack of CDK2/cyclin A could lead to biological apoptosis. Therefore, inhibition of CDK2/cyclin A leads to cytotoxicity (Davies et al., 2002; Knockaert et al., 2002; Lapenna and Giordano, 2009). The internal inhibitors such as (Cip-Kip) or improper expression of CDK2 lead to diverse tumors (Lapenna and Giordano, 2009).

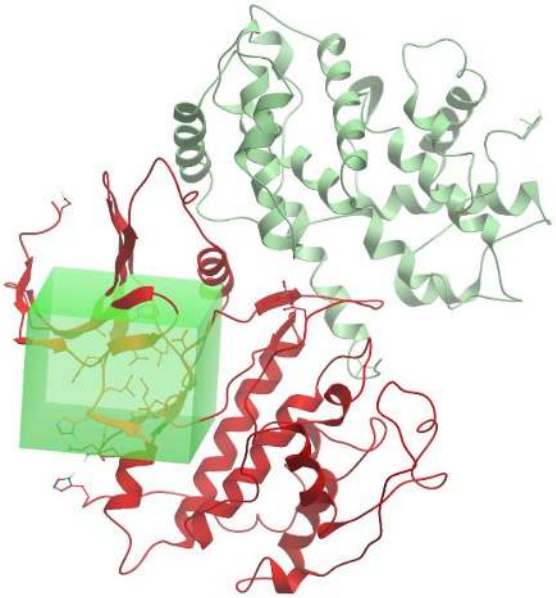

Figure 1.9 3D structure of CDK2 (Red)/Cyclin A complex (PDB: 5NEV) and green box represents the binding site.

CDK4/cyclin D1

The first CDK/cyclin holoenzyme known to be activated is constituted of cyclin D and cdk4. Cyclin D1-cdk4-pRb pathway is regarded as a fundamental player in controlling cell cycle promotion and its deregulation is noted in many types of malignancies (Vasanthakumari et al., 2019). The cyclin D1-cdk4/6/INK4/pRb/E2F pathway is controlling efficiently the passage from G1 to S phase during the cell cycle. Thus, focusing on cdk4 target for designing new remedial molecules to suspend or promote cell cycle regulation is a rising field (Dickson, 2014). CDK4/Cyclin D1 and CDK6/Cyclin D1 are of specific regard on mutation at the genome level (Hall and Peters, 1996) or overexpression of CDK4/Cyclin D1 and CDK6/Cyclin D1 are certainly substantial in the proliferation of various tumors.

Retinoblastoma protein (pRb) is a tumor suppressor gene that phosphorylates the active *CDK/Cyclin* complexes (Fry et al., 2004; Konstantinidis et al., 1998). Involvement of CDK/cyclin systems are activated during the subsequent stages of cell cycle, accordingly, CDK/cyclin systems are identified as pharmacological targets of importance for the advancement of anticancer therapy (Bruyère and Meijer, 2013; Lapenna and Giordano, 2009).

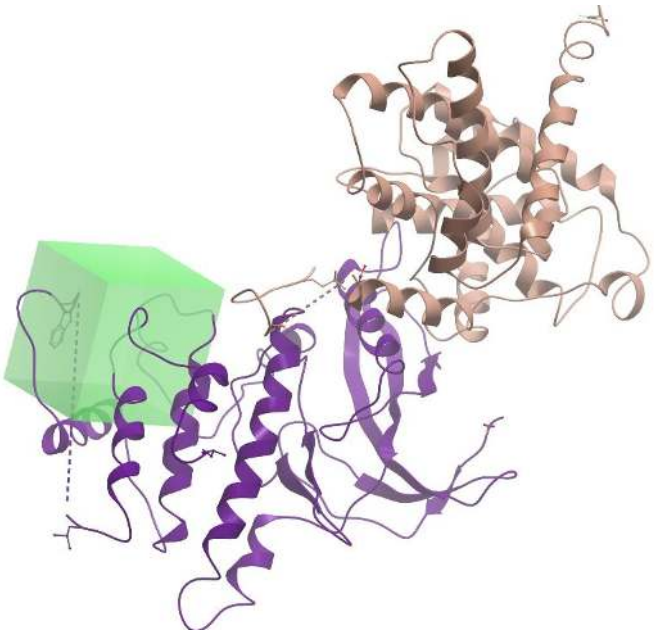

Figure 1.10 3D structure of CDK4 (Magenta)/Cyclin D1 complex (PDB: 2W96) and green box represents the binding site.

1.8.3 Inhibition of Metastasis and Invasion

The metastasis is well-defined single-valued characteristic only for cancer. In turn, this renders any potential cancer can be transferable to another site of body. This opens the door for about 90 percent of universal death of cancer due to metastasis (Fidler, 2002a, 2002b). Cancer cells penetrate across blood vessels to remote organs and invade neighboring tissues. It is necessary to note that not only tumor cell interacts with epithelial-mesenchymal and extracellular matrix components, but also the angiogenesis is main way for invasion (Wittekind and Neid, 2005). Clearly, whenever metastasis is established, set of processes are involved in progression of cancer invasion where the signals between tumor cells and the tumor extracellular matrix (ECM) drive for cancer migration or invasion (Desgrosellier and Cheresh, 2010). The changes in extracellular matrix composition orders the structure

activation of many subcellular biomechanics, predominantly G-protein-coupled receptors, integrin receptors, cytokine receptors and tyrosine kinases receptors, are assessed at their contributions to tumor invasion (Gkretsi and Stylianopoulos, 2018). The experimental statistics are rather questionable, and there is no sufficient therapy against metastasis. A much better systematic finding of treatment against cancer is that how can a medicine interact with distinct targets that are supposed to be responsible for cancer infiltration.

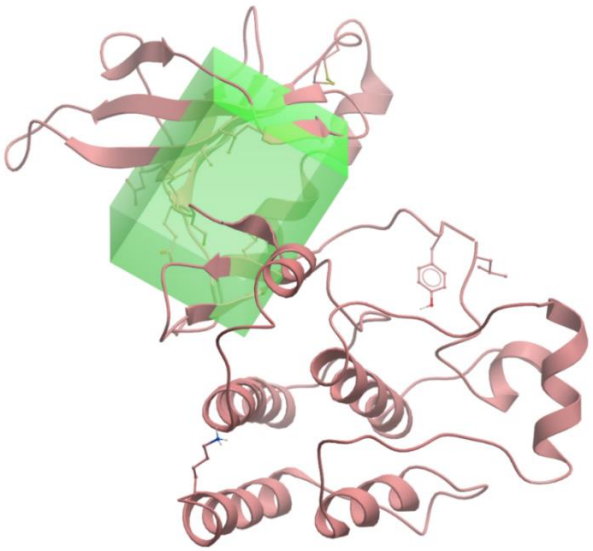

Figure 1. 11 3D structure of FAK1 complex (PDB: 4K8A) and green box represents the binding site

FAK1

Overexpression of focal adhesion kinase (FAK1) has been correlated with several kinds of tumours (Chen et al., 2014; Owens et al., 1995; Vanamala et al., 2011; Yoon et al., 2014; Zhang et al., 2014). FAK1 is tyrosine kinase and is involved in cancer metastasis by modulating focal adhesions. FAK1 has an activity linked to aggressive tumor features as the cell adhesion and spreading (Li et al., 2018; Thamilselvan et al., 2007). The adhesion kinases are dynamic intracellular proteins, they use integrin proteins to combine the extracellular matrix to the cell cytoskeleton. Experimentally, it has been demonstrated that the uncontrollable division of cell is associated with the phosphorylation of tyrosine 397 in FAK1 (Daniel and João, 2015). This phosphorylation arises from the interaction between a non-receptor tyrosine kinase with chemical signals and integrin proteins. Some declared that the inhibition of

FAK1 may diminish the metastatic power of breast tumor cells (Rigiracciolo et al., 2019).

ILK

Integrin-linked kinase (ILK) is a commonly expressed threonine or serine protein kinase in focal adhesions. These adhesion locations are crucial intracellular signaling centers. And ILK shows a basic task in transducing many of the biochemical signals that are established by cell-matrix interactions. This controls the elementary processes such as proliferation, growth, survival, migration, angiogenesis, differentiation and invasion (Hannigan et al., 2005). Evidence now refers to ILK as a crucial and multifaceted element in the normal functions of several tissues but ILK is overexpressed in different cancers. (Hannigan et al., 2005; Persad and Dedhar, 2003; Xu et al., 2003). Further, *in vivo* models demonstrated that the overexpression of ILK drives to the emergence of mammary cancers in mice (White et al., 2001). Comprehending the functions of ILK under natural and pathological conditions will present observations into how ILK leads to illness, and under which situations the ILK can be employed therapeutically (Legate et al., 2006). Thus, ILK is an interesting therapeutic object in human malignancy (McDonald et al., 2008).

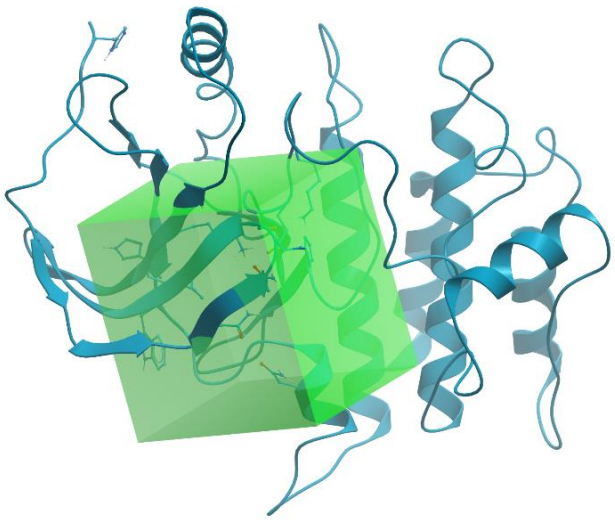

Figure 1. 12 3D structure of ILK complex (PDB: 3KMW) and green box represents the binding site.

AKT1

Protein kinase B (AKT or AKT1) has been noted to apply a crucial task in promoting the invasiveness of carcinoma cells (Jean et al., 2014; Taliaferro-Smith et al., 2015; Zhang et al., 2017). The AKT1 protein kinase transduces signals from growth elements and oncogenes to downstream objects that regulate essential ingredients in carcinoma expansion. The AKT1 route is one of the most often hyper-activated signaling pathways in human tumors. AKT1 has been proved to promote cell proliferation and to suppress the apoptosis. Consequently, stimulated AKT1 is correlated with cell invasion and migration in various mammalian processes. Therefore, suppressing the activity of AKT1 has been recognized as an interesting object for curative interference (Liu et al., 2006). This renders AKT1 a valuable therapeutic target for interrupting the invasion and metastasis (Nitulescu et al., 2018).

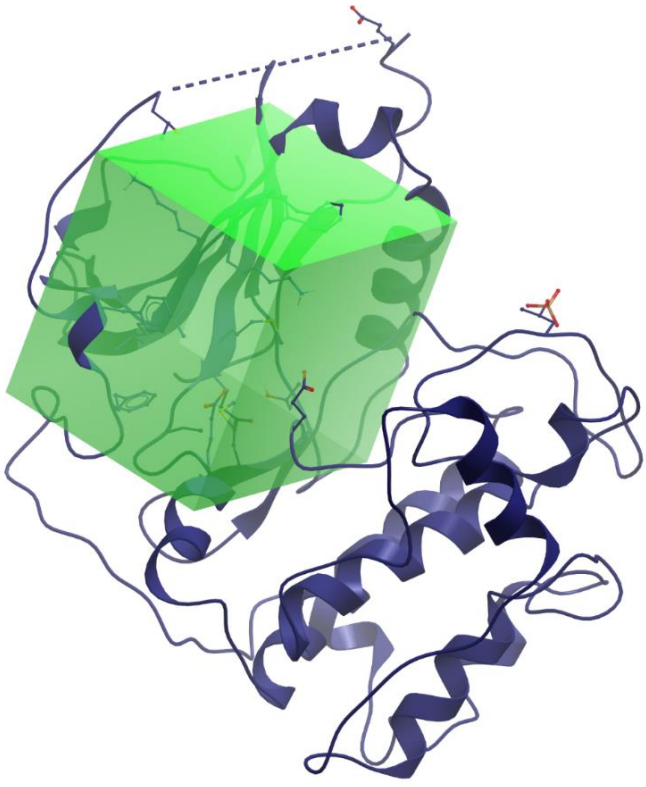

Figure 1. 13 3D structure of AKT1 complex (PDB: 6CCY) and green box represents the binding site

CHAPTER II

THEORETICAL BACKGROUND

2.1 Introduction

Molecular modeling science taught us how build the biological model: molecular modeling science has also taught us how to study the function of the system through using mathematical terms and physics (Honarparvar et al., 2014; Schlick, 2010). The term of "model" was firstly used in Oxford English Dictionary's which defined as 'a simplified description of a system. The model undergoes theoretical computations: theoretical computations include *semi-empirical quantum mechanics*, *ab initio,* molecular dynamics, and empirical (molecular) mechanics, free energy and solvation methods, *Monte Carlo* etc. The experimental data refinement was obtained from X-ray crystallography or nuclear magnetic resonance (NMR) can be regarded as regarded as main component of biomolecular modeling.

2.2 Molecular Mechanics

Molecular mechanics (MM) utilizes the classical physics' law of for explaining and interpreting the properties and behaviors of atoms and molecules (Atkins and Paula, 2006; Bultinck et al., 2003). The advantages of molecular mechanics become clear that it is treating huge molecules because it does not compute the electronic properties and it depends mainly on forcefields with embedded empirical parameters (Bultinck et al., 2003; Rogers, 1990). The most important applications of molecular mechanics are energy minimization and conformational analysis (Soliman, 2009). On the other hand, the important components of a force field contain a collection of equations describing the variation in the potential energy the molecule with locations of its atoms of molecule through characteristics of an atom of the element within a specific chemical context (Sharma, 2011). However, the drawbacks of molecular mechanics (Rogers, 1990) are: firstly, limited in the description of the equilibrium

for geometries and equilibrium of conformations; secondly, unable to estimate electronic properties.

Therefore, molecular mechanics unable to provide information about the bonding and it also unable to predict the bond formation or breaking. It cannot be used for the calculation of bond formation/breaking. Based on aforementioned notes, molecular mechanics cannot predict the selectivity and chemical reactivity. Third, the mostly used force fields nowadays are parameterized by using ab initio techniques or experimental data where the accuracy of molecular mechanics depends on both the on experimental studies and choice of parameters (Rogers, 1990; Soliman, 2009). Each distinct force field was designed for a specific set of molecules (proteins etc.).

Moreover, molecular mechanics considers that the molecule is a group of masses interacting with each other through harmonic forces. Consequently, the molecular mechanics total energy of a molecule is equal to the summation of contributions raised from bonded interactions: bond angles, bond length, torsions and non-bonded interactions (Van der Waals and electrostatic) (Hinchliffe, 2011; Jensen, 1989).

$$\boldsymbol{E_{tot} = E_{str} + E_{bend} + E_{tors} + E_{vdw} + E_{elec}} \quad (2.1)$$

where E_{tot} is representing the total energy, E_{str} is representing the bond-stretching energy, E_{bend} is representing the angle-bending energy, E_{tors} is representing the torsional energy, E_{vdw} is symbolizing the van der Waals energy and E_{elec} is symbolizing the electrostatic energy. The combination of the set energies forms the molecular mechanics force fields (Jensen, 1989; Rogers, 1990; Sansom and Smith, 2010; Weiner et al., 1983).

The development of numerous molecular mechanics force fields over the last several years has used for simulation for biomolecules. Many academic groups have announced force fields — such as AMBER, CHARMM, OPLS and GROMOS — to better understanding of the biomolecular system behaviors (Bures, 1999). All force fields vary in intrinsic properties because of changes in the parameterization treat also in atom types and the reference data. To that purpose consider a set of variables have to be regulated to render the results as similar global good fitting (Bures, 1999). In present study, CHARMM force field was used to investigate the multifunctional activities of amygdalin.

2.3 Molecular Docking

Computational techniques are developing into more powerful in investigating the construction and behave of biomolecules due to the number of protein X-ray systems (Rudnitskaya et al., 2010). Molecular docking is chiefly employed in structure-based rational drug design to determine the right conformations of small molecule ligands and again to evaluate the effectiveness of the protein-ligand interaction. The substrates, inhibitors or another remedy candidate are determined in the binding site of the macromolecule. Macromolecules are proteins such as a receptor, enzyme or nucleic acid with an established 3-dimensional structure (Plewczynski et al., 2011). Molecular docking intimates how can macromolecule interact with ligand (Olson and Goodsell, 1998). The molecular mechanics is used to analyze the binding energy between macromolecule with the ligand (Rudnitskaya et al., 2010). The binding potential is measured as follows:

$$E_{binding} = E_{receptor} + E_{ligand} - E_{receptor\text{-}ligand} \quad (2.2)$$

It is approximately that there are more than sixty docking tools are available as academic or commercial at present moment such as Dock (Ewing et al., 2001), AutoDock (Morris, 1998), AutoDockFR (Ravindranath et al., 2015) FlexX (Rarey et al., 1996), Surflex (Jain, 2003), Gold (Jones et al., 1997), Glide (Friesner et al., 2004) and others. These tools were categorized as fragment-based, stochastic Monte Carlo, , evolutionary-based and the shape complementary methods (Plewczynski et al., 2011). Because of the computational expense, the docking softwares do not apply a systematic search to inspect the degrees of fully freedom (Plewczynski et al., 2011). Two types of docking were made, these being the rigid docking, and the flexible docking. In the case of rigid docking, ligand and macromolecule are preserved rigid. But for flexible docking, both of macromolecule and ligand were allowed to be flexible (Erickson et al., 2004). In our work, we utilized the AutodockFR (Ravindranath et al., 2015) to enable the ligand to reach deep grooves of the binding pockets. And then we have hired AutoDock 4.2 (Morris and Huey, 2009) for docking a flexible ligand within binding pockets of the targeted proteins to evaluate the potential of the protein-ligand interaction. AutoDock performs conformational searches based on the Lamarckian version of genetic algorithm to

generate an evolutionary picture for the protein-ligand interactions. The implemented Lamarckian genetic algorithm (Morris, 1998) can handle the high number of degrees of freedom of ligands (Teodoro et al., 2002). Each new conformation becomes adaptive from changes after having optimized by using in situ optimization, after which the binding affinity can be assessed after generating ligand-protein interaction (Plewczynski et al., 2011). From the experiments which directed upon the docking engines, they revealed that maximum errors were due to the scoring function at 1.5-2.0 Å. Accordingly, it was confirmed that general deficiencies in docking are unquestionably due to scoring functions than sampling (Mukherjee et al., 2010). Unfortunately, no scoring method has been developed for identifying the correct binding mode for protein-ligand so far (Bultinck et al., 2003). It was also reported when the number of rotatable bonds is above 32 can affect the results of scoring methods. The ranking of success rate for ligands containing rotatable bonds were 7-0> 8-15> 15 (Mukherjee et al., 2010). Therefore, the using docking tools through combining them can enhance the results and reduce the disadvantages (Floudas et al., 2001).

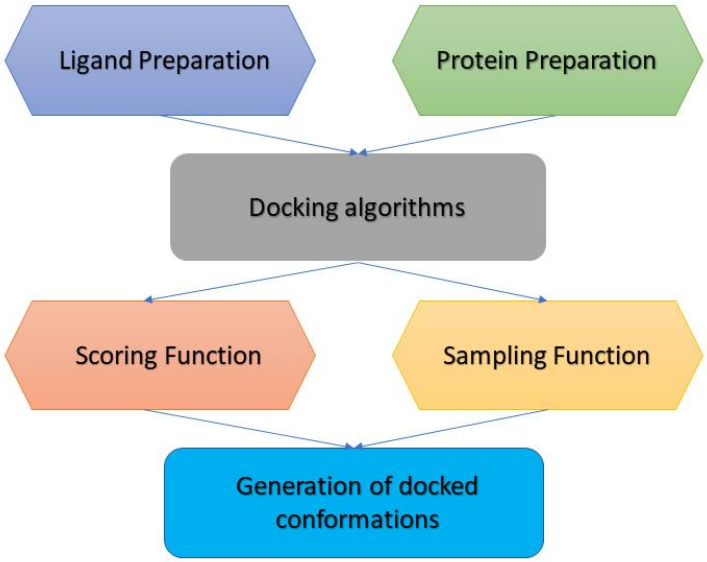

Figure 2.1 A simplified scheme of a general setup of protein-ligand docking.

A docking experiment requires that the base preparation for ligand and protein structures, however note that, the algorithm requires these molecules preparations for being ready to implement (Figure 2.1). Under the preparation's protocols for proteins are included addition of hydrogen atoms, assignment of partial charges, and the

assign the atom types to the ligand. The results of the docking experiment can be a sorted ranked according to the RMSD values and docking scores which they predicted by the implemented algorithms.

2.4 Molecular Dynamics (MD)

The importance of the molecular dynamics (MD) simulation is that it reproduces the time-dependent behavior (Khan, 2009; Parrill and Lipkowitz, 2016; Wang et al., 2001) a molecule because of atom vibrations and movements and collisions. In turn, this results from the interactions between the atoms and molecules periodically through of known physical characteristics for a system of particles at a specific temperature (Parrill and Lipkowitz, 2016; Sharma, 2011). In a molecular dynamic simulation, the molecule being set in motion through elevating the system to specific temperature to exceed the barriers of potential energy and reach more conformations at high temperature (Atkins and Paula, 2006; Sansom and Smith, 2010). Molecular dynamics computations were built on molecular mechanics basics (Cozzini et al., 2004; Sansom and Smith, 2010). The integrating Newton's laws motion (Jensen, 1989; Taylor et al., 2002) generate conformations. The obtained file from MD simulation is trajectory which exhibits how the positions and velocities of the atom in systems vary regarding time (Parrill and Lipkowitz, 2016; Sharma, 2011). This is can be got depending on the force on each particle (Fi) first as a function of time: force on each particle is a negative gradient of the potential energy.

$$\boldsymbol{F_i} = -\frac{\partial \boldsymbol{U}}{\partial \boldsymbol{ri}} \tag{2.3}$$

where r is the position of the particle and U is the potential energy. The acceleration (a) of a particle is obtained by dividing the force acting on it by the mass of the particle according to Newton's Law of motion (Jensen, 1989; Parrill and Lipkowitz, 2016).

$$\mathbf{ai} = -\frac{\boldsymbol{Fi}}{\boldsymbol{mi}} \tag{2.4}$$

The change in speed of the atom is equivalent to the integral of acceleration over time.

$$dv = \int a dt \tag{2.5}$$

Eventually the kinetic energy can be characterized in terms of both the velocities and momentum of the atoms or particles (Jensen, 1989; Parrill and Lipkowitz, 2016).

$$K(v) = \frac{1}{2}\sum_{i=1}^{N} m_i v_i^2 \tag{2.6}$$

$$K(p) = \frac{1}{2}\sum_{i=1}^{N} \frac{pi2}{mi} \tag{2.7}$$

Thus, the total energy of the system (Hamiltonian (H)) is resulted from the sum of the kinetic and potential energies:

$$H(q,p) = K(p) + U(q) \tag{2.8}$$

where q represents the Cartesian coordinates, p represents the momentum of the atoms. The velocities, are derived from the first derivative of the positions with regard to time:

$$v_i(t) = \frac{d}{dt} q_i(t) \tag{2.9}$$

where $q_i(t)$ points out to the atomic locates at a specific time, t. Depending on the initial coordinates of atom in the system, the atoms will move to new positions. Consequently, the new conformations are created (Jensen, 1989; Sharma, 2011). The temperature however is directly proportional to kinetic energy.

2.5 Binding Free Energy

The binding free energy for molecular system the plays a substantial role that in predicting the ability for association and reaction (Kamerlin et al., 2009; Kollman, 1993). In this work, the binding free energy computations are implemented for the amygdalin binding to different targets by using the Molecular mechanics Poisson-Boltzmann surface area (MM-PBSA) approach through running g_mmpbsa tool (Kumari et al., 2014). But unfortunately, there is still no consensus on the details of the method (Genheden and Ryde, 2015). The binding free energy $\Delta G_{binding}$ is obtained by following the below equation:

$$\Delta G_{binding} = \Delta G_{MM} + \Delta G_{sol} - T\Delta S \tag{2.10}$$

where ΔG_{MM} refers to molecular mechanics energy which is referring to the interaction between ligand and protein, ΔG_{sol} represents the solvation energy and $T\Delta S$ reflects the entropy contributions which can be neglected due their too small values (Al-Khafaji and Taskin Tok, 2020b). Moreover, the ΔG_{MM} term is derived from the MM interaction energies as follows:

$$\Delta G_{MM} = \Delta G_{vdW} + \Delta G_{elec} \quad (2.11)$$

where, ΔG_{vdW} and ΔG_{elec} refer to energy of Van der Waals interaction and energy electrostatic interaction, respectively (Meiselbach et al., 2007; Yang et al., 2011). While the solvation energy can be computed from the below equations:

$$\Delta G_{sol} = \Delta G_{pol} + \Delta G_{nonpol} \quad (2.12)$$

Here, ΔG_{pol} and ΔG_{nonpol} are the polar solvation energy and nonpolar solvation energy. Where ΔG_{nonpol} is measured through linear function of the solvent accessible surface area (SA) (Meiselbach et al., 2007; Yang et al., 2011).

$$\Delta G_{nonpol} = \gamma SA + b \quad (2.13)$$

where γ is 0.00542 kcal.mol^{-1}. Å^{-2} and b = 0.92 kcal. mol

-1

CHAPTER III

MATERIALS AND METHODS

3.1 Preparations of the 3D Structures of Amygdalin and Proteins

3D structure of amygdalin was downloaded from PubChem database (Kim et al., 2015) with ID: 656495. Then we used the module 'prepare ligand' of Discovery Studio 2013 (BIOVIA, 2013) to refine the 3D coordinates of amygdalin. We employed this module to standardize the charges for common groups and optimize of 3D coordinates for each atom of amygdalin molecule. Next, the PDBQT format of amygdalin had been saved through using Autodock Tools (*Autodocktools, the Free Gui for Autodock*).

3D structures of chosen proteins as presented in Table 3.1 were acquired from Protein Data Bank (PDB) (Berman et al., 2002). Water groups were detached from downloaded pdb files, polar hydrogen atoms were added to the protein and finally the charge were adjusted by using Gasteiger charges as required for Lamarckian Genetic Algorithm. Additionally, we corrected the missing residues by exploiting the repair missing atoms in AutoDock Tools and later saved as (PDBQT) format (*Autodocktools, the Free Gui for Autodock*).

Table 3.1 All the of elected proteins with their PDB-IDs

Name of Protein	PDB id	Structural chain	Resolution Å X-RAY
Bcl-2/BAX	2XA0	A/B	2.30
Caspase-3	1RHQ	A/C	2.97
PARP-1	4RV6	A	2.30
CDK1/Cyclin B	4Y72	A/B	2.30
CDK2/Cyclin A	5NEV	A/C	2.97
CDK4/Cyclin D1	2W96	B/A	2.30
AKT1	6CCY	A	2.18
FAK1	4K8A	A	2.97
ILK	3KMW	A	2.00

3.2 Amygdalin-Protein Dockings

Molecular docking tests executed utilizing the docking software Autodock Flexible Residue (ADFR) (Ravindranath et al., 2015) in partnership with the AutoGrid Flexible Residue (AGFR version 1). We employed ADFR computations to figure out flexible side-chains of proteins by setting the corresponding residues in the configuration file.

AGFR 1.0 employed for creating flexible receptor's side chains more flexible, to permit the amygdalin reaches buried grooves (Ravindranath et al., 2015). AutoGrid maps were particularly determined by applying the location of reference ligand inside the binding site selected receptors. Also, the best poses of amygdalin within the active site of each protein were achieved by running of ADFR based on probable specifications (Ravindranath et al., 2015). Secondly, all generated amygdalin-protein complexes were doubly docked utilizing Autodock 4.2 for more-precise estimation of amygdalin pose and also to promote the estimation of binding energies by

adopting Autodock 4.2 program. The scoring function of Autodock 4.2 uses the empirical free energy scoring function (Morris and Huey, 2009) to evaluate the binding energy of protein-ligand. While the poses of amygdalin were achieved based on the sampling (global search) function (built on the Lamarckian Genetic Algorithm) (Pandey et al., 2017). The grid points on the x, y, and z axes to 40 × 40 × 40 with 0.375 Å grid spacing were centered on the position of reference ligands. Docking parameters were set as default where, the number of energy evaluations is 250,000, and the number of generations is 50 (Sathishkumar et al., 2012). The AutoGrid 4.2 program was applied to construct grid maps whilst AutoDock 4.2 program was hired to obtain the docking results. The highest negative values of binding energies of amygdalin were chosen which have also values of RMSD less than 2 A^0. Discovery Studio 2013 (BIOVIA, 2013) was utilized for visualization of the protein-amygdalin conformations.

3.3 MD Simulation

MD simulation is a now considered as decision-making step in the computational investigations of drug discovery (Al-Khafaji and Taskin Tok, 2020d). It exhibits the dynamical changes with the time scale where we can evaluate the target-ligand complex is stable or not (Al-Khafaji and Taskin Tok, 2020a). In the present thesis, we subjected the amygdalin/protein complexes of with the selected proteins (Table 3.1) to 10-ns timescale MD simulations of ligand-free and ligand-bound form. We utilized GROMACS 2018.1 package (Abraham, Murtola, Schulz, Páll, et al., 2015) to run MD simulations. The protein-ligand complexes parametrized by using Charmm 27 force field for all atoms (Bjelkmar et al., 2010). As a part of parametrization, SwissParam was used to produce the amygdalin topologies. The three-point transferable intermolecular potential (TIP3P) was chosen as solvent to solvate the protein/amygdalin complex and inimate it as biological systems as shown in Figure 3.1. And the charge was adjusted by adding Na^+ or $d\ Cl^-$ ions by imitating the environment of physiological systems. These systems were then energy minimized by using the steepest descent algorithm at the tolerance value of 1000 kJ/mol.nm (Appendix E). In the next step, NVT and NPT ensembles counterpoised the complexes with position restraint on the protein molecules for 0.1ns. During equilibrations, systems were coupled with the Parrinello-Rahman barostat (Parrinello

and Rahman, 1981) for controlling pressure at 1 atm and the temperature was controlled by using velocity rescaling thermostat (Bussi et al., 2007) at 300 K. The Particle Mesh Ewald (PME) (Essmann et al., 1995) was appointed for dealing with the long range of Coulomb interactions through a Fourier grid spacing of 0.12 nm. While the short-range van der Waals interactions were calibrated through the Lennard-Jones potential with a cut-off distance of 1 nm. Moreover, the linear constraint solver (LINCS) method (Hess et al., 1997) was adopted to compel all bond lengths. All of the paramters were used, are presented in Appendix E. Now the MD simulations were carried out without any restraint on the ligand or protein molecules to determine the stability for 10 ns. Finally, the MD trajectories were analyzed by using gmx rmsd program to plot the root mean square deviation (RMSD) for each frame against time and gmx rmsf program to measure the root mean square fluctuation (RMSF) of the protein backbone (more details are presented in Appendix D).

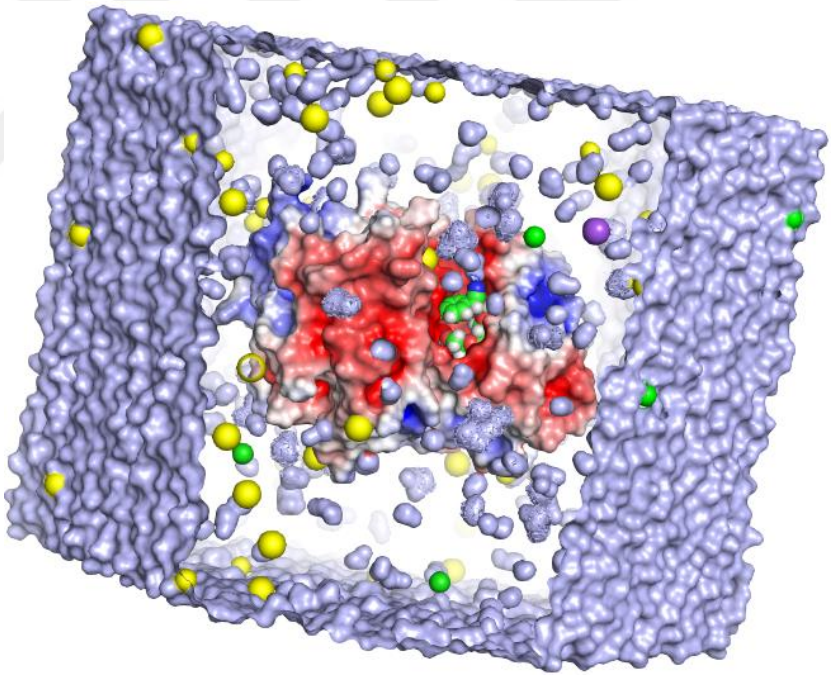

Figure 3.1 The immersed protein/amygdalin complex in imitative-biological PBC box.

3.4 Principal Component Analysis (PCA) and Free Energy Landscape (FEL)

PCA approach (Amadei et al., 1993) of GROMACS 2018.1 package (Abraham, Murtola, Schulz, Pall, et al., 2015) was applied to implement the calculations of the

first two principal components. It is employed to diminish the complexity of the data of functioning dynamics of proteins. In addition, it extracts the dynamic motion in simulations that are presumably meaningfully for biological function (Amadei et al., 1993). The dynamic motions of proteins in the principal subspace were established by projecting the Cartesian trajectory coordinates onward the most effective eigenvectors from the investigation. Trajectories of backbone atoms of the targeted proteins were analyzed by running gmx covar and gmx anaeig of Gromacs programs (Appendix D). Furthermore, the FEL (Al-Khafaji and Taskin Tok, 2020b) graphs were estimated based on the PCA values via utilizing gmx sham script (more information are in Appendix D).

3.5 Estimation of Binding Free Energy Using MM/PBSA

The MM-PBSA binding free energy of ligand/protein interactions for all the complexes was calculated by using the Molecular Mechanics/Poisson-Boltzmann Surface Area (MMP/BSA) tool which is used to analyse the MD trajectories snapshots and this is one of the appropriate methods for this type of studies (Kumari et al., 2014). The g_mmpbsa (Kumari and Lynn, 2011) tool is employed in conjunction with GROMACS and estimates the binding free energy for more details are presented in Appendix F and G . This tool represents the binding energy which is the average three energetic terms, first is the non-polar solvation energy second is the polar-solvation energy and last is the potential energy in the vacuum. Three amygdalin bound targets were selected for binding energy calculation through all 10 ns.

CHAPTER IV

RESULTS AND DISCUSSION

4.1 Amygdalin as Apoptotic Inducer

4.1.1 Double Function of Amygdalin Versus Bcl-2/BAX

4.1.1.1 Molecular Docking

Molecular docking results of top ranked with best pose of amygdalin with the apoptotic targets are presented in Table 4.1. The full information of docking results of all generated poses is in (Appendix A). Closer inspection of the Table 4.1 exhibits that the lowest estimated binding energy was for Bcl-2/BAX/amygdalin of -8.69 kcal/mol. Amygdalin docked in a hydrophobic region in the interface of BAX/Bcl-2 (Figure 4.1). The best pose of amygdalin inside the interface region was elected from the DLG file depending upon two criterions: choosing the lowest binding energy value the lowest RMSD value. Then the generated complex of amygdalin analyzed. The interactions amygdalin-BAX/Bcl-2 is disclosing that the benzene ring of amygdalin was placed to hydrophobic surface through establishing three pi-alkyl bonds with each of Val133 and Arg129 residues of Bcl-2, and Leu59 residue of BAX. Where the two-glucose moieties of amygdalin created three hydrogen-bonding interactions with both of Bcl-2/BAX while the fourth hydrogen bond was between cyano group and Ser60 as shown in Figure 4.1. As a result, the Lys57 and Arg129 of Bcl-2 contributes decisively in the interaction between Bcl-2/BAX and amygdalin in both hydrophobic and hydrophilic interactions. Comparison of the findings with those of other studies confirms this result, where quercetin and taxifolin interacted with BAX/Bcl-2 through Arg129 residue (Verma et al., 2015).

Table 4.1 Docking results synopsis of amygdalin with nominated target for targeting apoptosis (Al-Khafaji and Taskin Tok, 2020c).

Protein Target	Binding Affinities (kcal/mol)	RMSD (A^0)	Ki (inhibition constant, uM)
Bcl-2/BAX	-8.69	2.12	0.424
Caspase-3	-8.98	2.19	0.260
PARP-1	-9.84	2. 76	0.121

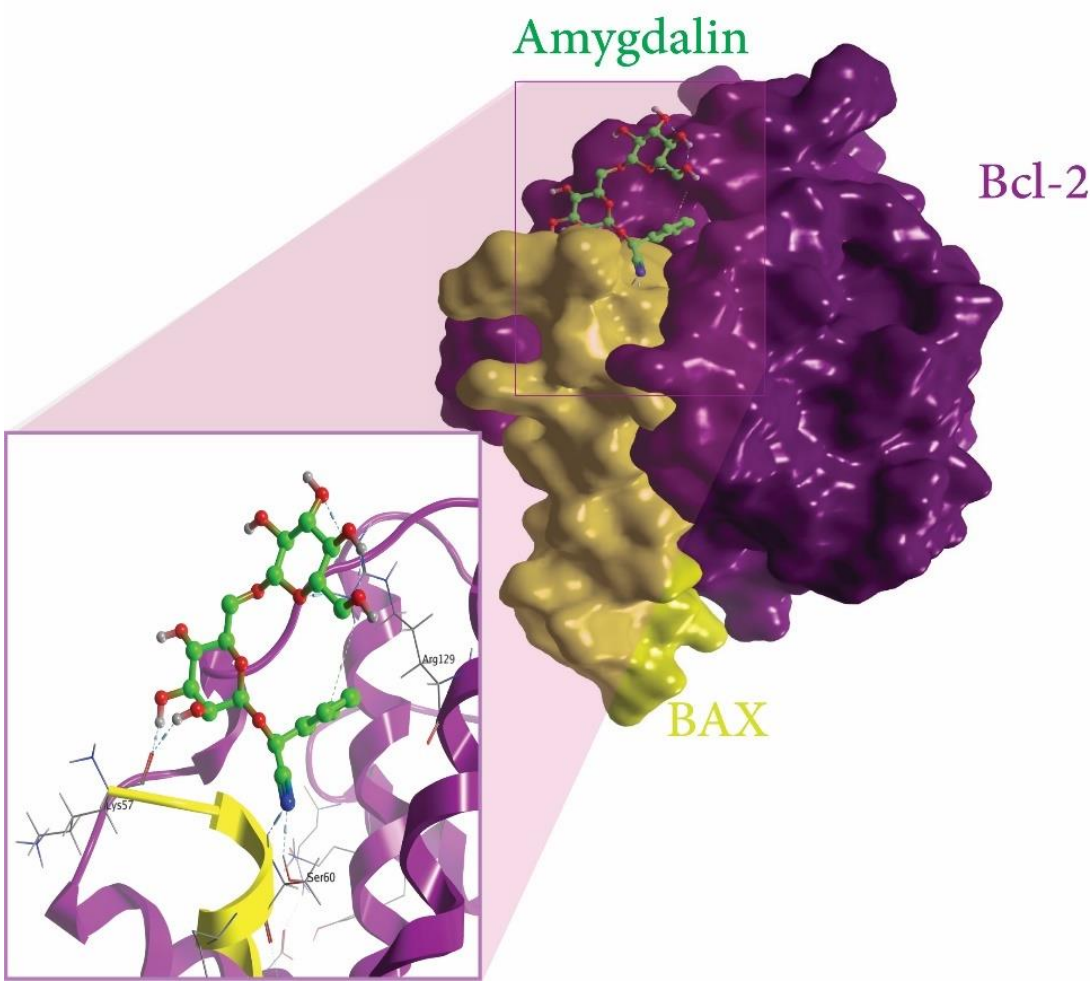

Figure 4.1 The generated conformation of amygdalin with Bcl-2/BAX.

4.1.1.2 MD Simulations

Before we conduct MD simulations to investigate the stabilities of Bcl-2/BAX/amygdalin and the Bcl-2/BAX complexes, we investigated the interface residues that are responsible for stabilizing the Bcl-2/BAX interactions via employing Discovery Studio 2013 (BIOVIA, 2013). This investigation revealed that Arg110, Arg144 and Arg107 of Bcl-2 and Asp68, Glu69 and Asp71 play a crucial role in stabilizing the of Bcl-2/BAX interaction. This study supports evidence from previous observations (Pinto et al., 2004). In the following stage, the BAX/Bcl-2/amygdalin was subjected to MD simulation to investigate the effect of amygdalin on BAX/Bcl-2 stability. Meanwhile, Figure 4.2 exhibits the RMSD values of the backbone atoms of Bcl-2 in amygdalin-bound Bcl-2/BAX was constantly less than 2.6 A^0 up to ~8 ns, thus, as soon as RMSD decreased dramatically, yet RMSD has again risen at twice the RMSD value in the first increase. We noted a moderate initial rise in the RMSD, which is derived from the separation of amygdalin from the complex for a too short duration, later, a continuous rise was marked with up and down for tiny-time intervals. We found this rise in RMSD is to be in proper accord with the snapshots recorded after 9 ns, which declared the departure of BAX peptide from Bcl-2 (Figure 4.2). These results seem to justify the experimental studies that reported the amygdalin inhibits Bcl-2 and promotes the BAX (Chang et al., 2006; Chen et al., 2013; Lee and Moon, 2016).

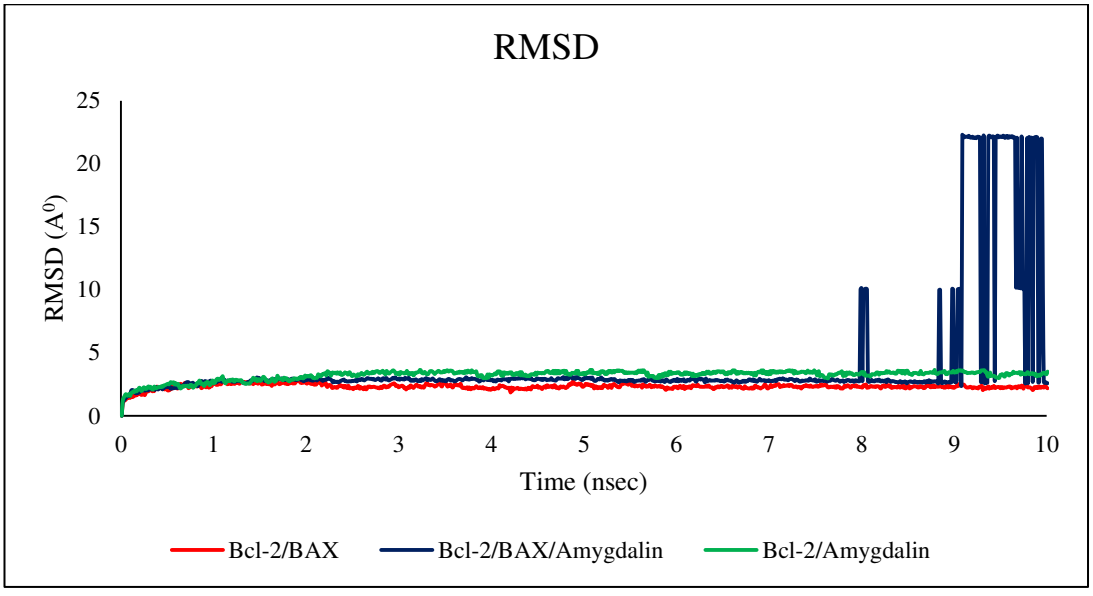

Figure 4.2 The evaluation root means square deviations (RMSDs) of Protein's backbone atoms versus 10 ns of MD simulation.

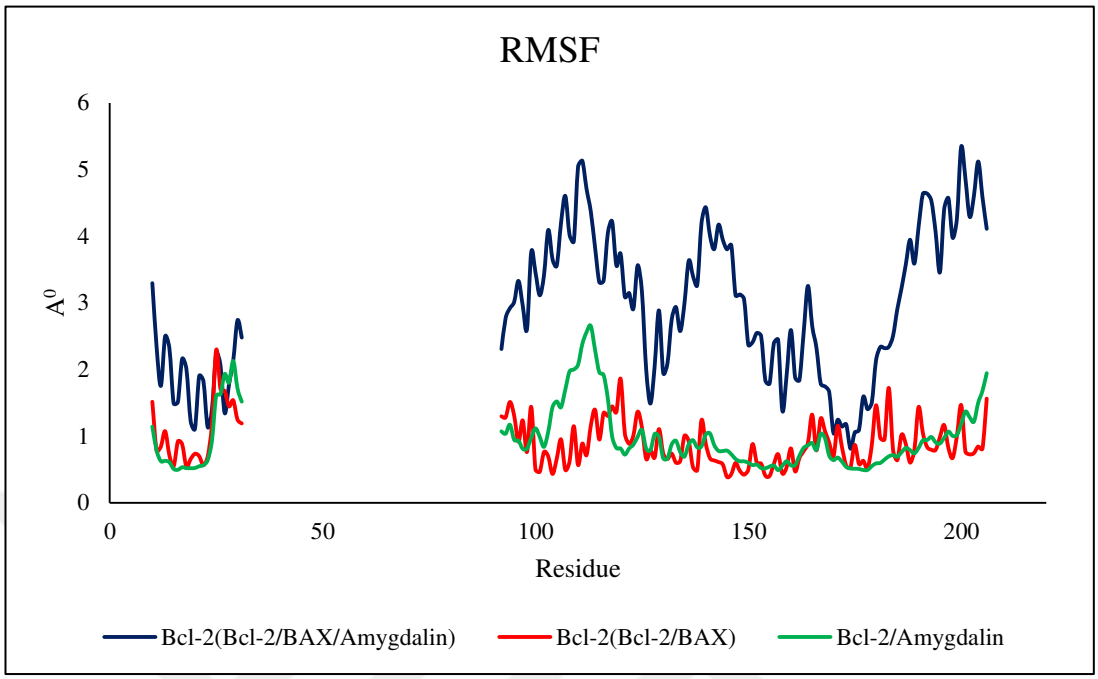

Figure 4.3 Residual fluctuations (RMSF) of protein backbone's atoms during 10 ns MD simulations.

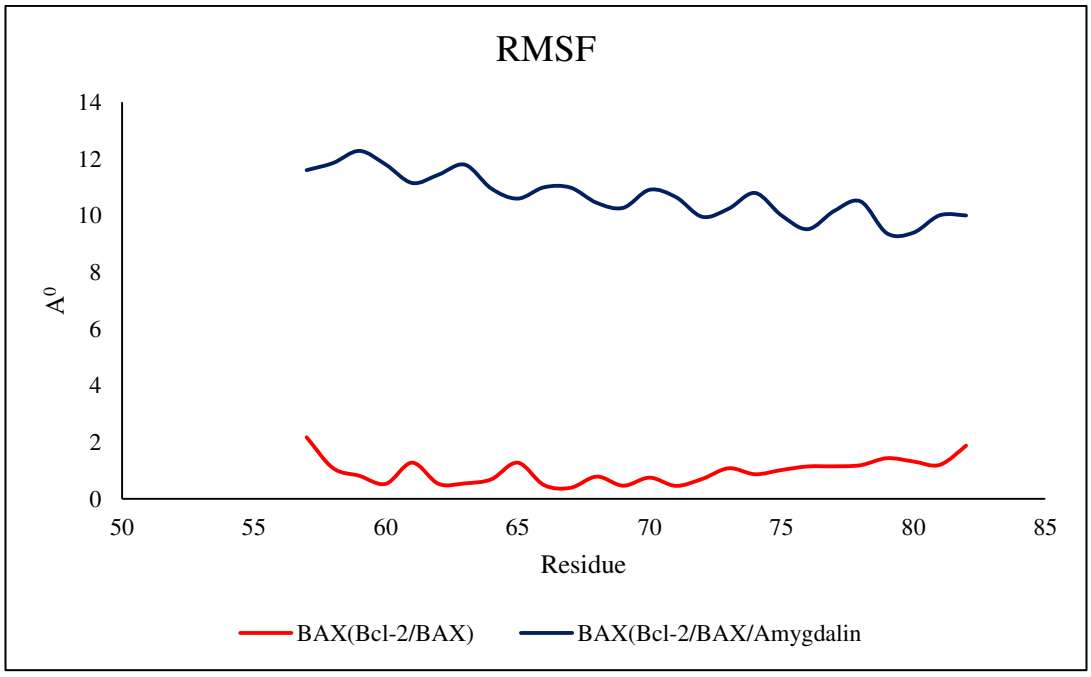

Figure 4.4 Residual fluctuations (RMSF) of BAX backbone's atoms during 10 ns MD simulations.

RMSF of backbone atoms were also used to examine the disruptive effect of amygdalin on the protein/protein system. The RMSF values for Bcl-2 (apo BAX/Bcl-2, amygdalin-bound BAX/Bcl-2, and Bcl-2/ amygdalin) were compared in Figure 4.3, while Figure 4.4 compares between backbone atoms BAX before dealing the protein-protein complex with amygdalin and after. What stands out in Figure 4.3 and Figure 4.4 is the amygdalin destabilized the stable complex (i.e., stable interaction between BAX and Bcl-2), and causes separation between the chain of BAX and Bcl-2 chain. Extra investigation indicated that (Figure 4.3) RMSF values for the backbone atoms of Bcl-2 in complex with BAX is little higher value than those of Bcl-2 with amygdalin but for BAX/Bcl-2 in presence of amygdalin, it high further varied. In Figure 4.4, is in agreement with Figure 4.3, it's clearly Bcl-2/BAX is disrupted when amygdalin interlinked with the complex. These results suggested that amygdalin disrupted the stable interactions of residues at the Bcl-2/BAX interface which remained consistent in ligand-unbound form. This finding broadly supports the work of other studies in the idea of disrupting Bcl-2/BAX by taxifolin and quercitrin during 12 ns MD simulation (Verma et al., 2015). This mechanism is considered an sufficient demonstration of *in vitro* investigation of amygdalin (Chen et al., 2013; Lee and Moon, 2016).

4.1.1.3 PCA and FEL

PCA was utilized to assay the effect of amygdalin on essential dynamics of Bcl-2 and then compare it Bcl-2/BAX complex's behavior. Figure 4.5 compares between the PCA of Bcl-2/BAX and Bcl-2/amygdalin, and also contrasts the differences between the FEL values of Bcl-2/BAX and Bcl-2/BAX. Interestingly, the essential dynamics of Bcl-2 was significantly decreased when it bound to amygdalin (Figure 4.5(A)). The computing of FEL is a computationally useful task; FEL differentiates the kinetic and thermodynamic properties of holo and apo forms of protein. The FEL results were formed merely rely on the possibility of existence of a combination of certain data points which are later translated into a free- energy value by simple contact. Figure 4.5 (B) and (C) present the free energy landscapes projected onto the first two principal components of backbone atoms of Bcl-2 in the both of Bcl-2/BAX and Bcl-2/amygdalin complexes. The shape and size and of the minimum energy

space (in red) in the free energy contour map shows the complex has much more stability. Narrower and more unified blue areas propose that the corresponding complex is higher durable. As presented in Figure 4.5 (B) and (C) the Bcl-2/amygdalin complex is much more reliable than Bcl-2/BAX**.** This means that Bcl-2 prefers to bind to amygdalin and be more thematically stable.

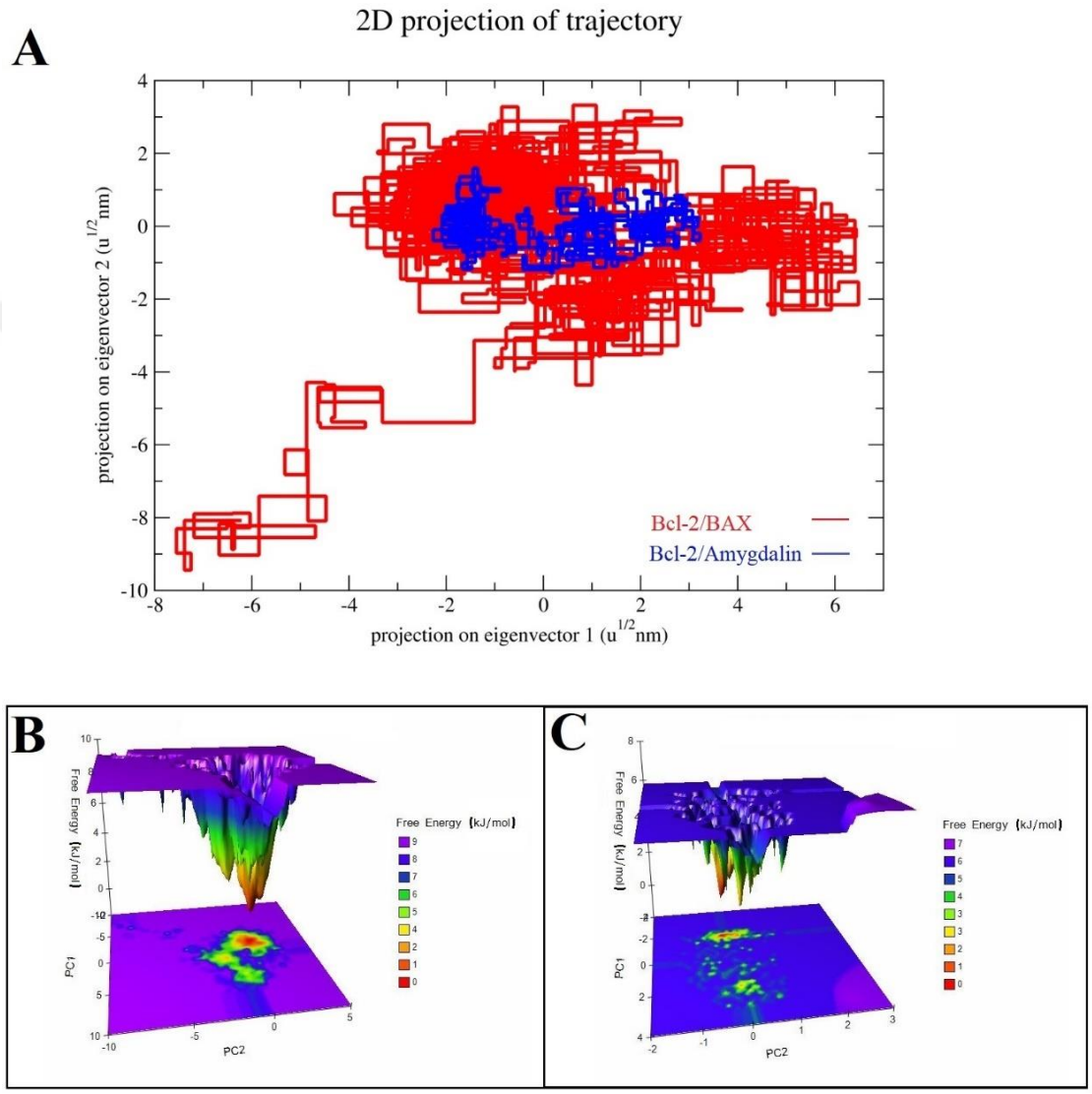

Figure 4.5 (A) PCA of 10 ns MD trajectories of apo and holo form of Bcl-2's backbone residues, (B) FEL of Bcl-2/BAX and (C) FEL interpretations of Bcl-2/Amygdalin.

4.1.1.4 Binding Free Energy Through by Computations

The calculation of binding free energy has a pivotal function in evaluating the binding ability of the ligands towards targets; it quantifies the binding affinity between biomolecules. The g_mmpbsa tool, which runs through GROMACS was employed to estimate the binding free energy of amygdalin toward targeted proteins. The 10 ns MD trajectory of Bcl-2/amygdalin complex were submitted to g_mmpbsa tool to evaluate the binding free energy between amygdalin with Bcl-2. The binding free energy $\Delta G_{binding}$ was -5.386 kcal/mol as shown in Table 4.2. Also, the stability of the Bcl-2/amygdalin interactions were analyzed overall the time of MD simulation (Appendix B). This indicates that Bcl-2/amygdalin complex is binding tightly and stable. This also accords with our earlier observations of double docking.

The most noticeable finding emerge from the MMPBSA energies is that value of $\Delta G_{binding}$ that refers to stable Bcl-2/amygdalin interaction. These results corroborate the findings from RMSD, RMSF, PCA and FEL of a great integration of results in this work. These results emphasize the anti-cancer activities did not come from cyano group.

Table 4. 2 The estimated free binding energies of amygdalin/Bcl-2 complex by using g_mmpbsa tool.

ΔG_{vdW} (kcal/mol)	-20.049
ΔG_{elec} (kcal/mol)	-7.612
ΔG_{pol} (kcal/mol)	24.968
ΔG_{nonpol} (kcal/mol)	-2.692
$\Delta G_{binding}$ (kcal/mol)	-5.386

4.1.2 Mechanism of Caspase-3 Activation by Amygdalin

4.1.2.1 Molecular Docking

The docking results revealed that amygdalin interacted with the active pocket of caspase-3. The docking results shows a higher negative binding energy was for caspase-3/amygdalin of -8.98 kcal/mol. Amygdalin engaged to caspase-3 via hydrogen bonding within the binding site (Figure 4.6). Chen et al. previously observed that amygdalin activates caspase-3 in Breast cancer Cells (Chen et al., 2013). Further investigational tests were done by running MD simulation for caspase-3/amygdalin complex to investigate the conformational influence of amygdalin upon the dynamic behavior of caspase-3. Before we conducted the dynamic simulation. The residues: Tyr153, Phe280, Lys278, Glu289, Ala284, Arg286, Asp291 and Asn151 of chain A and; B, Glu397, ASP326, Asp326, Leu328, Gly336, Gly336, Ser339 and Glu397.

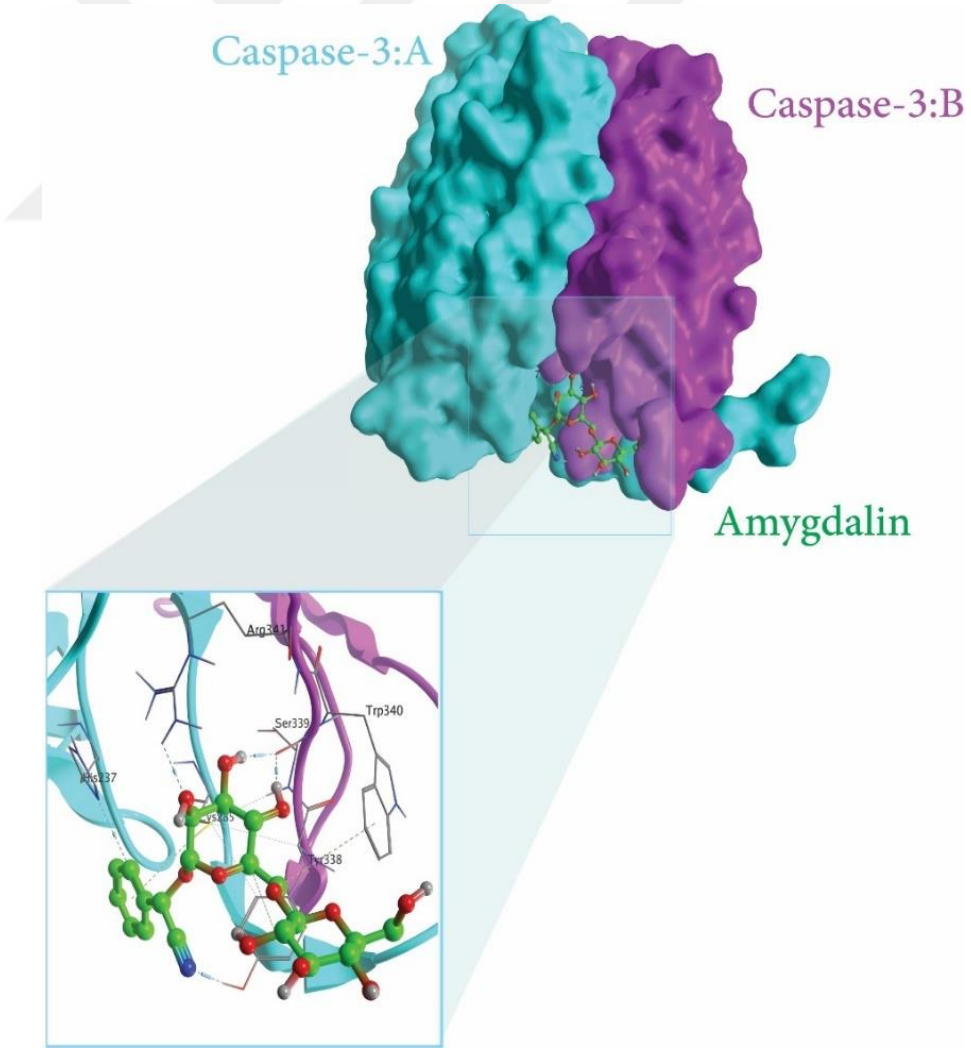

Figure 4.6 The docked pose of amygdalin with caspase-3.

4.1.2.2 MD Simulations

MD simulations were implemented to assess the action of amygdalin toward the caspase-3 during 10 ns MD simulation. Figure 4.7 presents that the RMSD value with snapshots of conformation changes during the MD course of amygdalin/caspase-3. RMSD value for Caspase-3 was less than 2.4 A^0 through 10 ns. While RMSD value for caspase-3/amygdalin it went up and down through 10 ns MD simulation. It obviously was less than 2.6 A^0 up to ~3.3 ns, RMSD increased to ~ 30 A^0, this indicates that the amygdalin destabilized the interaction between chain A and C and led to disrupting the interaction of two chains as explained in snapshots. RMSD decreased dramatically, at 4.7 ns, this indicated that chain And C joined together. From 5.5 ns to ~6 ns the RMSD values fluctuated between increasing and decreasing. After 6 ns the RMSD was ~ 2.5 A^0 till 9 ns and RMSD rocked again out and fell down suddenly and again increased from 9.5 ns to 9.9 ns. This indicated the A and C chains are clustered and leaving up in the presence of amygdalin in the binding pocket of caspase-3. Overall, the behavior of the caspase-3 in presence of amygdalin has two periods of stable complex and two periods of disrupted protein chains.

We used RMSF of backbone values to assess the impact of amygdalin on the dynamic behavior. The RMSF of backbone atoms of caspase-3 showed elevated fluctuation in the amygdalin-bound caspase-3 as compared to amygdalin-unbound caspase-3 during 10 MD simulation. This stipulates that the amygdalin's interaction pulls apart the stable interaction between two chains and this derives to high flexibility when caspase-3 bound to amygdalin as presented in Figure 4.8. These proposed that amygdalin has the ability to disrupt the stable interactions between the interacted chain A and B. Here the dynamic simulation success to exhibit what is the process of caspase-3 activation. Moreover, Walter et., al stated that "The direct activation of caspase-3 through a conformational switch rather than by chain cleavage" (Walters et al., 2009), and this agrees completely with our MD results of caspase-3 with amygdalin. This result is regarded as a comprehensive explanation about the mechanism of amygdalin of how can amygdalin activates the caspase-3 (Chen et al., 2013; Lee and Moon, 2016).

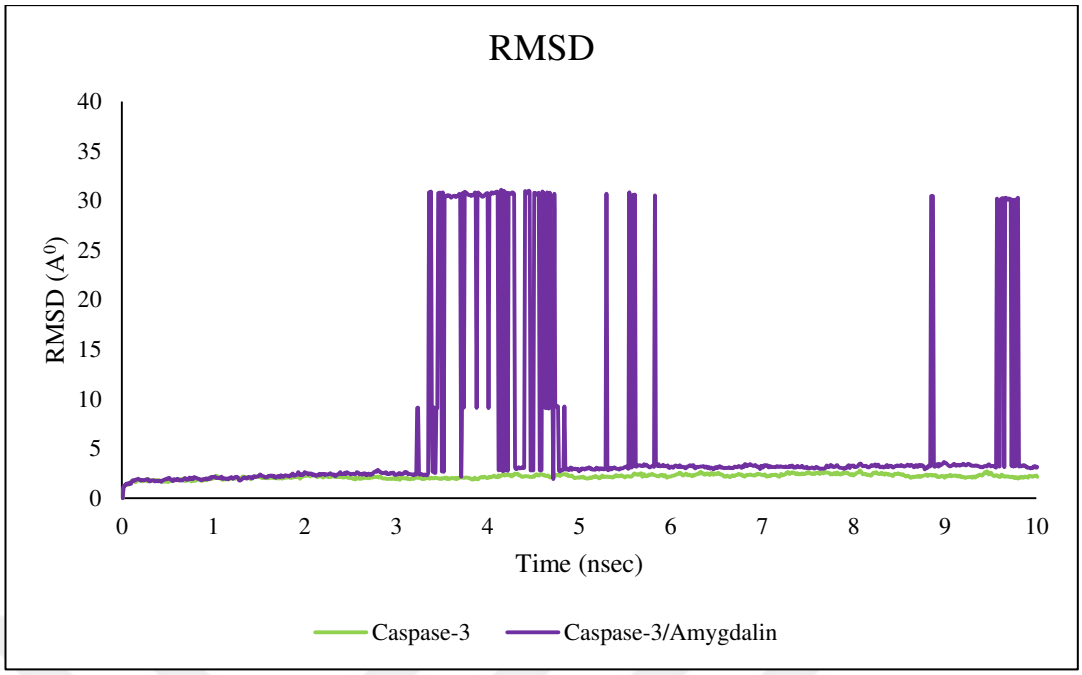

Figure 4.7 The evaluation root means square deviations (RMSDs) of caspase-3's backbone atoms versus 10 ns of MD simulation.

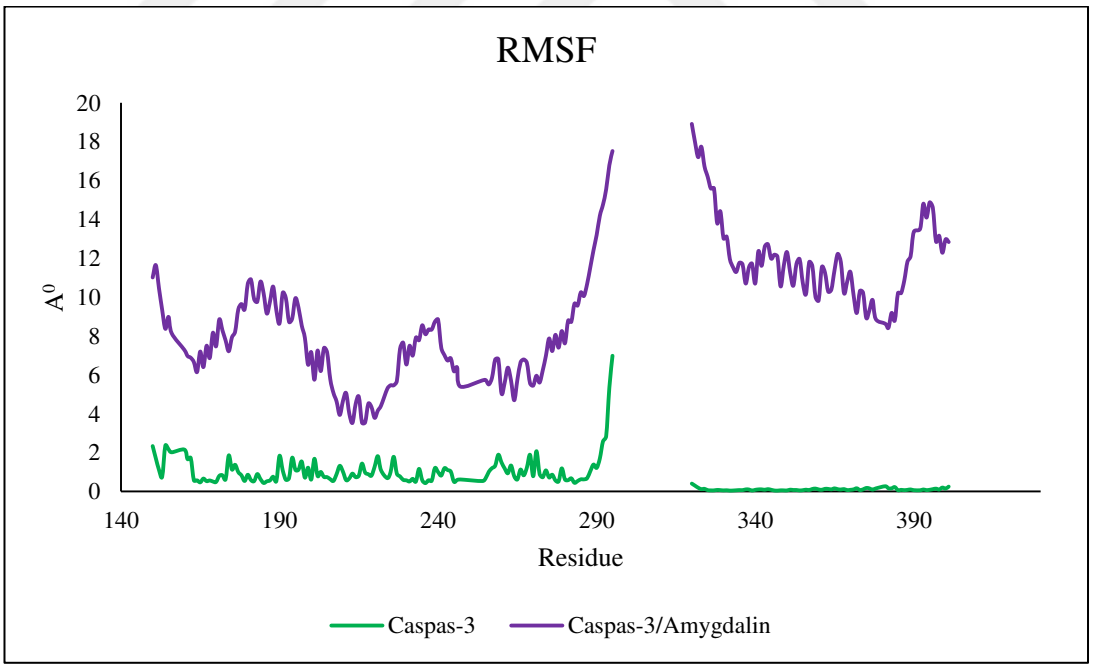

Figure 4.8 Residual fluctuations (RMSF) of caspase-3 backbone's atoms during 10 ns MD simulations.

4.1.3 Inhibition Mechanism of PARP-1 by Amygdalin

4.1.3.1 Molecular Docking

The binding energy of amygdalin inside the active site of PARP-1 is -9.84 kcal/mol. It was again noticed that amygdalin successfully docked and amygdalin fits completely inside the binding site (Feinstein and Brylinski, 2015; Ferreira et al., 2015). Figure 4.9 displays that amygdalin and PARP-1 interlinked with each other, and amygdalin created three hydrogen bonds with the binding site's residues: Gly862, Met898 and Tyr907. It affirms the good inhibitory property of amygdalin against PARP-1. To examine the effect of amygdalin on the conformation behavior of PARP-1 we conducted 10 ns MD simulation to examine the PARP-1/amygdalin complex stability.

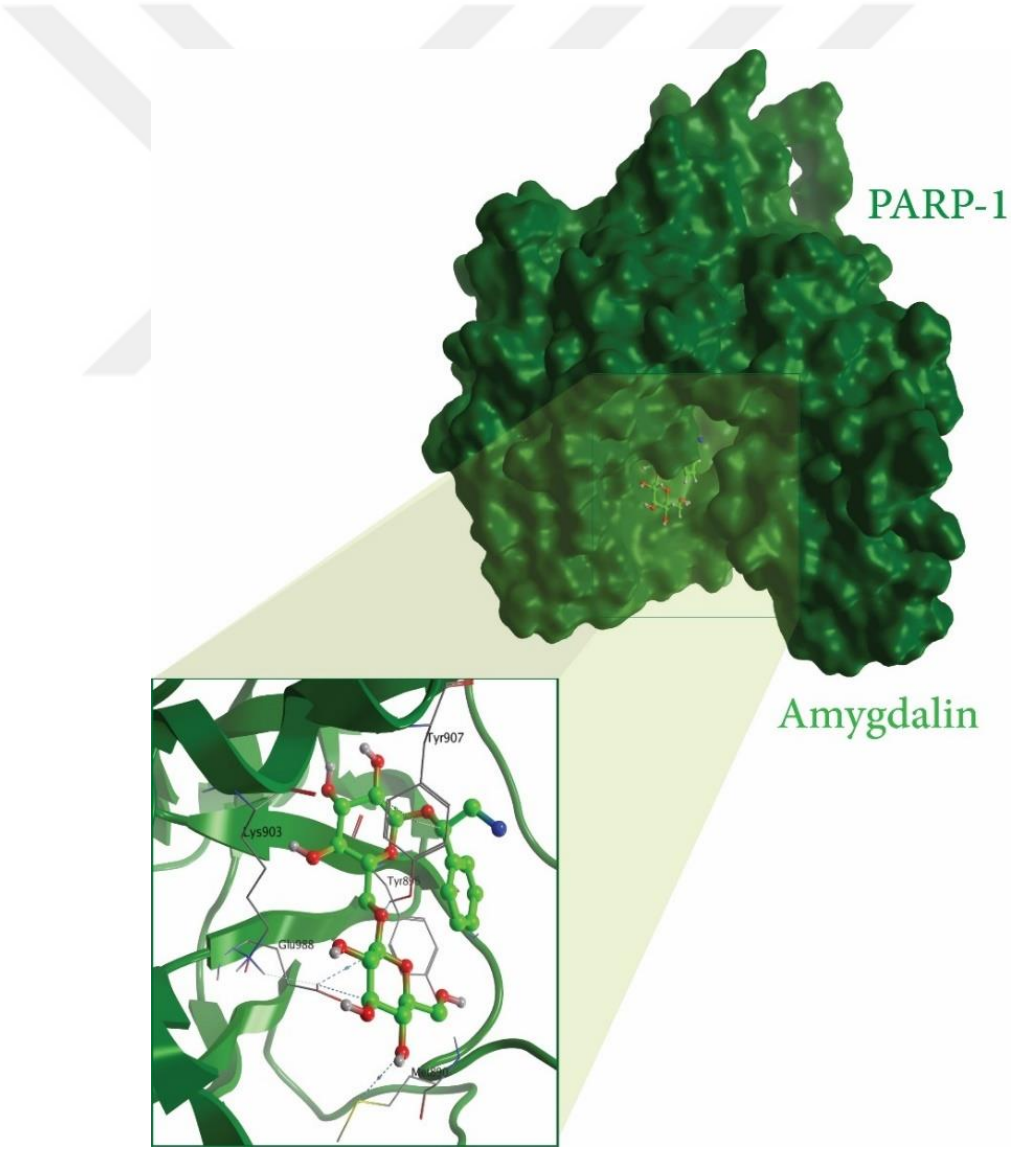

Figure 4.9 The docked pose of amygdalin with PARP-1.

4.1.3.2 MD Simulations

MD simulations were implemented for amygdalin-unbound PARP-1 and amygdalin-bound PARP-1 for 10 ns MD simulation. First, we assessed the dynamical stability, by analyzing molecular dynamics trajectories for PARP-1/amygdalin complex and ligand-unbound PARP-1 including RMSD and RMSF. First, we evaluated the structural stability of the PARP-1-amygdalin complex using the RMSD of the backbone of PARP-1 inbound with amygdalin status relative to the initial structure. The RMSD of the PARP-1 was nearly less than 2 A^0 during 10 ns whereas RMSD of PARP-1/amygdalin slowly increased to exceed the barrier 2 A^0 at 4.5 ns and gradually diminished as the time progresses to reach RMSD values of unbound-ligand PARP-1 at 7.4 ns (Figure 4.10). The overall agreement between the bound-amygdalin PARP-1 and unbound-amygdalin PARP-1 simulations and the behaviors are also quite similar indicating that the models considered here are stable.

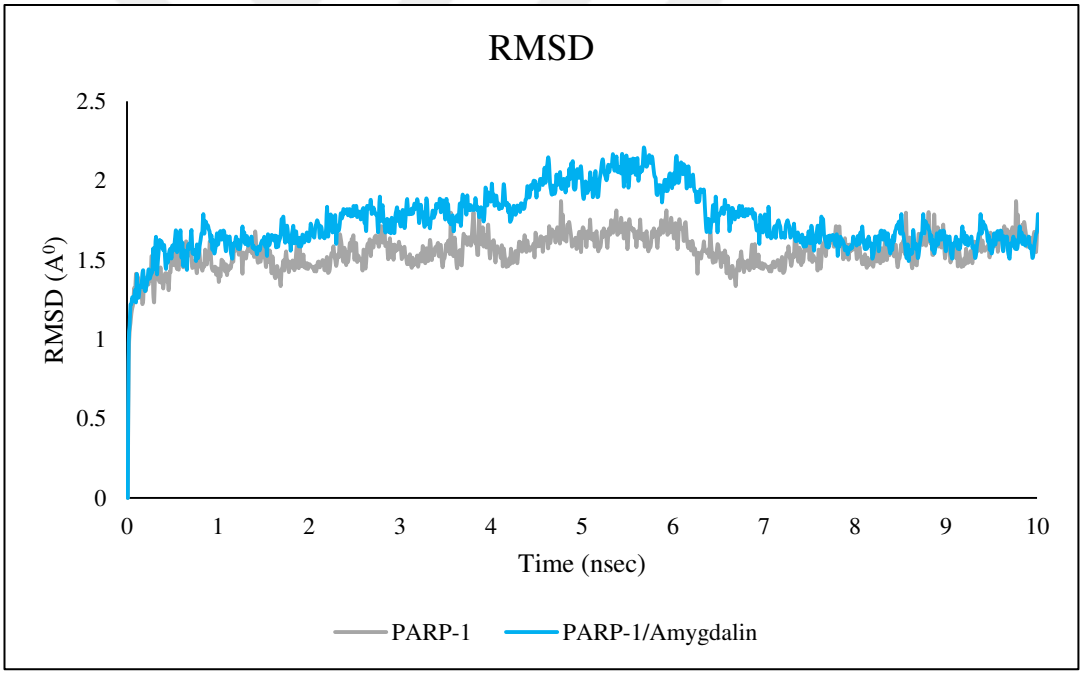

Figure 4.10 The evaluation root means square deviations (RMSDs) of Protein's backbone atoms versus 10 ns of MD simulation.

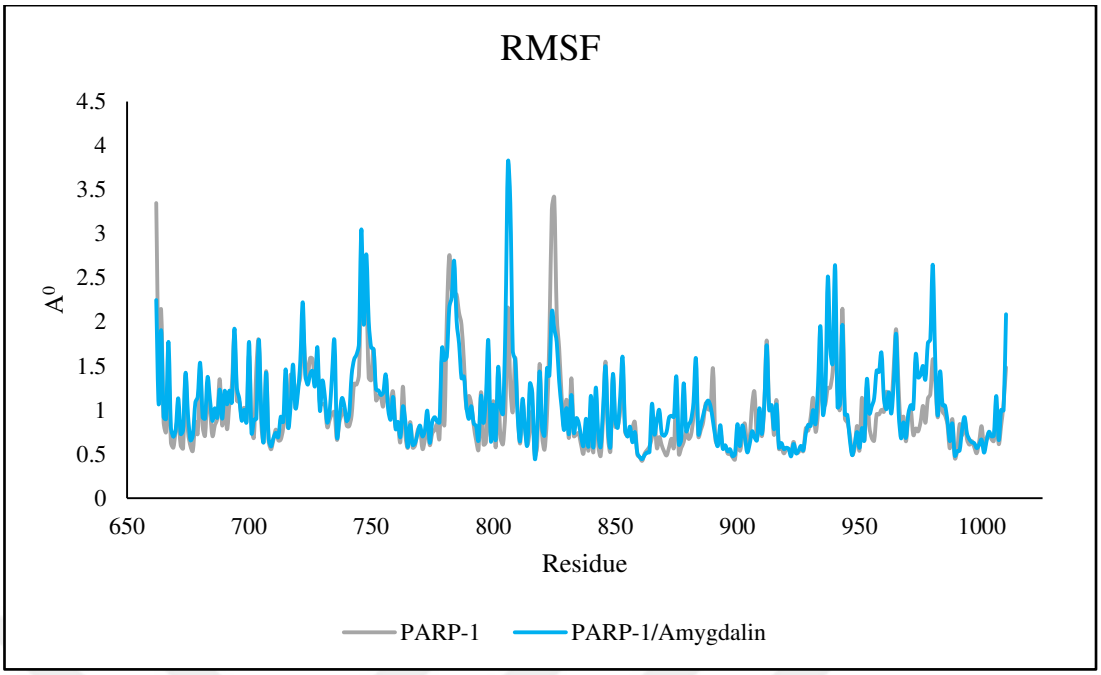

Figure 4.11 Residual fluctuations (RMSF) of protein backbone's atoms during 10 ns MD simulations.

We also evaluated RMSF values to describe the regions of significant variations. We outlined the results in Figure 4.11. We noticed a comparable RMSF distribution for the amygdalin-unbound PARP-1 and amygdalin-bound PARP-1. We analyzed RMSF of the amino acid residues of binding site to investigate how many variations occur during the simulation course and we found that the main amino acids in the active site were less fluctuated. This shows amygdalin was extremely stable inside of the binding pocket of PARP-1. There may be a fortuitous merit in the Figure 4.11; the RMSF quite varies in the three-loop regions (residues 934–940, 957–960, and 973–980) of PARP-1. These changes may induce variations in the binding capacities of the ligands. However, the RMSF evaluation revealed the complexes showed similar dynamics through the 10 ns MD simulations. This points out that amygdalin possesses a steady inhibitory effect inside the active site of PARP-1, and in silico research thoroughly complied with experimental research by Chen's group (Lee and Moon, 2016).

4.1.3.3 PCA and FEL

Figure 4.12 (A) shows the differences in the essential dynamics of apo and amygdalin-bound PARP-1. The most surprising aspect of the data is in the Figure

4.12 (A) that amygdalin constringed the dynamics of PARP-1. It can be concluded that amygdalin blocks the PARP-1. Further, the FEL contour maps Figure 4.12 (B) and (C) is illustrating the effect of amygdalin on the thermal stability of PARP-1. As indicated in Figure 4.12 (B) and (C) the PARP-1/amygdalin complex has higher stability than apo PARP-1. This indicates that PARP-1 is less dynamically and more thermally stable that apo form of PARP-1.

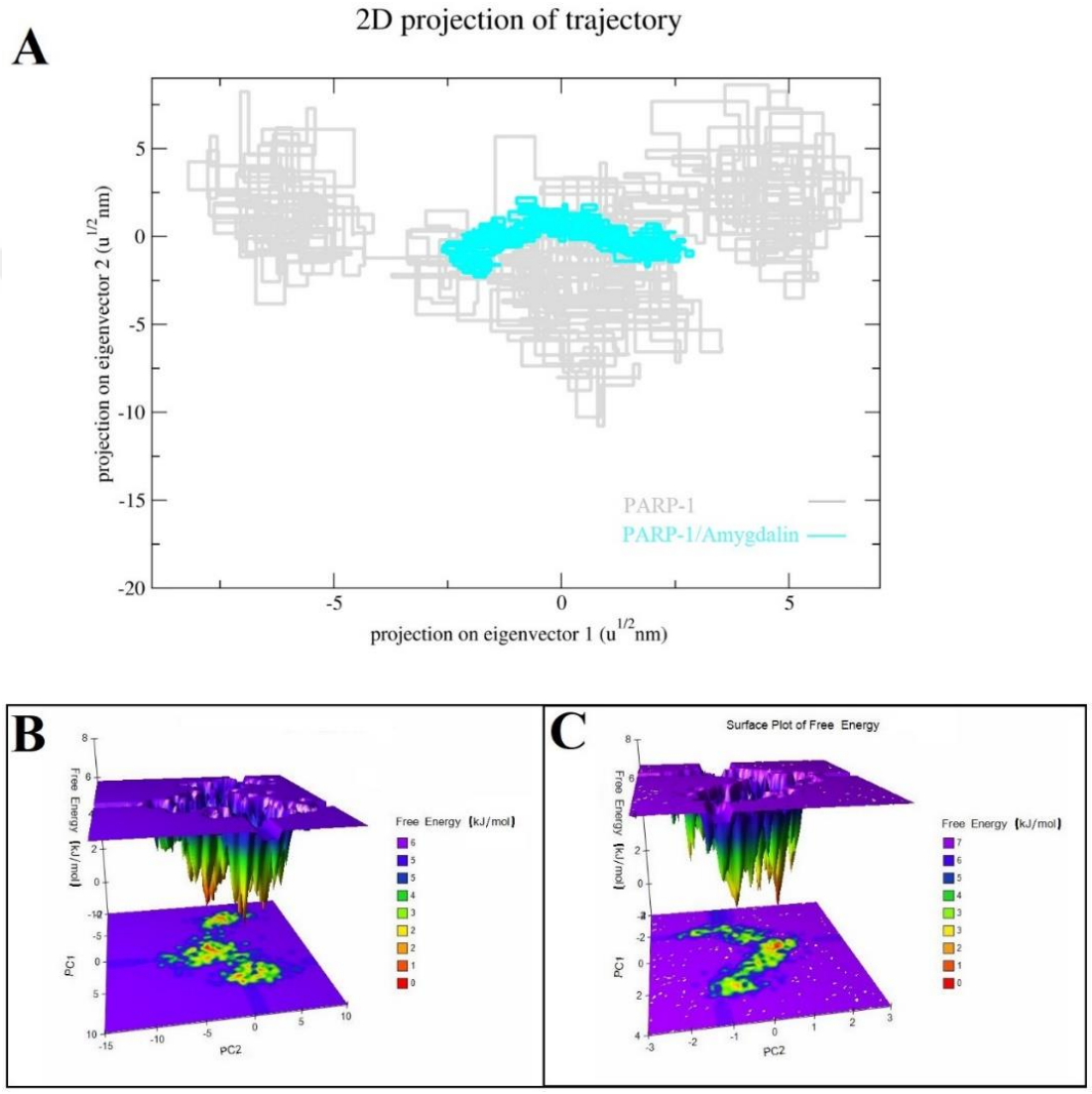

Figure 4.12 (A) PCA of 10 ns MD trajectories of apo and holo forms of PARP-1's backbone residues, (B) FEL of PARP-1 and (C) FEL of PARP 1/Amygdalin.

4.1.3.4 Binding Free Energy by MM/PBSA Computations

The binding energy of PARP-1/amygdalin presented in Table 4.3. The binding free energy $\Delta G_{binding}$ was 0.569 kcal/mol as shown in Table 4.3. And the MM/PBSA analysis was illustrated alongside the 10-ns MD simulation in Appendix B. This indicates that amygdalin is not well bound inside the PARP-1's binding site. But van der Waals energy was good. However, polar solvation energy was responsible for making the binding free energy was not good.

Table 4.3 The estimated free binding energies of amygdalin/PARP-1 complex by using g_mmpbsa tool.

ΔG_{vdW} (kcal/mol)	-40.763
ΔG_{elec} (kcal/mol)	-16.417
ΔG_{pol} (kcal/mol)	60.544
ΔG_{nonpol} (kcal/mol)	-4.793
$\Delta G_{binding}$ (kcal/mol)	0.569

4.2 Amygdalin as Cell Division Inhibitor

4.2.1 Inhibition of CDK1/Cyclin B by Amygdalin

4.2.1.1 Molecular docking

The molecular docking results of amygdalin inside the ATP sites of CDKs/Cyclins are given in Table 4.4 (for more information Appendix A). It is evident from this table that the measured binding energies are very similar and highly negative value between amygdalin and CDKs/Cyclins. The conformation of amygdalin is generated by adopting double docking which sticks in the ATP pocket of CDK1/Cyclin B of -9.24 kcal/mol and presented in Figure 4.13 and Table 4.4. The Interaction between amygdalin and CDK1/Cyclin B reveals that all of amygdalin fitted well to ATP-binding pocket. Amygdalin interacted with CDk1/Cyclin B through establishing three pi-alkyl interactions between the benzene ring with Val18, Leu135, and Ala145 of CDK1's chain. While the two glucose groups of amygdalin constructed a four

hydrogen bonds with Lys33, Glu51, Leu83 and Asp146 of chain CDK1. To further investigation both of the effects of amygdalin upon CDk1/Cyclin B/amygdalin complex stability in the 10 ns MD simulation and correlate it with the MD simulations of amygdalin-unbound CDK1/Cyclin B, GROMACS has been employed.

Table 4.4 Docking results synopsis of amygdalin with nominated target for targeting apoptosis (Al-Khafaji and Taskin Tok, 2020a).

Protein Target	**Binding Affinities (kcal/mol)**	**RMSD (A^0)**	**Ki (inhibition constant, uM)**
CDK1/Cyclin B	-9.24	0.778	0.168 uM
CDK2/Cyclin A	-9.02	2.19	0.014 uM
CDK4/Cyclin D1	-10.6	2. 76	0.453 uM

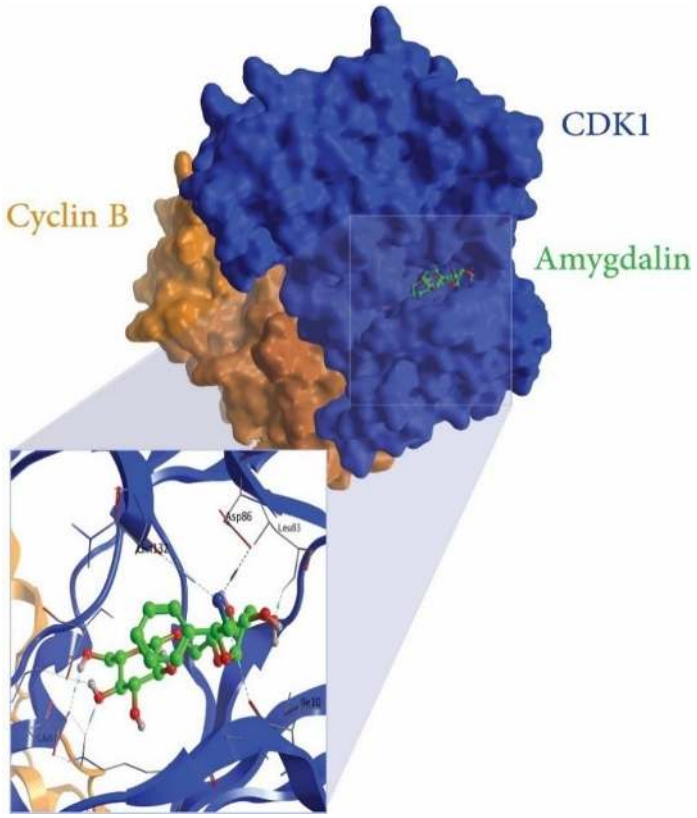

Figure 4.13 The docked pose of amygdalin with CDK1/Cyclin B.

4.2.1.2 MD Simulations

The complex of CDK1/Cyclin B and amygdalin was admitted to MD simulation to assess the effect of amygdalin upon conformational differences of CDK1/Cyclin B. The RMSD and RMSF were adopted for this purpose. Figure 4.14 reveals that the RMSD of backbone atoms of CDK1/Cyclin B of amygdalin-bound CDK1/Cyclin B and amygdalin-bound CDK1/Cyclin B profiles exhibited identical shape of fluctuation during all 10 ns, were consistently fewer than 2.5 A^0 for the full simulation which offered the stability of CDK1/Cyclin B/amygdalin complex. The downhill was initially rising in the RMSD for the first, ~0.65 ns and later a stable profile was noted for the amygdalin-unbound CDK1/Cyclin B and amygdalin-bound CDK1/Cyclin B, exhibited the similar average RMSD values.

To identify the impact of amygdalin upon the flexibility of backbone atoms of CDK1/Cyclin B before and after binding with amygdalin, RMSF of backbone residues position was measured. Amygdalin-bound CDK1/Cyclin B form showed obviously the same variations as correlated to amygdalin-unbound form (Figure 4.15). This means that the CDK1/Cyclin B/amygdalin complex is reliable as in unbound ligand CDK1/Cyclin B. Further, these observations of amygdalin are in agreement with experimental results which exhibited that amygdalin suppresses the cell division of cancer cells through blocking the CDK1/Cyclin B (Juengel et al., 2016; Makarević, Rutz, Juengel, Kaulfuss, Reiter, et al., 2014).

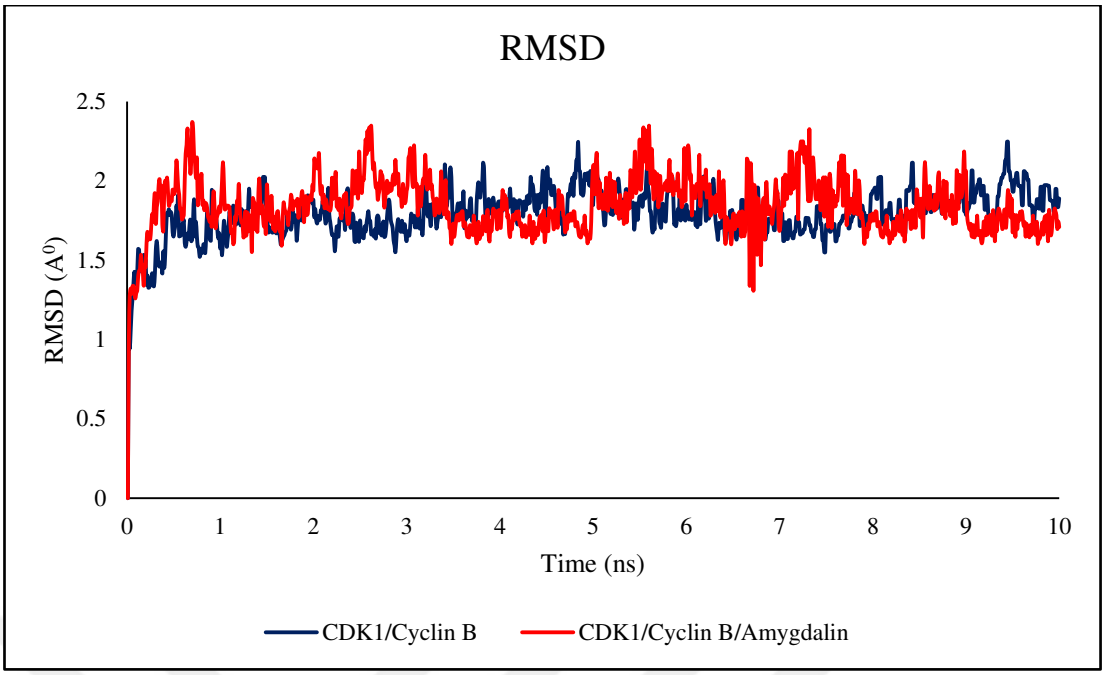

Figure 4.14 The evaluation root means square deviations (RMSDs) of Protein's backbone atoms versus 10 ns of MD simulation.

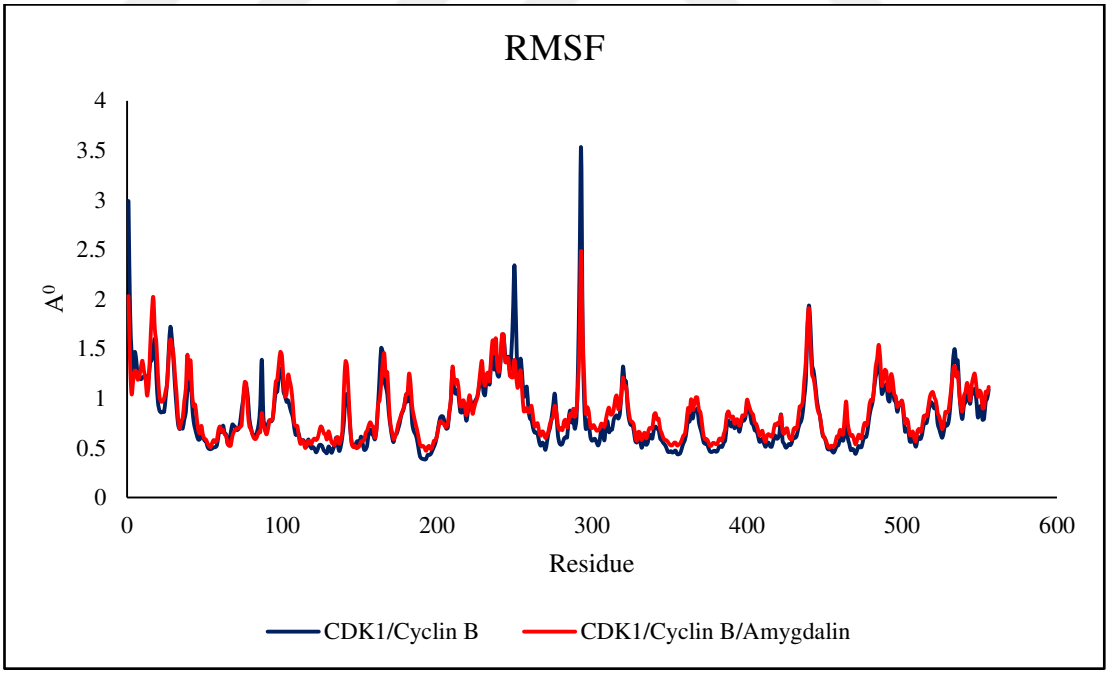

Figure 4.15 Residual fluctuations (RMSF) of protein backbone's atoms during 10 ns MD simulations.

4.2.1.3 PCA and FEL

Figure 4.16 (A) illustrates the distinctions in the essential dynamics of apo and amygdalin-bound CDK1/Cyclin B. It can be seen from Figure 4.16 (A) that amygdalin makes the essential dynamics alittle lesser than the essential dynamics of apo CDK1/Cyclin B. Therefore, looking at the FEL contour maps can give deep comprehension to evaluate the effect of amygdalin CDK1/Cyclin B. Figure 4.16 (B) and (C) present the effect of amygdalin on the thermal stability of CDK1/Cyclin B. As indicated in Figure 4.16 (B) and (C) the CDK1/Cyclin B/amygdalin complex much more stable than CDK1/Cyclin B. This indicates that CDK1/Cyclin B has more thermally stability than apo form of CDK1/Cyclin B.

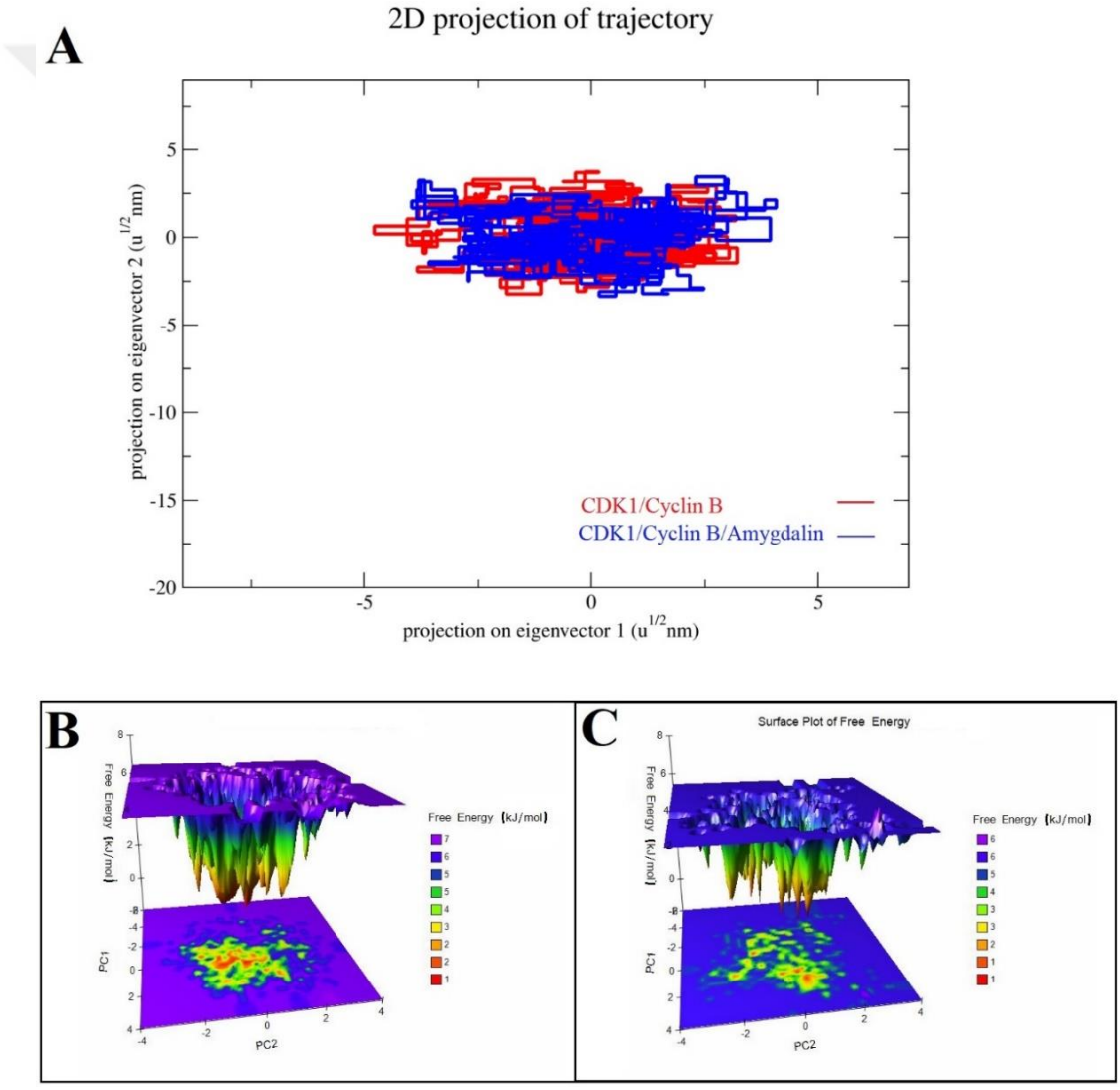

Figure 4. 16 (A) PCA of 10 ns MD trajectories of apo and holo forms of CDK1/Cyclin B's backbone residues, (B) FEL of CDK1/Cyclin B and (C) FEL of CDK1/Cyclin B/Amygdalin.

4.2.1.4 Binding Free Energy by MM/PBSA Computations

Table 4.5 provides the summary of the energies and total binding free energy of CDK1/Cyclin B/amygdalin. The binding free energy $\Delta G_{binding}$ was -2.260 kcal/mol which is considered as good to show high affinity of amygdalin toward CDK1/Cyclin B. Furthermore, the fashion of $\Delta G_{binding}$ overall time of MD simulation reveals that amygdalin is stable within the binding site of CDK1/Cyclin B (Appendix B).

Table 4. 5 The estimated free binding energies of amygdalin/CDK1/Cyclin B complex by using g_mmpbsa tool.

ΔG_{vdW} (kcal/mol)	-15.111
ΔG_{elec} (kcal/mol)	-5.863
ΔG_{pol} (kcal/mol)	20.786
ΔG_{nonpol} (kcal/mol)	-2.072
$\Delta G_{binding}$ (kcal/mol)	-2.260

4.2.2 Inhibition of CDK2/Cyclin A by Amygdalin

4.2.2.1 Molecular Docking

To assess possible pose of amygdalin that can inhibit of the CDK2/Cyclin A complex, Double docking generated the inhibitive conformation of amygdalin in the ATP-active pocket. Docking results disclosed that amygdalin interacted with CDK2/Cyclin A inside the pocket with the binding energy of -9.02 kcal/mol (Table 4.4). Amygdalin formed three traditional H-bond with the residues: Glu81, Leu83, and Gln131 of CDK2 chain (Figure 4.17). The lowest binding energy conformation recovered from DLG file, and used as initiating complex for MD simulation, in order to probe the stability of CDK2/Cyclin A/amygdalin complex, and correlate it with the MD simulation of amygdalin-unbound CDK2/Cyclin A and free-amygdalin CDK2/Cyclin A.

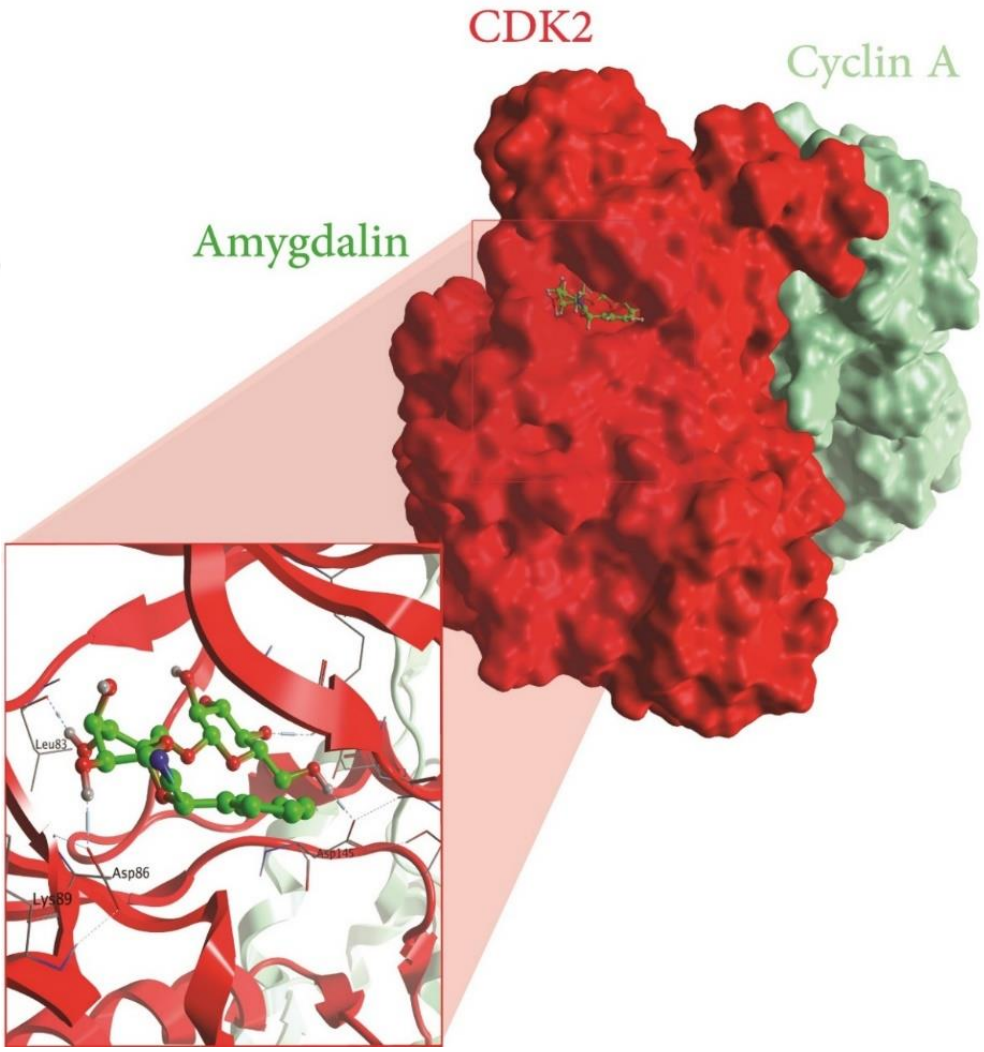

Figure 4.17 The docked pose of amygdalin with CDK2/Cyclin A.

4.2.2.2 MD Simulations

The CDK2/Cyclin A/amygdalin complex with the binding energy of -9.02 kcal/mol has been taken as an introductory complex for conducting MD simulation. The conformational influence of amygdalin on CDK2/Cyclin have evaluated based on the RMSD and RMSF. To explore the stability of amygdalin within the active site of CDK2/Cyclin A, the RMSD values of backbone residues were calculated as a function of time. RMSD profiles were regularly fewer than 2.9 A^0 for the entire simulation which represented the stability of CDK2/Cyclin A/amygdalin system as displayed in Figure 4.18. In contrast to steep of RMSD value for the amygdalin-bound CDK2/Cyclin A, RMSD steep was much more shaper. This indicates CDK2/Cyclin A/amygdalin complex needs 1.5 ns from MD simulation's beginning to reach a stability state. After 2.5 ns amygdalin-bound and amygdalin-unbound CDK2/Cyclin A appeared relatively the same average RMSD values. The declared results of trajectories of the MD simulations highlight the CDK2/Cyclin A-amygdalin complex after arriving was respectable for post evaluations.

Moreover, it is noteworthy to analyze the flexible parts of the CDK2/Cyclin A by depending on RMSF of backbone residues. CDK2/Cyclin A in amygdalin-bound state showed strikingly the same variations as related to unbound form (Figure 4.19). This implies that the CDK2/Cyclin B/amygdalin complex is reliable as in unbound-amygdalin CDK2/Cyclin B.

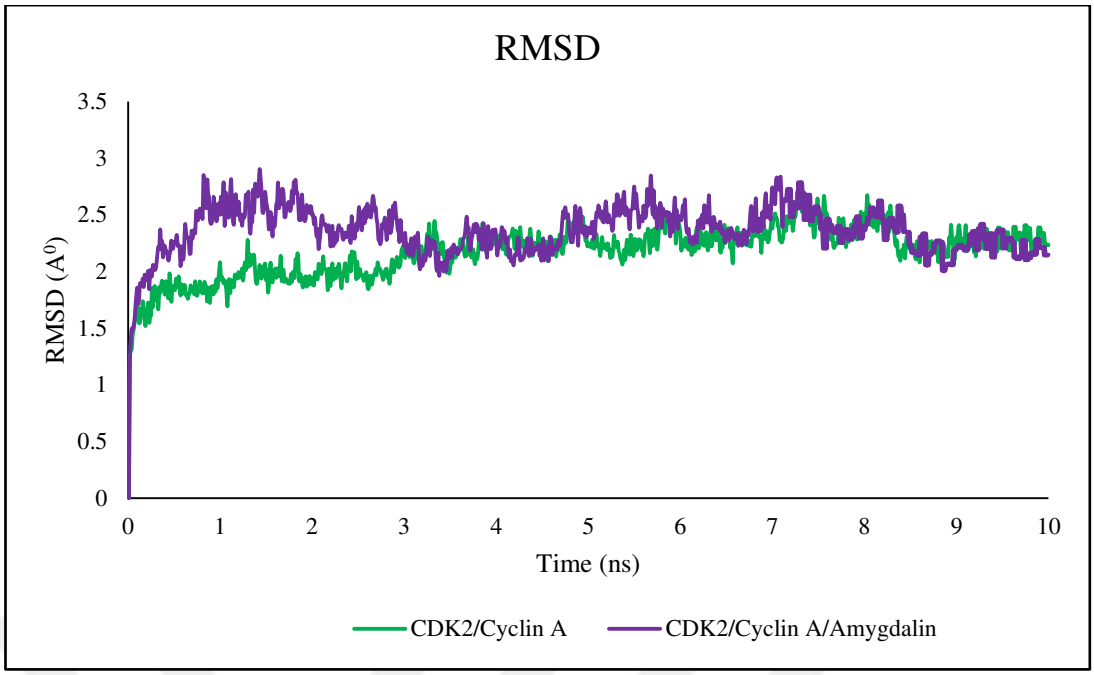

Figure 4.18 The evaluation root means square deviations (RMSDs) of Protein's backbone atoms versus 10 ns of MD simulation.

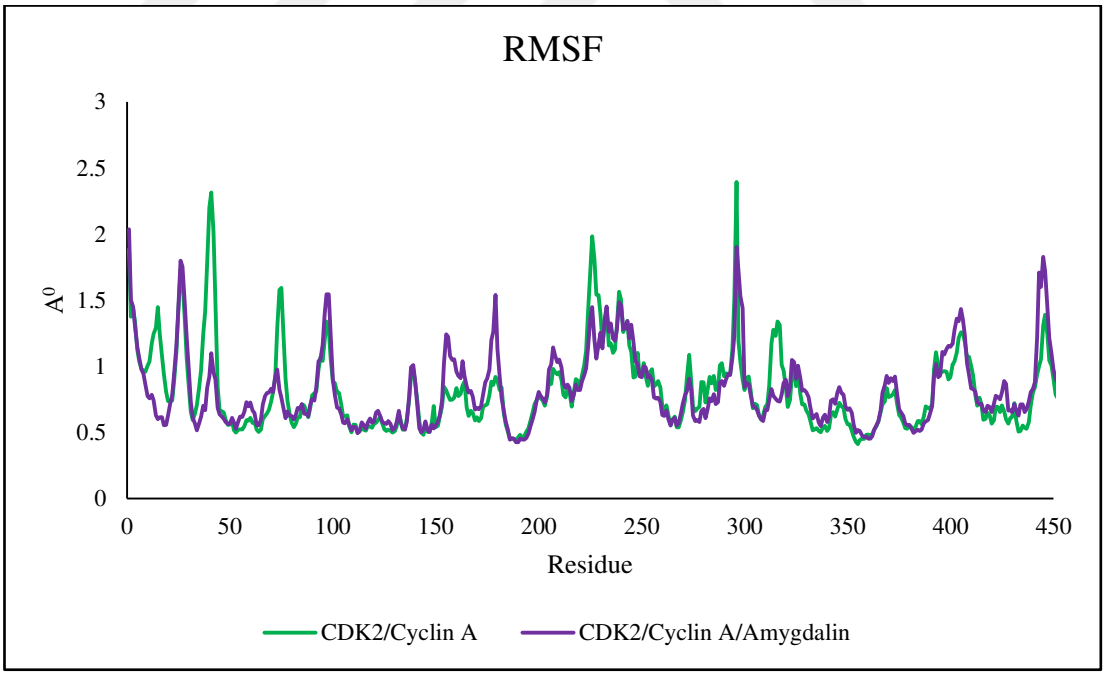

Figure 4.19 Residual fluctuations (RMSF) of protein backbone's atoms during 10 ns MD simulations.

4.2.2.3 PCA and FEL

Figure 4.20 (A) presents the essential dynamics of both apo and amygdalin-bound CDK2/Cyclin A. It can be seen from Figure 4.20 (A) that the essential dynamics for both of CDK2/Cyclin A and CDK2/Cyclin A/amygdalin are approximately same. Therefore, looking at the FEL contour maps (Figure 4.20 (B) and (C)) shows a little enhancement in the thermal profile when CDK2/Cyclin A bound to amygdalin. It can be concluded from Figure 4.20 (B) and (C) that the CDK1/Cyclin B/amygdalin complex a little bit more stable than CDK1/Cyclin B.

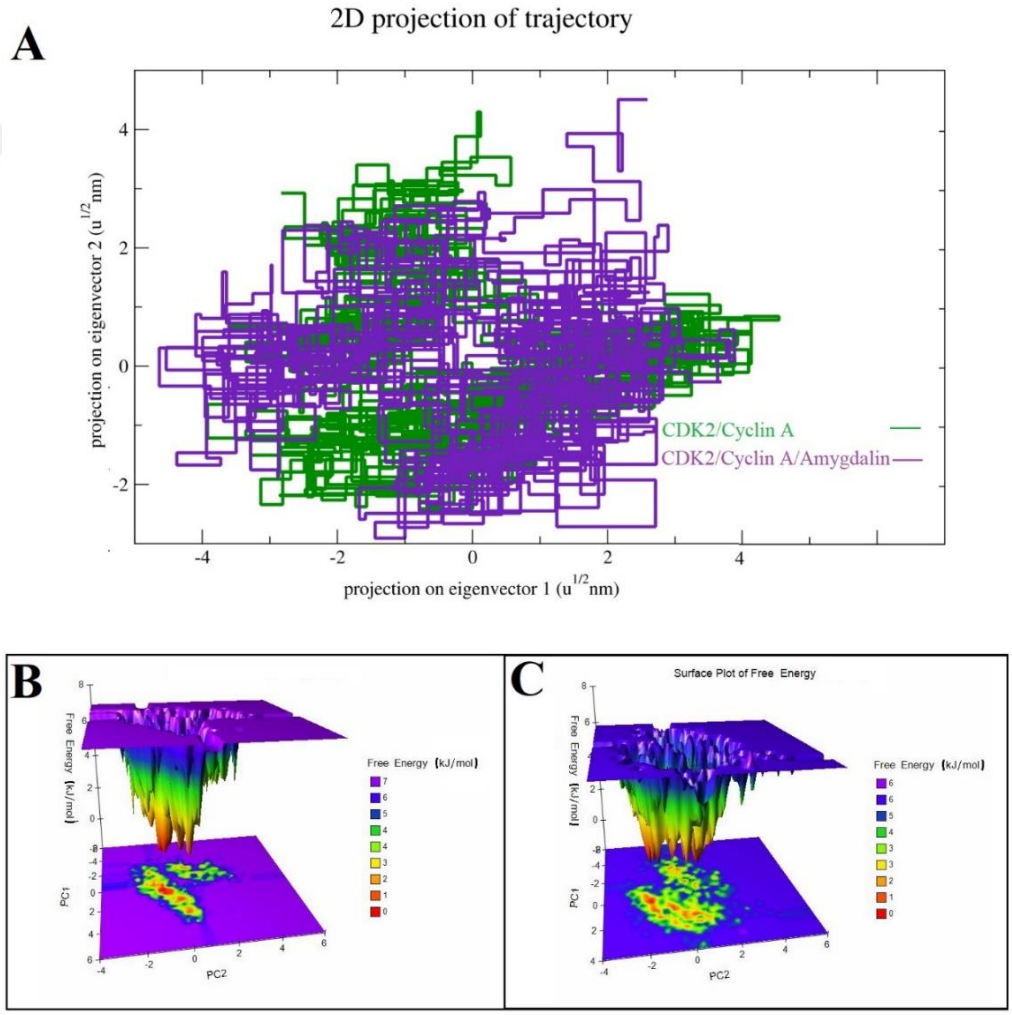

Figure 4.20 (A) PCA of 10 ns MD trajectories of apo and holo forms of CDK2/Cyclin A's backbone residues, (B) FEL of CDK2/Cyclin A (C) FEL of CDK2/Cyclin A/Amygdalin.

4.2.2.4 Binding Free Energy by MM/PBSA Computations

The estimated energies of CDK2/Cyclin A/amygdalin which obtained from g_mmpbsa computations are summarised in Table 4.6. The binding free energy $\Delta G_{binding}$ is -14.393 kcal/mol which is highest value which reflects very strong interactions between CDK2/Cyclin A and amygdalin for more details are presented in Appendix B. This value was quite enough to denote which type the amygdalin is a good inhibitor for CDK2/Cyclin A. Furthermore, $\Delta G_{binding}$ of amygdalin to CDK2/Cyclin A proved that the amygdalin blocks the CDK2/Cyclin A as presented in experimental studies (Juengel et al., 2016; Makarević, Rutz, Juengel, Kaulfuss, Reiter, et al., 2014).

Table 4.6 The estimated free binding energies of amygdalin/CDK2/Cyclin A complex by using g_mmpbsa tool.

ΔG_{vdW} (kcal/mol)	-44.395
ΔG_{elec} (kcal/mol)	-16.122
ΔG_{pol} (kcal/mol)	51.073
ΔG_{nonpol} (kcal/mol)	-4.949
$\Delta G_{binding}$ (kcal/mol)	-14.393

4.2.3 Inhibition of CDK2/Cyclin A by Amygdalin

4.2.3.1 Molecular Docking

The disclosed results of Molecular docking is that the amygdalin binds in the binding site of CDK4 (Dong et al., 2017) with value -10.6 kcal/mol (Table 4.4). The interactions between amygdalin and CDK4/Cyclin D1 are presented are the relevant hydrogen bonding established with residues Val14, Gly18, Tyr17, Asn145, Glu144 and Asp158 of CDK4 chain (Figure 4.21). Carbonyl (hydrogen acceptor) and hydroxyl (hydrogen donor) groups of amygdalin were involved in hydrogen bonding. This docked conformation of amygdalin within the ATP-active site of CDK4/Cyclin was chosen as initial complex for MD simulations.

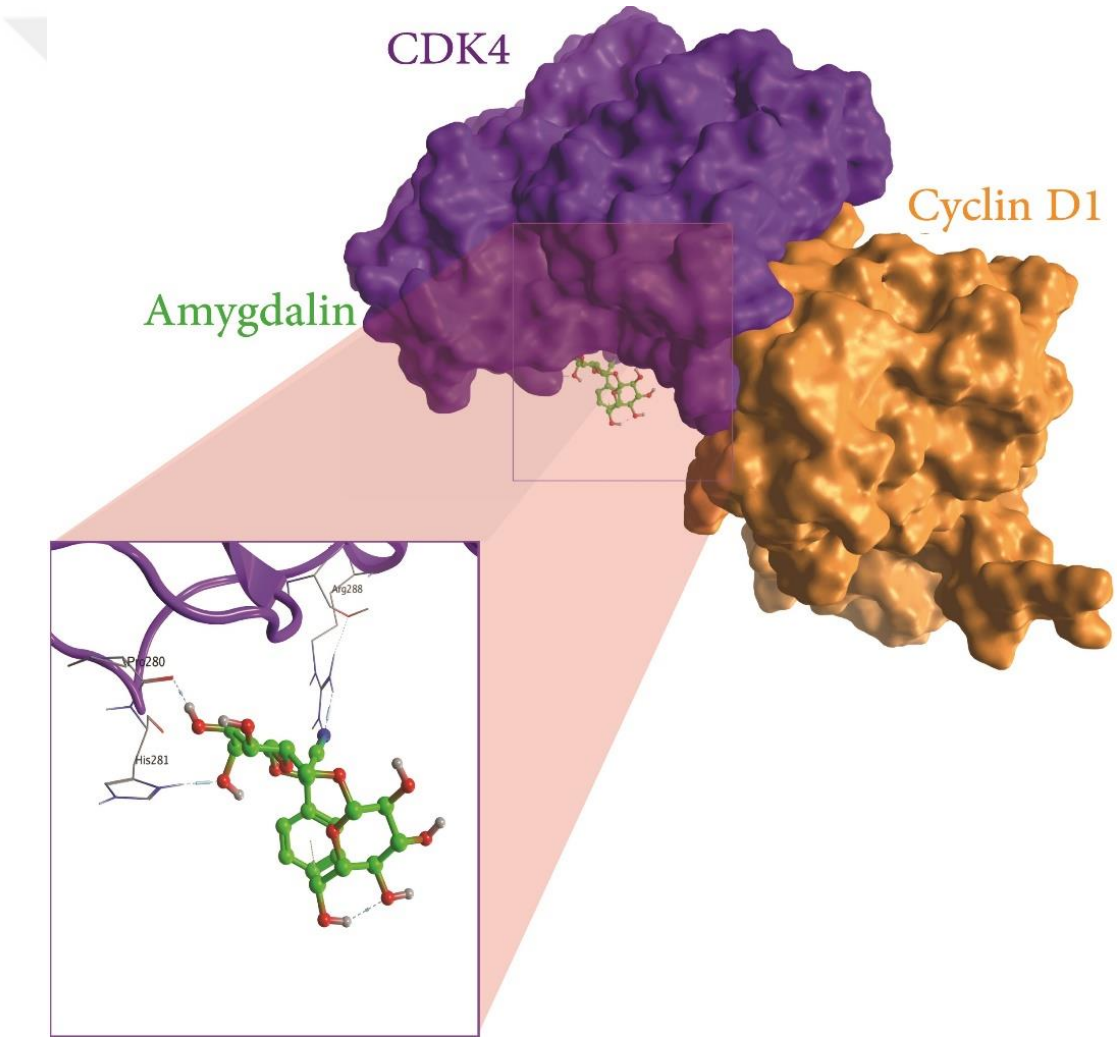

Figure 4.21 The docked pose of amygdalin with CDK4/Cyclin D1.

4.2.3.2 MD Simulations

The CDK4/Cyclin D1/amygdalin complex was used as an initial complex for MD simulation running. In order to estimate the effect of amygdalin on conformational stability through the time of MD simulation of the CDK4/Cyclin D1, we adopted RMSD and RMSF for this purpose. Figure 4.22 reveals that the RMSD for CDK4/Cyclin D1/ amygdalin was growing till 6.6 ns to achieve ~3.1 A^0. From 6.6 to 8.7 ns the RMSD profile leaped to 4 A^0 and fell to 3 A^0. After 8.7 ns RMSD values had the similar style of amygdalin-unbound CDK4/Cyclin D1. This manner is because of the interaction of approximately polar molecule amygdalin inside the active site, which is comprising hydrophobic grove.

To inspect the flexible regions of the protein, (RMSF) of backbone residues was studied. CDK4/Cyclin D1/amygdalin complex showed distinctly the same variations as compared to amygdalin-bound CDK4/Cyclin D1 (Figure 4.23).

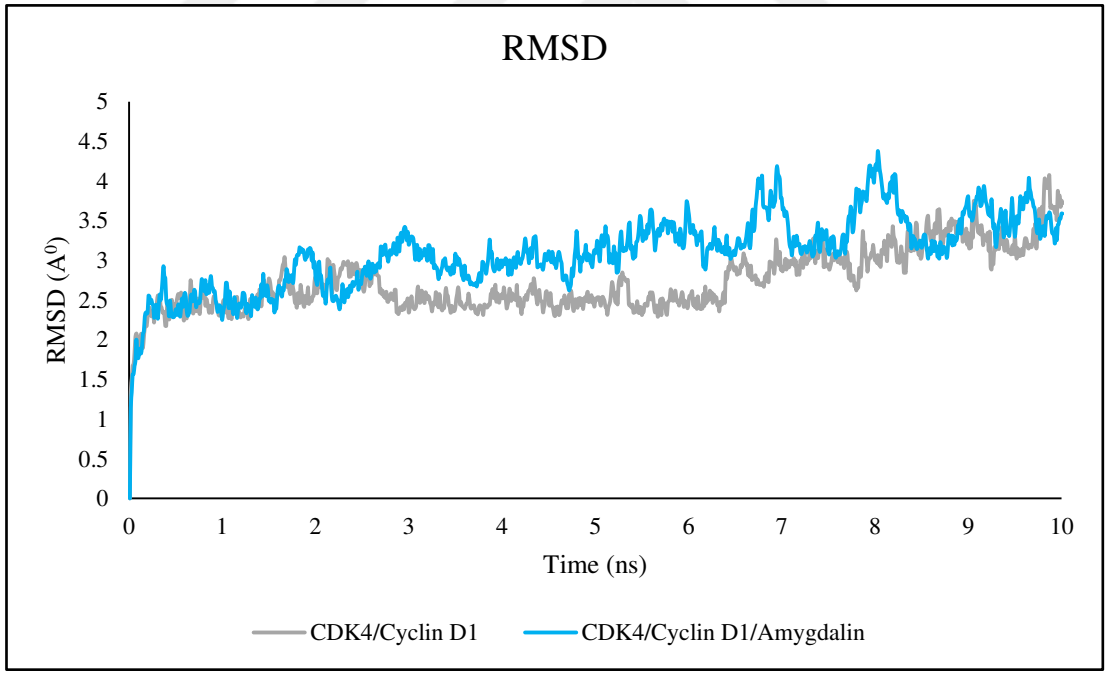

Figure 4.22 The evaluation root means square deviations (RMSDs) of Protein's backbone atoms versus 10 ns of MD simulation.

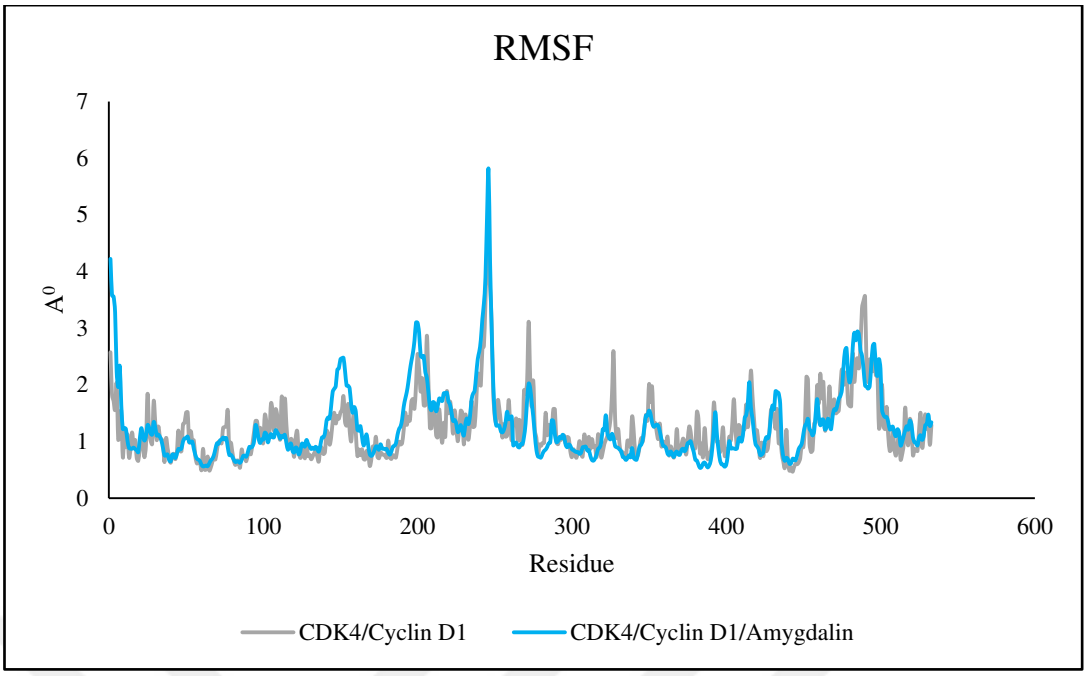

Figure 4.23 Residual fluctuations (RMSF) of protein backbone's atoms during 10 ns MD simulations.

4.2.3.3 PCA and FEL

Figure 4.24 (A) exhibits the essential dynamics for both apo and amygdalin-bound CDK4/Cyclin D1. It is apparent from Figure 4.24 (A) that the essential dynamics for both of CDK4/Cyclin D1/amygdalin is more arbitrary and the increased significantly if it compared with essential dynamics of apo CDK4/Cyclin D1. And also, the FEL contour maps (Figure 4.24 (B) and (C)) shows a that the thermal profile of CDK4/Cyclin D1 is little better than amygdalin-bound CDK4/Cyclin D1.

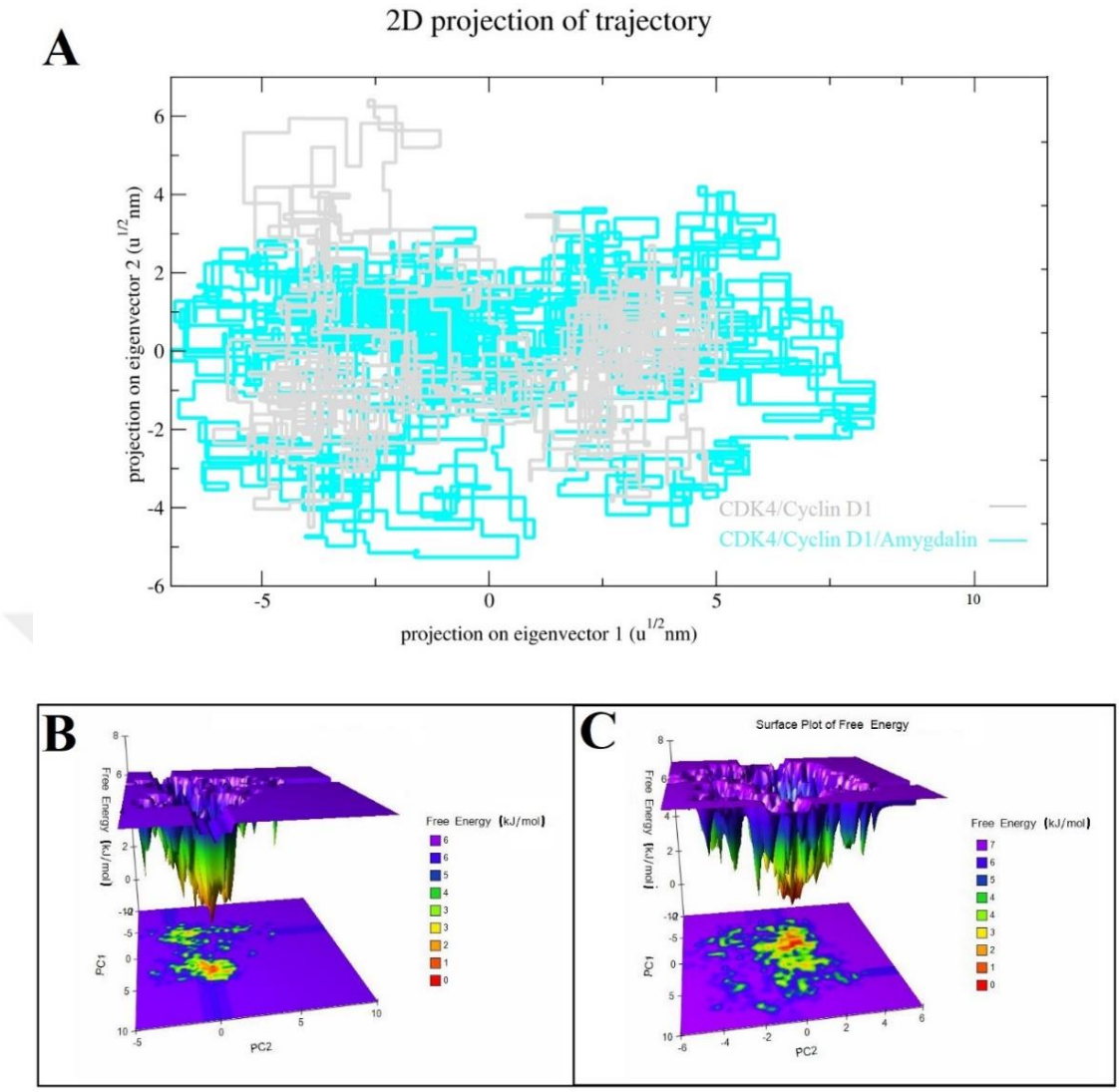

Figure 4. 24 (A) PCA of 10 ns MD trajectories of apo and holo forms of CDK4/Cyclin D1's backbone residues, (B) FEL of CDK4/Cyclin D1 (C) FEL of CDK4/Cyclin D1/Amygdalin.

4.2.3.4 Binding Free Energy by MM/PBSA Computations

Table 4.5 provides the synopsis of the energies and total binding free energy of CDK4/Cyclin D1/amygdalin that generated through utilizing g_mmpbsa tool. Also, the details about binding free energy during MD simulations are presented in Appendix B. From the below table that the binding free energy $\Delta G_{binding}$ is -0.766 kcal/mol which is considered as good to show high affinity of amygdalin toward CDK4/Cyclin D1.

Table 4.7 The estimated free binding energies of amygdalin/CDK4/Cyclin D1 complex by using g_mmpbsa tool.

ΔG_{vdW} **(kcal/mol)**	-20.647
ΔG_{elec} **(kcal/mol)**	-6.536
ΔG_{pol} **(kcal/mol)**	29.444
ΔG_{nonpol} **(kcal/mol)**	-3.025
$\Delta G_{binding}$ **(kcal/mol)**	-0.766

4.3 Amygdalin as Inhibitor of Metastasis and Cancer Invasion

4.3.1 Inhibition of AKT1 by Amygdalin

4.3.1.1 Molecular Docking

To check the mechanism of AKT1/amygdalin interactions, we adopted double docking. Double docking results disclosed that amygdalin binds at ATP binding pocket (Eduardo Sanabria-Chanaga et al., 2019) with binding energy of −7.321 kcal/mol (Table 4.8). The AKT1/amygdalin complex which generated by double docking is stabilized by three hydrogen bonds are between amygdalin and Glu191, Asp274 and Glu198 residues of AKT1 (Figure 4.25).

Table 4.8 Docking results synopsis of amygdalin with nominated target for targeting apoptosis (Al-Khafaji and Taskin Tok, 2020b).

Protein Target	**Binding Affinities (kcal/mol)**	**RMSD (A^0)**	**Ki (inhibition constant**, uM)
AKT1	-7.321	2.155	2.15 uM
FAK1	-8.61	1.944	1.2 uM
ILK	-7.6	2.413	0.55 uM

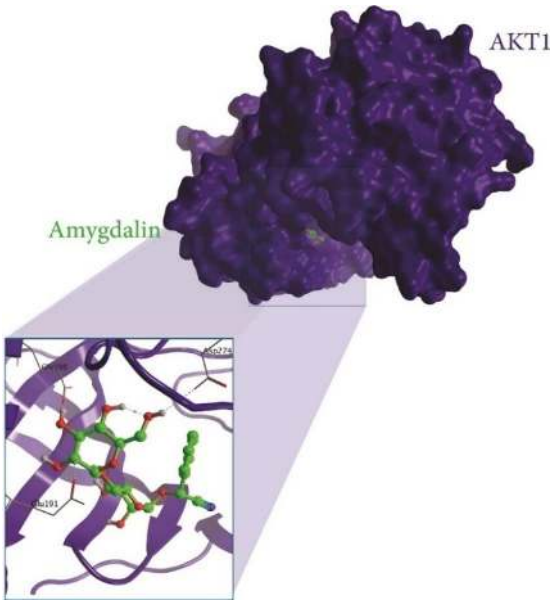

Figure 4. 25 The docked pose of amygdalin with AKT1.

4.3.1.2 MD simulations

The RMSD values were measured for both the amygdalin-unbound AKT1 and amygdalin-bound AKT1 are presented in Figure 4.26. The average RMSD value for amygdalin-unbound AKT1 and AKT1/amygdalin were 1.65 and 1.64 A^0, respectively. After 2 ns AKT1/amygdalin complex exhibit much more stability during MD simulation as compared with amygdalin-unbound AKT1. From RMSF analysis, we can deduce that both apo AKT1 and AKT1-amygdalin show a similar pattern of RMSF values ranged between 5.6 A^0 and 0.43 A^0 (Figure 4.27). Except in the loop 11 (302-318) and loop 21 (441–449) regions, AKT1-amygdalin exhibited more flexibility. Nevertheless, in AKT1-amygdalin complex less flexibility in the loop 22 (449-470) region.

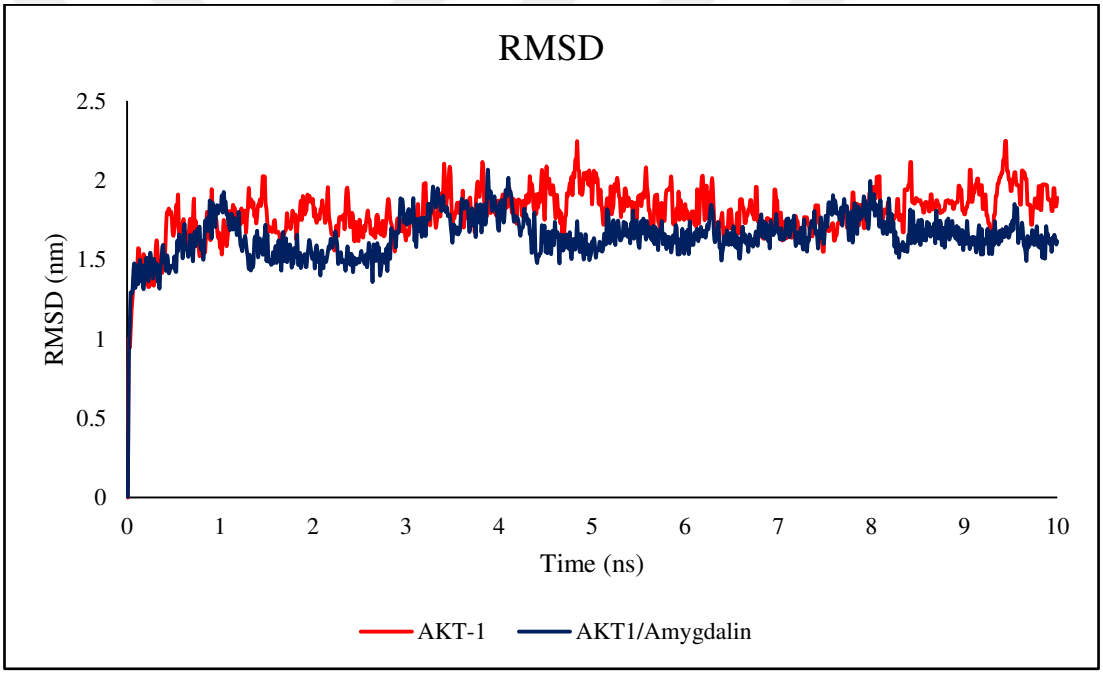

Figure 4. 26 The evaluation root means square deviations (RMSDs) of Protein's backbone atoms versus 10 ns of MD simulation.

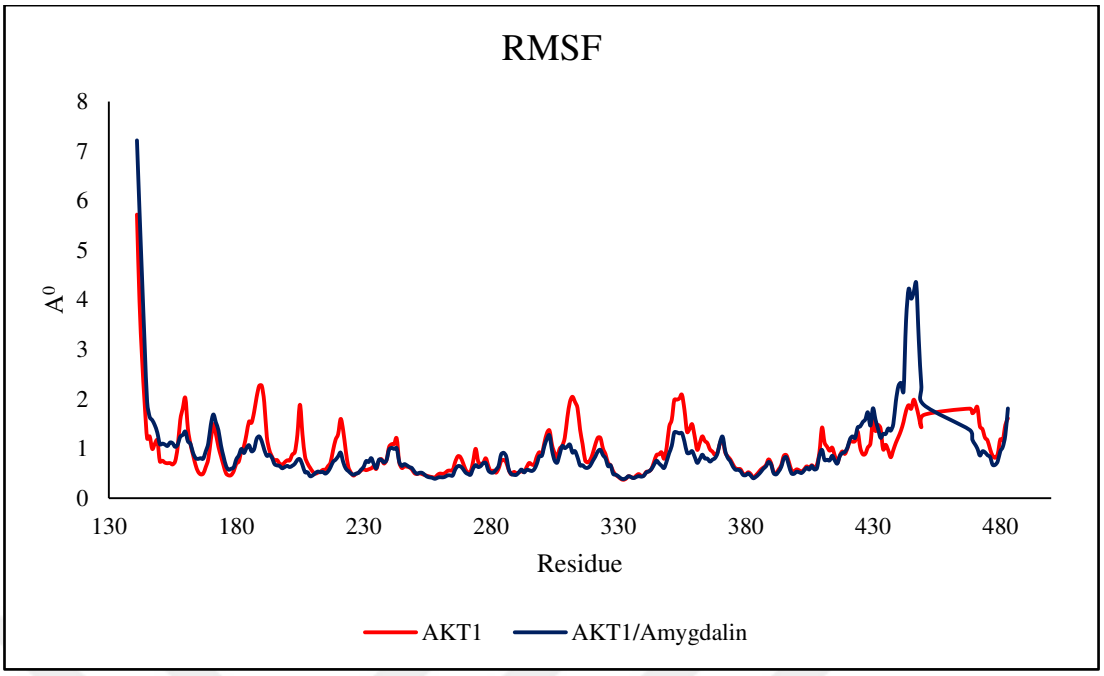

Figure 4. 27 Residual fluctuations (RMSF) of protein backbone's atoms during 10 ns MD simulations.

4.3.1.3 PCA and FEL

Figure 4.28 (A) depicts the essential dynamics of apo AKT1 and holo AKT1. It is apparent from Figure 4.28 (A) that the essential dynamics for both of AKT1/amygdalin is more oriented when it compared with essential dynamics of apo AKT1. But, the FEL contour maps (Figure 4.28 (B) and (C)) illustrates that the thermal profile of apo AKT1 is more favoured than amygdalin-bound AKT1.

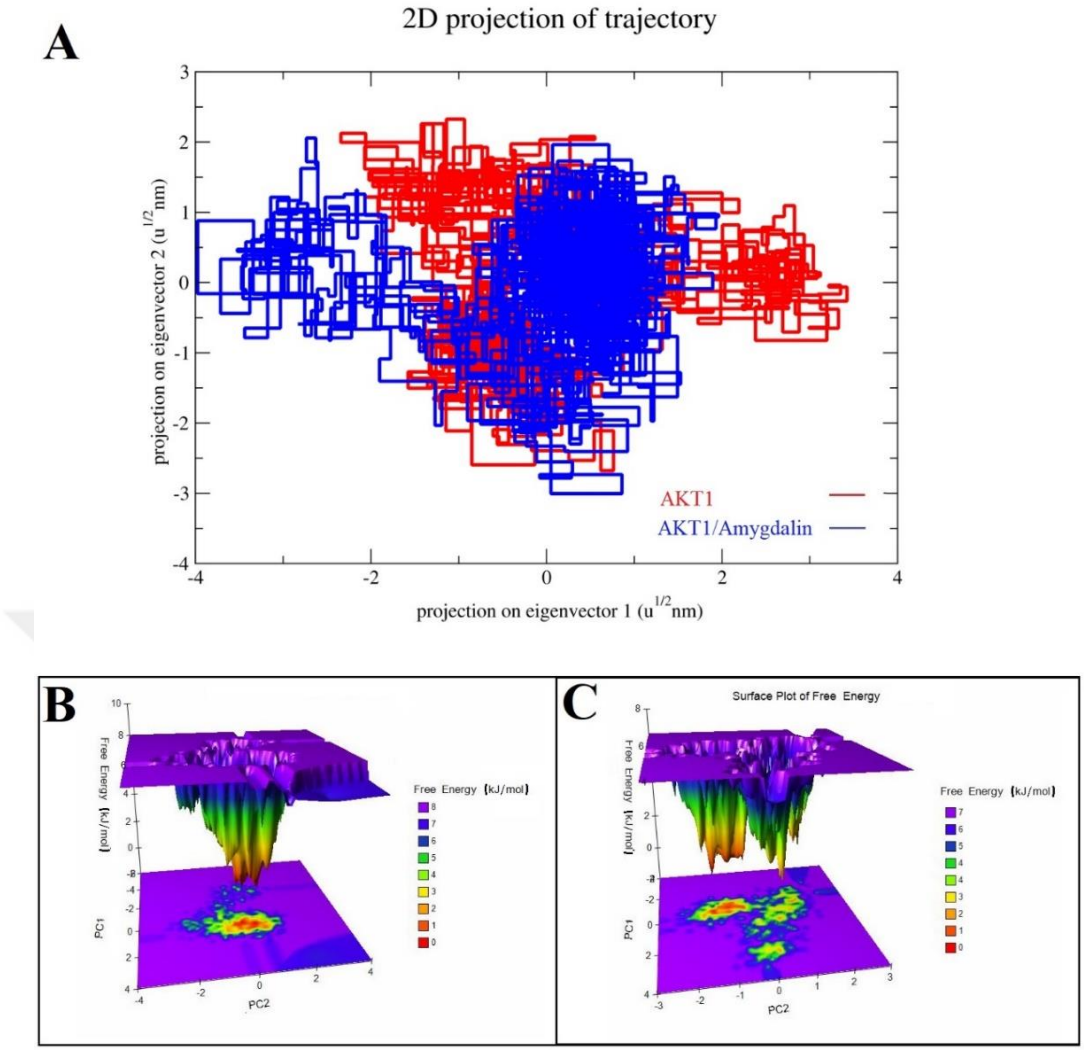

Figure 4.28 (A) PCA of 10 ns MD trajectories of apo and holo forms of AKT1's backbone residues, (B) FEL of AKT1 (C) FEL of AKT1/Amygdalin.

4.3.1.4 Binding Free Energy by MM/PBSA Computations

The summarized energies for the interactions between AKT1 and amygdalin are presented in Table 4.9 (details are presented in Appendix B). From below table we can see that the binding energy $\Delta G_{binding}$ is -3.281 kcal/mol which is indicating that amygdalin binds inside the active site of AKT1.

Table 4.9 The estimated free binding energies of amygdalin/AKT1 complex by using g_mmpbsa tool.

ΔG_{vdW} **(kcal/mol)**	-34.049
ΔG_{elec} **(kcal/mol)**	-15.760
ΔG_{pol} **(kcal/mol)**	50.365
ΔG_{nonpol} **(kcal/mol)**	-3.837
$\Delta G_{binding}$ **(kcal/mol)**	-3.281

4.3.2 Inhibition of FAK1 by Amygdalin

4.3.2.1 Molecular Docking

The result of the molecular dockings of revealed that amygdalin docked pose inside the binding site of FAK1 is presented in Figure 4.29. Amygdalin binds with FAK1 of binding energy of -8.61 kcal/mol (Table 4.8.). It is apparent from this table that the estimated binding energy of amygdalin with FAK1 protein has the lowest negative magnitude of -8.61 kcal/mol. Figure 4.29 illustrates that amygdalin interacts within the binding site of FAK1 and amygdalin forms six hydrogen bonds with Lys454, Glu500, Cys502, and Glu430 of FAK1 chain. Our docking output confirm previous docking studies of ligands toward the binding site of FAK1 (Cheng et al., 2017; Daneial et al., 2017; Zhan et al., 2015). Ultimately, the FAK1/amygdalin complex was introduced to 10 ns MD simulation.

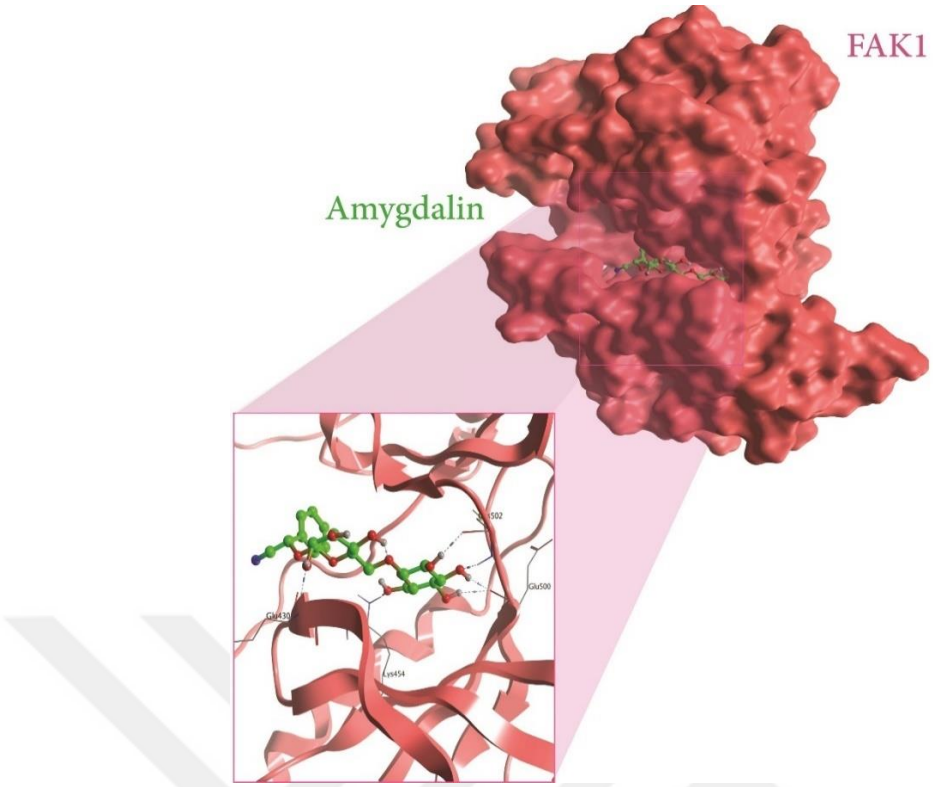

Figure 4.29 The docked pose of amygdalin with FAK1.

4.3.2.2 MD Simulations

RMSD values for backbone residue of FAK1 of free and holo form are shown in Figure 5 (A). Figure 4.30 exhibits the stability (RMSD) of FAK1-apo and FAK1-amygdalin during 10 ns. Both of RMSD trends for apo-FAK1 and holo-FAK1 were almost the same. The average of RMSD were 1.66 and 1.64 A^0 for free bound FAK1 and amygdalin-bound FAK1 respectively. Again, here amygdalin enhanced the stability of the target protein. The RMSF of FAK1 protein as shown in Figure 4.31, when amygdalin bound to FAK1 protein, it is clear that amygdalin stabilized the FAK1 regions. From the RMSF report, we have deduced that the amygdalin induced fewer conformational variations through binding and can serve as a stabilizer for FAK1 protein.

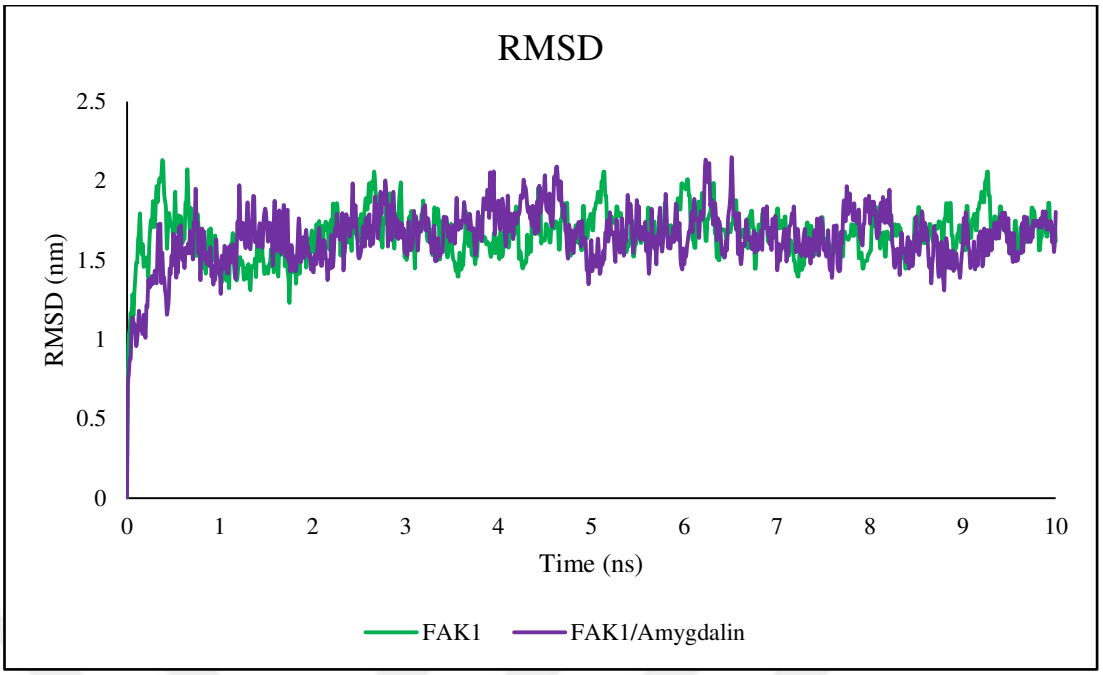

Figure 4. 30 The evaluation root means square deviations (RMSDs) of Protein's backbone atoms versus 10 ns of MD simulation.

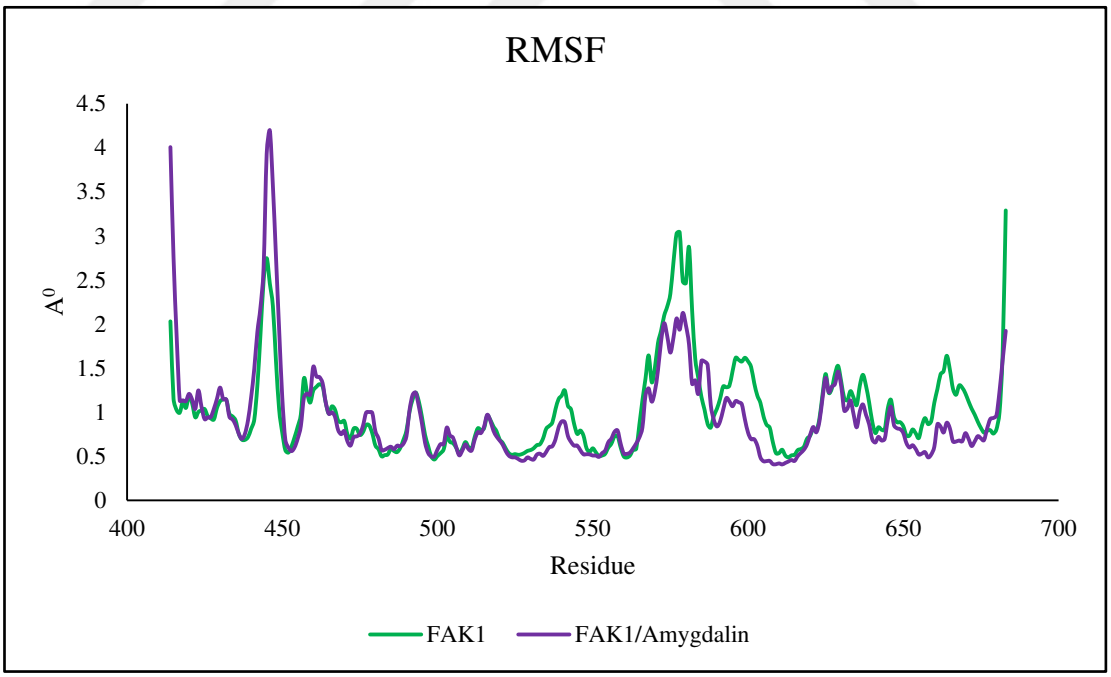

Figure 4. 31 Residual fluctuations (RMSF) of protein backbone's atoms during 10 ns MD simulations.

4.3.2.3 PCA and FEL

Figure 4.32 (A) epitomizes the essential dynamics of apo FAK1 and amygdalin-bound FAK1. This figure is quite revealing in several ways. First, the essential dynamics of amygdalin-bound FAK1 is more centralized unlike the essential dynamics of apo FAK1, second amygdalin-bound FAK1 has less arbitrary. And the FEL contour maps (Figure 4.32 (B) and (C)) shows the red region is also more centralized for amygdalin-bound FAK1, this indicates that the energy landscape is more stable.

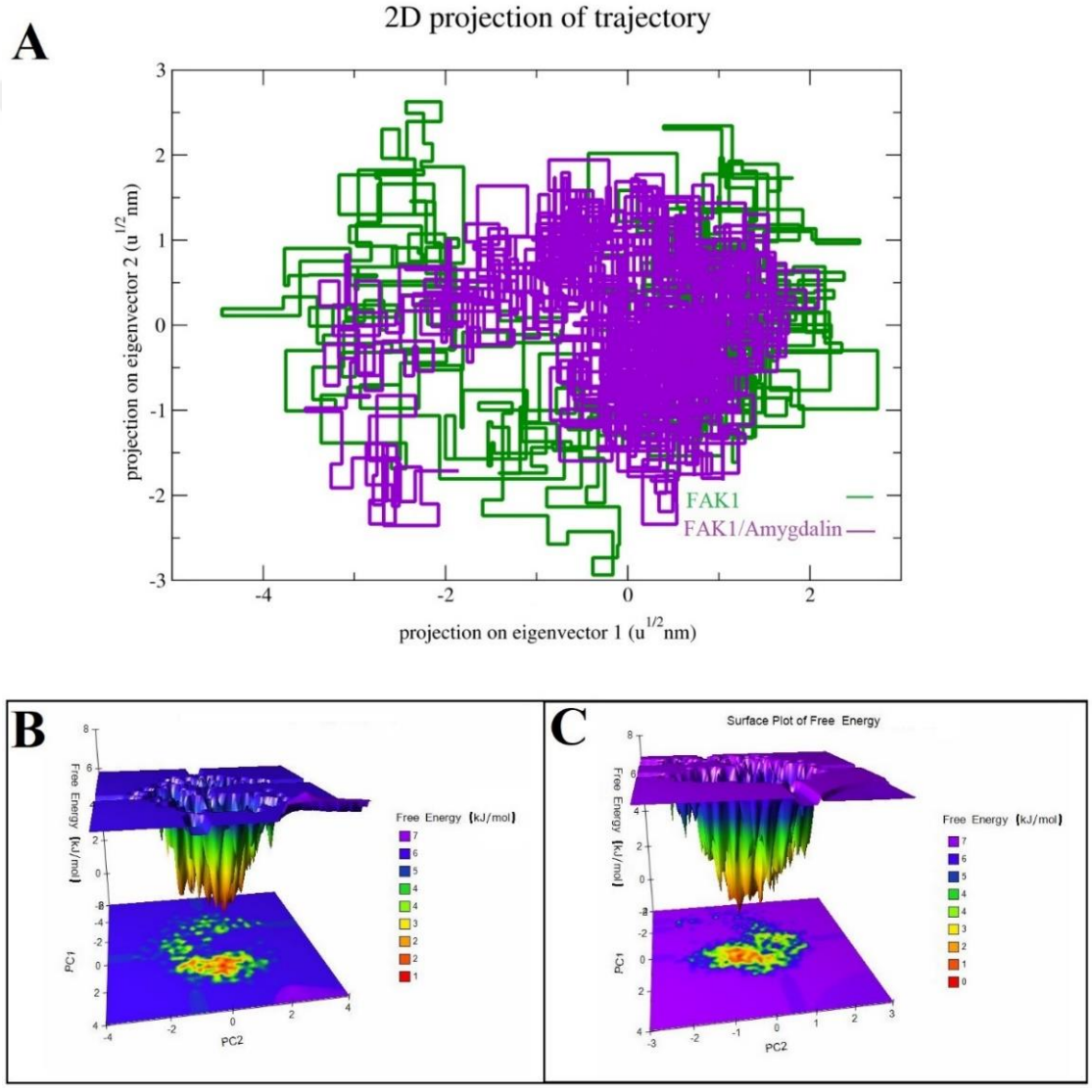

Figure 4. 32 (A) PCA of 10 ns MD trajectories of apo and holo forms of FAK1's backbone residues, (B) FEL of FAK1 (C) FEL of FAK1/Amygdalin.

4.3.2.4 Binding Free Energy by MM/PBSA Computations

Table 4.9 gives a summary of energies for the interactions between FAK1 and amygdalin. As Table 4.9 shows, there is a stately binding free energy $\Delta G_{binding}$ of -13.052 kcal/mol. This can indicate that amygdalin locates inside the binding site of FAK1 tightly.

Table 4.10 The estimated free binding energies of amygdalin/FAK1 complex by using g_mmpbsa tool.

ΔG_{vdW} (kcal/mol)	-37.308
ΔG_{elec} (kcal/mol)	-20.788
ΔG_{pol} (kcal/mol)	49.474
ΔG_{nonpol} (kcal/mol)	-4.429
$\Delta G_{binding}$ (kcal/mol)	-13.052

4.3.3 Inhibition of ILK by Amygdalin

4.3.3.1 Molecular docking

As can be seen from the Figure 4.33, that amygdalin forms a stable interaction inside the ILK active-binding site (Gulzar, Ali, et al., 2019; Gulzar, Syed, et al., 2019), which is generated by double docking. It created a four hydrogen bonds with Lys220, Met272, His270 and Asp339 (Figure 4.33) with binding energy of -7.6 Kcal/mol (Table 4.8). Yet, the docked complex between amygdalin and ILK/amygdalin complex was proposed to 10 ns MD simulation.

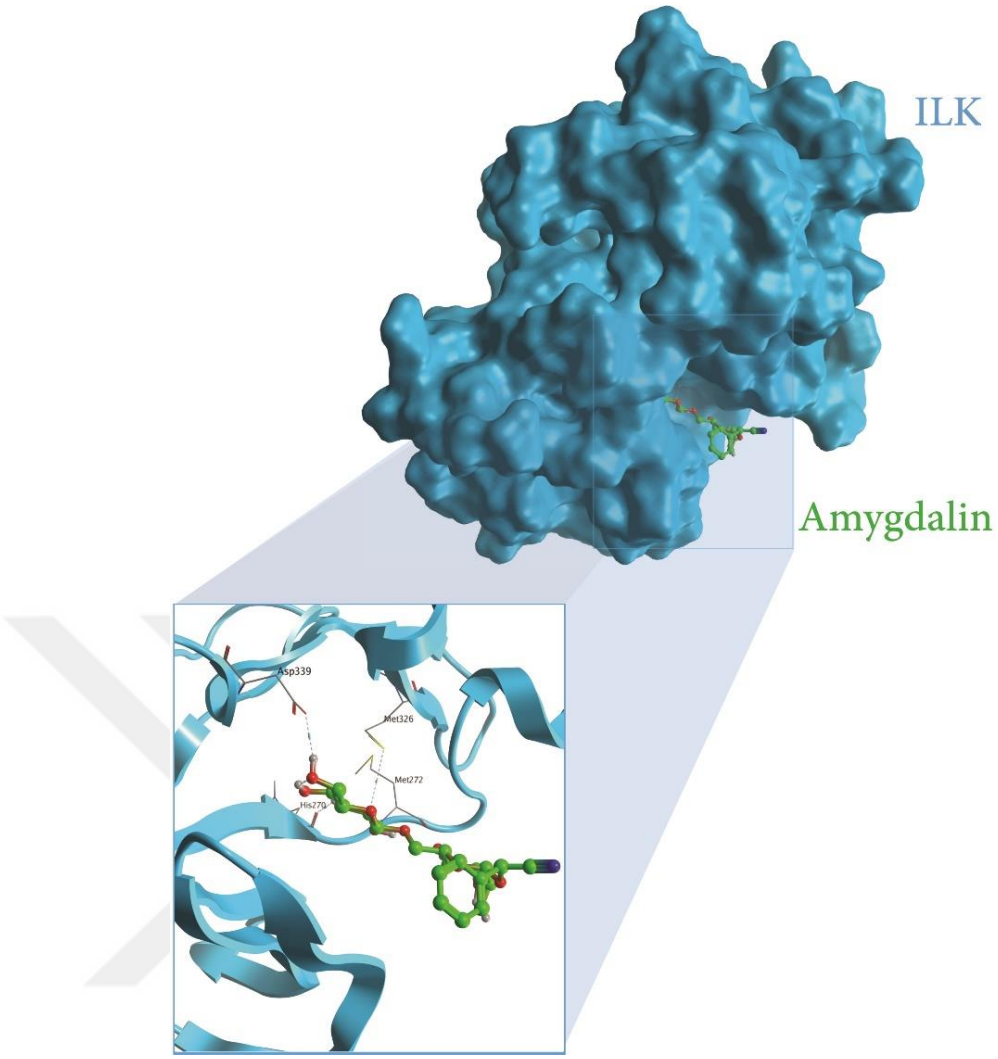

Figure 4.33 The docked pose of amygdalin with ILK.

4.3.3.2 MD Simulations

The RMSD values of amygdalin-unbound and amygdalin-bound forms of ILK were summarized in Figure 4.34. That general style of RMSD for amygdalin-unbound ILK and amygdalin-bound ILK is dissimilar during the time of MD simulation. Where, Figure 4.34 demonstrates that the RMSD of amygdalin-unbound ILK from 2.5 ns till 6.3 ns has greater value than RMSD of amygdalin-bound ILK. But noticeably, from 8.2 to 8.9 ns RMSD for ILK/amygdalin is greater than those of amygdalin-unbound ILK. The average of RMSD values of apo-ILK and ILK amygdalin 1.5 and 1.47 A^0 respectively. Moreover, amygdalin contributes to fix the ILK protein. From gained results, amygdalin overall offers further stability to targeted proteins by restrain the dynamics of proteins' backbones if correlated with apo forms of proteins. On account of RMSD magnitude of fluctuations all protein in free bound form or amygdalin

bound form are nearly close were preserved stable over the time, the simulation is stable conformation (Dash et al., 2019), based on this, further analysis is recommended.

ILK protein behaved when it bonded to amygdalin. Figure 4.35 shows amygdalin stabilized the (195-202 residue) and (285-292) regions to the behaviour. From the RMSF analysis, we have achieved that all of our predicted amygdalin inducing less conformational variations during binding and can act as a stable complex.

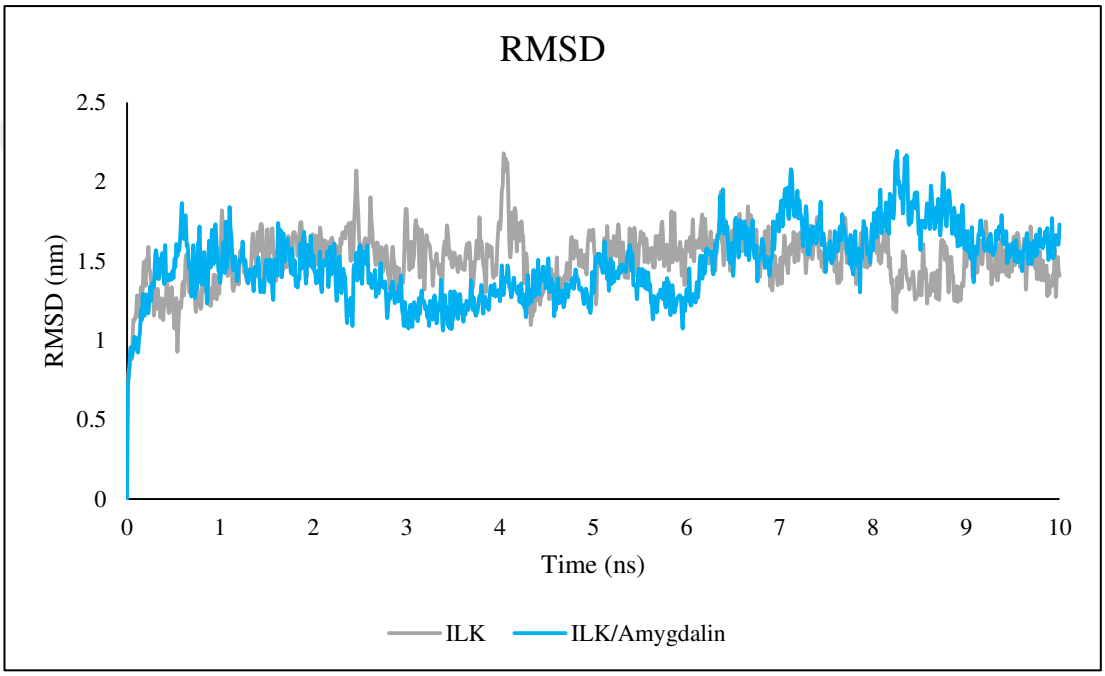

Figure 4.34 The evaluation root means square deviations (RMSDs) of Protein's backbone atoms versus 10 ns of MD simulation.

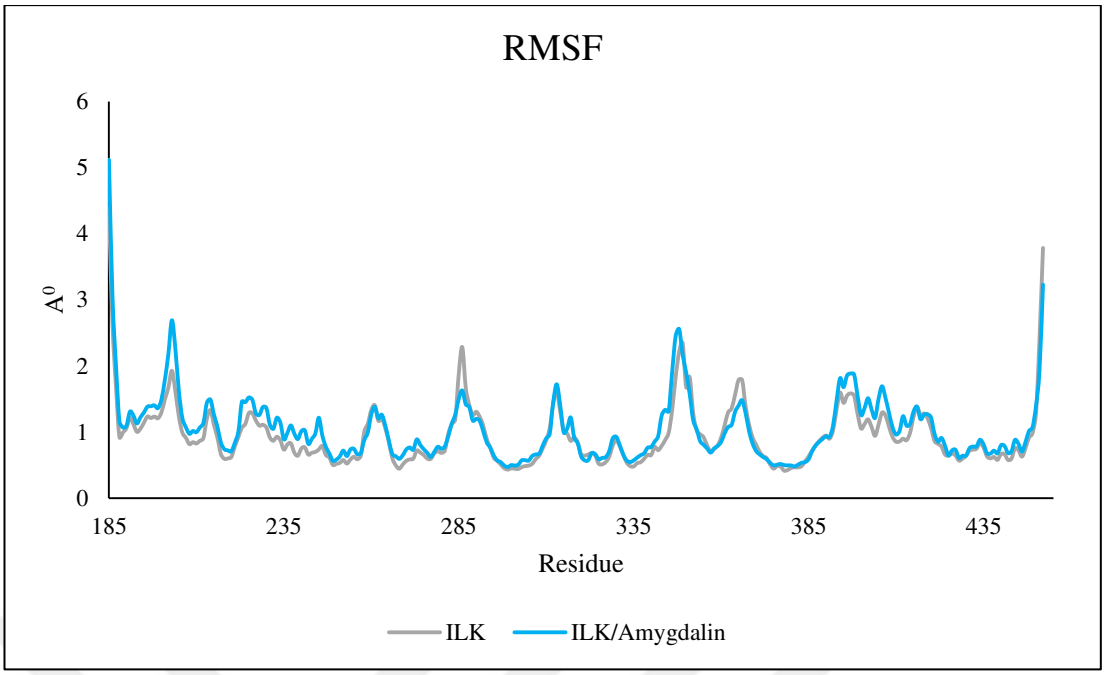

Figure 4.35 Residual fluctuations (RMSF) of protein backbone's atoms during 10 ns MD simulations.

4.3.3.3 PCA and FEL

After binding amygdalin with ILK, the FEL of ILK protein was occupying the centre and filled the least imaginable area in the contour map to state that ILK is plenty higher stable when it bound to amygdalin (Figure 4.36 (B) and (C)). These results suggest irrefutable demonstrate for the multi-targeting inhibitory of amygdalin which provides the logical explanations for experimental studies (Qian et al., 2015) and refute the idea that the of the anticancer activity of amygdalin's comes from "*Hydrogen cyanide is thought to kill cancer cells*" (Institute, 2018, April 5).

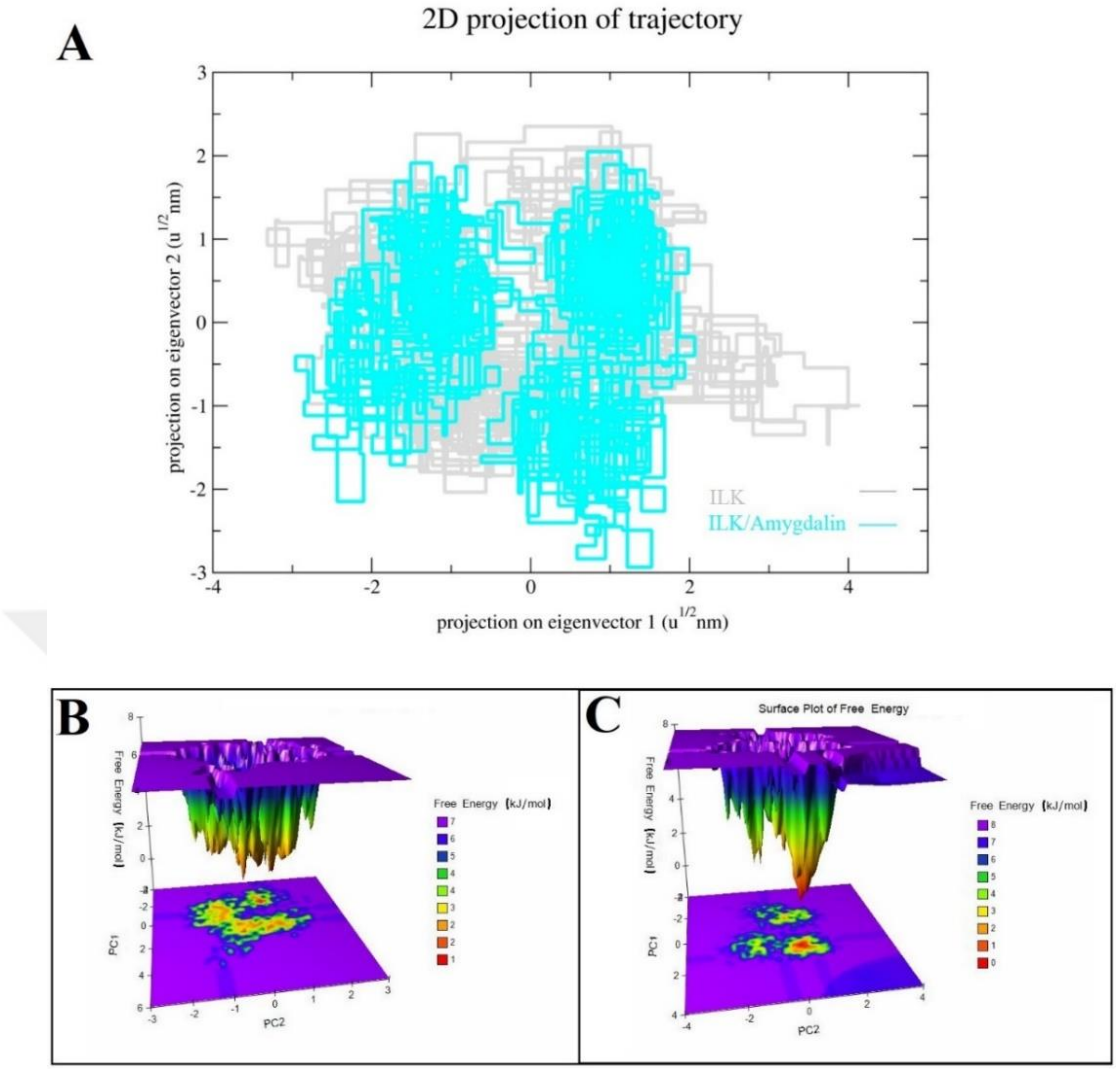

Figure 4.36 (A) PCA of 10 ns MD trajectories of apo and holo forms of ILK's backbone residues, (B) FEL of ILK (C) FEL of ILK/amygdalin.

4.3.3.4 Binding Free Energy by MM/PBSA Computations

Table 4.11 covers the summary of all energies for the interactions between ILK and amygdalin which are produced through using g_mmpbsa. Where the deep analysis of MM/PBSA values during MD simulations are presented in Appendix B. As Table 4.11 shows, there is a stately binding free energy $\Delta G_{binding}$ of -12.023 kcal/mol. This also accords with our earlier observations of double docking. This can indicate that amygdalin binds inside the binding site of ILK tightly. All of obtained results from computational investigations give deep information and evidence for the possibility of amygdalin to work as anti-metastasis drug (Al-Khafaji and Taskin Tok, 2020b). Also these are explanation for the experimental researches which reported that

amygdalin blocks the adhesion and invasion of different kinds of cancers (Makarević, Rutz, Juengel, Kaulfuss, Tsaur, et al., 2014; Qian et al., 2015).

Table 4.11 The estimated free binding energies of amygdalin/ILK complex by using g_mmpbsa tool.

ΔG_{vdW} (kcal/mol)	-39.318
ΔG_{elec} (kcal/mol)	-16.131
ΔG_{pol} (kcal/mol)	47.892
ΔG_{nonpol} (kcal/mol)	-4.465
$\Delta G_{binding}$ (kcal/mol)	-12.023

CHAPTER V

CONCLUSION AND RECOMMENDATIONS

Double docking, MD simulation and g_mmpbsa methods were implemented to elucidate the impact of amygdalin on the dynamic behaviors on BAX/Bcl-2 complex, caspase-3, PARP-1, CDK1/Cyclin B, CDK2/Cyclin A, CDK4/Cyclin D1, AKT1, FAK1 and ILK which are a key function in apoptotic pathways, cell division and metastasis as therapeutic targets for development cancer treatment. Efficiently, amygdalin bound to hydrophobic surface of Bcl-2/BAX. Further, the first finding from the MD simulation results that the amygdalin-unbound Bcl-2/BAX showed stable interaction during 10 ns MD simulation. Also, the MD simulation outcomes proved that the Bcl-2/amygdalin is stable complex too. But the second major finding was from MD simulation that when amygdalin bound to Bcl-2/BAX, the Bcl-2/BAX interaction is disrupted and separated from each other. Moreover, the results of PCA and FEL investigations show that amygdalin reduced the essential dynamics of backbone atoms of Bcl-2 while BAX did diminish the essential dynamics of backbone atoms of Bcl-2 during the time of MD simulation. Also, the thermal profile of Bcl-2 was enhanced when it bound to amygdalin. The most obvious finding to emerge from MM/PBSA which revealed that amygdalin binds strongly to Bcl-2 protein during time of MD simulation. The evidence from this study suggests that amygdalin blocks Bcl-2 and release BAX from Bcl-2/BAX complex efficiently. Before this study, evidence of amygdalin how to activate BAX and inhibit Bcl-2 was purely anecdotal.

Caspase-3 is another target of the apoptotic pathways. Amygdalin bound in the interface location of two chains. MD simulations of amygdalin/caspase-3 revealed that amygdalin makes construction of caspase-3 further dynamic through disrupting and binding of two chains of caspase-3 during the 10 ns MD simulation. This proposes that the activation of caspase-3 done by modifying conformation of caspas-

3 and it be further dynamic than stable conformation (amygdalin-unbound caspase-3).

Whilst for PARP-1 the case is different where amygdalin is bound to the PARP-1 active site. Amygdalin/PARP-1 complex is stabilized identical to the free PARP-1, and thereby this led to conclude that amygdalin is perfect inhibitor for PARP-1. The results of PCA investigations show that amygdalin impressively reduced the essential dynamics of PARP-1's backbone atoms for holo form.

Another three protein complexes are CDK1/Cyclin B, CDK2/Cyclin A, and CDK4/Cyclin D1. They are played determinant roles in cell cycle division pathways as therapeutic targets for cancer treatment. Docking results showed that amygdalin efficiently bound to ATP-binding site of CDK1/Cyclin B with binding free energy -9.41 kcal/mol. The obtained results from RMSD and RMSF of apo and amygdalin-bound CDK1/Cyclin B showed that amygdalin is giving much more stability to the CDK1/Cyclin B. As regards of PCA estimations, there is no significant difference to essential dynamics of apo and holo forms of CDK1/Cyclin B. Moving on now to consider the FEL investigations, the results revealed that amygdalin makes the Gibbs free energy profile more stable for holo form of CDK1/Cyclin B. Another significant aspect of investigation is MM/PBSA. The Binding free energy which is obtained from g_mmpbsa tool is -2.260 kcal/mol that is considered as good indicator for amygdalin as strong binder to CDK1/Cyclin B. Taken together, these results suggest that amygdalin inhibit the CDK1/Cyclin B complex efficaciously.

Turning now to second target of cell division which is CDK2/Cyclin A. The double docking results revealed that docking score of amygdalin to CDK2/Cyclin A is -9.02 kcal/mol. The results from molecular dynamic simulations analysis of complexes showed that amygdalin gives more stability to CDK2/Cyclin A as happened to CDK1/Cyclin when it bound to amygdalin. To study the influence of amygdalin of functioning dynamics of CDK2/Cyclin A, we utilized PCA computations. PCA results summarized both of amygdalin free and amygdalin-bound CDK2/Cyclin A are motioning in similar style. But the FEL estimations showed that apo form of CDK2/Cyclin A thermal style is more favored. The investigation of the binding free energy behavior gave highly reliable information on how can amygdalin binds tightly to the CDK2/Cyclin A. The binding free energy is -14.393 kcal/mol. The results of the investigations for inhibiting CDK2/Cyclin A by amygdalin, confirming that amygdalin is a good inhibitor of CDK2/Cyclin A.

For the last target of cell division, is CDK4/Cyclin D1. Docking results explored that docking score of amygdalin when it bound to CDK4/Cyclin D1 is -10.6 kcal/mol. The results from MD simulation did not show an enhancement upon the RMSD values of CDK4/Cyclin D1's backbone atoms. But the most obvious finding to emerge from PCA estimations is that the amygdalin increased the arbitrary of essential dynamics for holo form of CDK4/Cyclin D1. Further, the binding free energy of CDK4/Cyclin D1/amygdalin complex is -0.766 kcal/mol and it is not efficient. The results of computational investigations on the activity of amygdalin against CDK4/Cyclin D1 are in agreement of previous experimental results that amygdalin did not inhibited the CDK4/Cyclin D1.

For another function of amygdalin is as metastasis inhibitor through targeting primary targets: AKT1, FAK1 and ILK proteins. Results of docking presented that binding of amygdalin with AKT1, FAK1 and ILK showed strongest binding energy -8.61 with FAK1 kcal/mol as related to AKT1 and ILK. MD trajectories analysis (i.e., RMSD and RMSF) again showed amygdalin enhanced the overall stability FAK1's backbone atoms, where RMSD decrease from 1.66 A^0 of amygdalin-unbound FAK1 to 1.64 A^0 for amygdalin-bound FAK1. RMSF reveals amygdalin reduced substantially the variations of FAK1 residues. FEL analysis of amygdalin-target complexes revealed that the binding of amygdalin to FAK1 and ILK enhanced the Free energy landscape. Whereas, with AKT1, there is no noticeable distinction of the Free energy landscape, which reveals the amygdalin has no great effect on the dynamics of attitude of AKT1. MM/PBSA results displays that amygdalin fit well into the ATP binding site of both FAK1 and ILK better than binding of amygdalin with AKT1. The most noticeable finding to appear from this investigation is that the stability of binding energies of amygdalin toward FAK1 and ILK during overall 10 ns.

Overall, the computational studies may regard as satisfactory evidence to disprove the presence of the suggested theory, that hydrogen cyanide which produced from dissociation of amygdalin which is responsible for anticancer actions of amygdalin, thereby confirming that amygdalin has particular structure can be character for drug designers to invent modern molecules has same structure.

Further, this research supports the belief that amygdalin can be as a multi-objective or muti-target drug against different mechanisms of tumor. These data help in several respects to our understanding the actual processes of amygdalin which were curious and afford a basis for establishing a serious scientific instigation of amygdalin use against different malignancies. This research supports the opinion that of this examination disclose that, supporting that amygdalin has an exceptional structure can be a reference for drug designers to design new molecules against cancer has the same structure and also to apply this molecule in large in vitro, in vivo studies.

REFERENCES

Abraham, M. J., Murtola, T., Schulz, R., Páll, S., Smith, J. C., Hess, B., & Lindahl, E. (2015). Gromacs: High Performance Molecular Simulations through Multi-Level Parallelism from Laptops to Supercomputers. *SoftwareX*, **1**, 19-25.

Al-Khafaji, K., & Taskin Tok, T. (2020a). Amygdalin as Multi-Target Anticancer Drug against Targets of Cell Division Cycle: Double Docking and Molecular Dynamics Simulation. *Journal of Biomolecular Structure and Dynamics*, 1-10. https://doi.org/10.1080/07391102.2020.1742792

Al-Khafaji, K., & Taskin Tok, T. (2020b). Molecular Dynamics Simulation, Free Energy Landscape and Binding Free Energy Computations in Exploration the Anti-Invasive Activity of Amygdalin against Metastasis. *Computer Methods and Programs in Biomedicine*, **195**, 105660. https://doi.org/https://doi.org/10.1016/j.cmpb.2020.105660

Al-Khafaji, K., & Taskin Tok, T. (2020c). Understanding the Mechanism of Amygdalin's Multifunctional Anti-Cancer Action Using Computational Approach. *Journal of Biomolecular Structure and Dynamics*, 1-14. https://doi.org/10.1080/07391102.2020.1736159

Alberts, B. (2008). Molecular Biology of the Cell. Garland Science.

Amadei, A., Linssen, A. B., & Berendsen, H. J. (1993). Essential Dynamics of Proteins. Proteins: Structure, *Function, and Bioinformatics*, **17(4)**, 412-425.

Atkins, P., & Paula, J. (2006). Atkins' Physical Chemistry. Chemistry, 783-827.

Autodocktools, the Free Gui for Autodock. http://autodock.scripps.edu/resources/adt

Barford, D. (2011). Structural Insights into Anaphase-Promoting Complex Function and Mechanism. *Philosophical Transactions of the Royal Society B: Biological Sciences*, **366(1584)**, 3605-3624.

Bellocchi, D., Macchiarulo, A., Costantino, G., & Pellicciari, R. (2005). Docking Studies on Parp-1 Inhibitors: Insights into the Role of a Binding Pocket Water Molecule. *Bioorganic & medicinal chemistry*, **13(4)**, 1151-1157.

Berman, H. M., Battistuz, T., Bhat, T. N., Bluhm, W. F., Bourne, P. E., Burkhardt, K., Feng, Z., Gilliland, G. L., Iype, L., & Jain, S. (2002). The Protein Data Bank. *Acta Crystallographica Section D: Biological Crystallography*, **58(6)**, 899-907.

Bhatnagar, A., Mittal, S., & Garg, A. (2017). Laetrile: A Wonder Drug or Farce. *International Journal of Applied Dental Sciences*.

BIOVIA, D. S. (2013). *Discovery Studio*. In (Version 2013) San Diego: Dassault Systèmes.

Bjelkmar, P., Larsson, P., Cuendet, M. A., Hess, B., & Lindahl, E. (2010). Implementation of the Charmm Force Field in Gromacs: Analysis of Protein Stability Effects from Correction Maps, Virtual Interaction Sites, and Water Models. *Journal of Chemical Theory and Computation*, **6(2)**, 459-466.

Blaheta, R. A., Nelson, K., Haferkamp, A., & Juengel, E. (2016). Amygdalin, Quackery or Cure? *Phytomedicine*, **23(4)**, 367-376. https://doi.org/https://doi.org/10.1016/j.phymed.2016.02.004

Bray, F., Ferlay, J., Soerjomataram, I., Siegel, R. L., Torre, L. A., & Jemal, A. (2018). Global Cancer Statistics 2018: Globocan Estimates of Incidence and Mortality Worldwide for 36 Cancers in 185 Countries

[https://doi.org/10.3322/caac.21492]. CA: A Cancer Journal for Clinicians, **68(6)**, 394-424. https://doi.org/https://doi.org/10.3322/caac.21492

Broertjes, J. (2015). The Ten Hallmarks of Cancer in Cutaneous Malignant Melanoma. *UNAV Journal for Medical Students*, **1**, 6-12. https://doi.org/10.15581/005.1.6-12

Brown, N. R., Korolchuk, S., Martin, M. P., Stanley, W. A., Moukhametzianov, R., Noble, M. E., & Endicott, J. A. (2015). Cdk1 Structures Reveal Conserved and Unique Features of the Essential Cell Cycle Cdk. *Nature Communications*, **6**, 6769.

Bruyère, C., & Meijer, L. (2013). Targeting Cyclin-Dependent Kinases in Anti-Neoplastic Therapy. *Current opinion in cell biology*, **25(6)**, 772-779.

Bultinck, P., Winter, H., & Langeneaker, W. (2003). Computation Medicinal Chemistry for Drug Discovery. In.

Bures, M. G. (1999). Molecular Mechanics and Conformational Analysis in Drug Design by G. M. Keseru and I. Kolossvary. Blackwell Science, Oxford, U.K. 1999. Viii + 168 Pp. 18 × 25 Cm. Isbn 0-632-05289-9. £49.50. *Journal of medicinal chemistry*, **42(23)**, 4925-4926. https://doi.org/10.1021/jm990487q

Bussi, G., Donadio, D., & Parrinello, M. (2007). Canonical Sampling through Velocity Rescaling. *The Journal of chemical physics*, **126(1)**, 014101.

Chaffer, C. L., & Weinberg, R. A. (2011). A Perspective on Cancer Cell Metastasis. *Science*, **331(6024)**, 1559. https://doi.org/10.1126/science.1203543

Chang, H.-K., Shin, M.-S., Yang, H.-Y., Lee, J.-W., Kim, Y.-S., Lee, M.-H., Kim, J., Kim, K.-H., & Kim, C.-J. (2006). Amygdalin Induces Apoptosis through Regulation of Bax and Bcl-2 Expressions in Human Du145 and Lncap Prostate Cancer Cells. *Biological and Pharmaceutical Bulletin*, **29(8)**, 1597-1602. https://doi.org/10.1248/bpb.29.1597

Chashoo, G., & Saxena, A. (2014). Targetting Cdks in Cancer: An Overview and New Insights. *J Cancer Sci Ther*, **6(12)**, 488-496.

Chen, Q., Xu, R., Zeng, C., Lu, Q., Huang, D., Shi, C., Zhang, W., Deng, L., Yan, R., Rao, H., Gao, G., & Luo, S. (2014). Down-Regulation of Gli Transcription Factor Leads to the Inhibition of Migration and Invasion of Ovarian Cancer Cells Via Integrin B4-Mediated Fak Signaling. *PloS one*, **9(2)**, e88386-e88386. https://doi.org/10.1371/journal.pone.0088386

Chen, Y., Ma, J., Wang, F., Hu, J., Cui, A., Wei, C., Yang, Q., & Li, F. (2013). Amygdalin Induces Apoptosis in Human Cervical Cancer Cell Line Hela Cells. *Immunopharmacology and immunotoxicology*, **35(1)**, 43-51.

Cheng, P., Li, J., Wang, J., Zhang, X., & Zhai, H. (2017). Investigations of Fak Inhibitors: A Combination of 3d-Qsar, Docking and Molecular Dynamics Simulations Studies. *Journal of Biomolecular Structure and Dynamics*, **36**, 1-59. https://doi.org/10.1080/07391102.2017.1329095

Citrin, D., Bloom, D., Grutsch, J., Mortensen, S., & Lis, C. (2012). Beliefs and Perceptions of Women with Newly Diagnosed Breast Cancer Who Refused Conventional Treatment in Favor of Alternative Therapies. *The oncologist*, **17**, 607-612. https://doi.org/10.1634/theoncologist.2011-0468

Clute, P., & Pines, J. (1999). Temporal and Spatial Control of Cyclin B1 Destruction in Metaphase. *Nature cell biology*, **1(2)**, 82.

Cohen, P., & Alessi, D. R. (2013). Kinase Drug Discovery--What's Next in the Field? *ACS chemical biology*, **8(1)**, 96-104. https://doi.org/10.1021/cb300610s

Cole, M. P., Jones, C. T. A., & Todd, I. D. H. (1971). A New Anti-Oestrogenic Agent in Late Breast Cancer: An Early Clinical Appraisal of Ici46474. *British Journal of Cancer*, **25**, 270-275.

Cozzini, P., Fornabaio, M., Marabotti, A., Abraham, D. J., Kellogg, G. E., & Mozzarelli, A. (2004). Free Energy of Ligand Binding to Protein: Evaluation of the Contribution of Water Molecules by Computational Methods. *Current medicinal chemistry*, **11(23)**, 3093-3118.

Croce, C. M., & Reed, J. C. (2016). Finally, an Apoptosis-Targeting Therapeutic for Cancer. *Cancer Research*, **76(20)**, 5914-5920.

Curt, G. A. (1990). Unsound Methods of Cancer Treatment. *Principles Pract Oncol*, 4, 1-10.

Daneial, B., Joseph, J., & Ramakrishna, G. (2017). Molecular Dynamics Simulation Analysis of Focal Adhesive Kinase (Fak) Docked with Solanesol as an Anti-Cancer Agent. *Bioinformation*, **13**, 274-283. https://doi.org/10.6026/97320630013274

Daniel, A. B. d. O., & João, B. L. M. (2015). Qm/Mm (Oniom) Calculation on Fak/Dasatinib Docking. *Revista Processos Químicos*, **9(18)**. https://doi.org/10.19142/rpq.v9i18.259

Dash, R., Choi, H. J., & Moon, I. S. (2019). Mechanistic Insights into the Deleterious Role of Nasu-Hakola Disease Associated Trem2 Variants. *bioRxiv*, 705608. https://doi.org/10.1101/705608

Davies, T. G., Pratt, D. J., Endicott, J. A., Johnson, L. N., & Noble, M. E. (2002). Structure-Based Design of Cyclin-Dependent Kinase Inhibitors. *Pharmacology & therapeutics*, **93(2-3)**, 125-133.

Desgrosellier, J. S., & Cheresh, D. A. (2010). Integrins in Cancer: Biological Implications and Therapeutic Opportunities. *Nature Reviews Cancer*, **10(1)**, 9-22. https://doi.org/10.1038/nrc2748

Diamantopoulos, P. T., Sofotasiou, M., Papadopoulou, V., Polonyfi, K., Iliakis, T., & Viniou, N.-A. (2014). Parp1-Driven Apoptosis in Chronic Lymphocytic Leukemia. *BioMed research international*, 2014.

Dickson, M. A. (2014). Molecular Pathways: Cdk4 Inhibitors for Cancer Therapy. *Clinical Cancer Research*, **20(13)**, 3379-3383. https://doi.org/10.1158/1078-0432.ccr-13-1551

Ding, J., Zhang, Z., Roberts, G. J., Falcone, M., Miao, Y., Shao, Y., Zhang, X. C., Andrews, D. W., & Lin, J. (2010). Bcl-2 and Bax Interact Via the Bh1–3 Groove-Bh3 Motif Interface and a Novel Interface Involving the Bh4 Motif. *Journal of Biological Chemistry*, **285(37)**, 28749-28763.

Dong, K., Yang, X., Zhao, T., & Zhu, X. (2017). An Insight into the Inhibitory Selectivity of 4-(Pyrazol-4-Yl)-Pyrimidines to Cdk4 over Cdk2. *Molecular Simulation*, **43(8)**, 599-609.

Dorr, R., & Paxinos, J. (1978). The Current Status of Laetrile. *Annals of internal medicine*, **89**, 389-397. https://doi.org/10.7326/0003-4819-89-3-389

Eduardo Sanabria-Chanaga, E., Betancourt-Conde, I., Hernández-Campos, A., Téllez-Valencia, A., & Castillo, R. (2019). In Silico Hit Optimization toward Akt Inhibition: Fragment-Based Approach, Molecular Docking and Molecular Dynamics Study. *Journal of Biomolecular Structure and Dynamics*, **37(16)**, 4301-4311. https://doi.org/10.1080/07391102.2018.1546618

Erickson, J., Jalaie, M., Robertson, D., Lewis, R., & Vieth, M. (2004). Lessons in Molecular Recognition: The Effects of Ligand and Protein Flexibility on Molecular Docking Accuracy. *Journal of medicinal chemistry*, 47, 45-55. https://doi.org/10.1021/jm030209y

Essmann, U., Perera, L., Berkowitz, M., Darden, T., Lee, H., & Pedersen, L. (1995). A Smooth Particle Mesh Ewald Method. *J. Chem. Phys.*, **103**, 8577. https://doi.org/10.1063/1.470117

Ewing, T., Makino, S., Skillman, G., & Kuntz, I. (2001). Dock 4.0: Search Strategies for Automated Molecular Docking of Flexible Molecule Databases. *Journal of computer-aided molecular design*, **15**, 411-428. https://doi.org/10.1023/A:1011115820450

Feinstein, W. P., & Brylinski, M. (2015). Calculating an Optimal Box Size for Ligand Docking and Virtual Screening against Experimental and Predicted Binding Pockets. *Journal of cheminformatics*, **7(1)**, 18.

Ferreira, L., dos Santos, R., Oliva, G., & Andricopulo, A. (2015). Molecular Docking and Structure-Based Drug Design Strategies. *Molecules*, **20(7)**, 13384-13421.

Fidler, I. J. (2002a). Critical Determinants of Metastasis. *Seminars in Cancer Biology*, **12(2)**, 89-96. https://doi.org/https://doi.org/10.1006/scbi.2001.0416

Fidler, I. J. (2002b). The Organ Microenvironment and Cancer Metastasis. *Differentiation*, **70(9)**, 498-505. https://doi.org/https://doi.org/10.1046/j.1432-0436.2002.700904.x

Fischer, F. H., Lewith, G., Witt, C. M., Linde, K., von Ammon, K., Cardini, F., Falkenberg, T., Fønnebø, V., Johannessen, H., Reiter, B., Uehleke, B., Weidenhammer, W., & Brinkhaus, B. (2014). High Prevalence but Limited Evidence in Complementary and Alternative Medicine: Guidelines for Future Research. *BMC Complementary and Alternative Medicine*, **14(1)**, 46. https://doi.org/10.1186/1472-6882-14-46

Floudas, C., Pardalos, P., Mitchell, J., Phillips, A., Rosen, J., & Eyck, L. (2001). A Coupled Scanning and Optimization Scheme for Analyzing Molecular Interactions. https://doi.org/10.1007/978-1-4757-3218-4_11

Frei, E. (1984). General Motors Cancer Research Foundation Prizes Charles F. Kettering Prize. Acute Leukemia in Children. Model for the Development of Scientific Methodology for Clinical Therapeutic Research in Cancer. *CNCR Cancer*, **53(10)**, 2013-2025.

Frei, E., 3rd, Holland, J. F., Schneiderman, M. A., Pinkel, D., Selkirk, G., Freireich, E. J., Silver, R. T., Gold, G. L., & Regelson, W. (1958). A Comparative Study of Two Regimens of Combination Chemotherapy in Acute Leukemia. *Blood*, **13(12)**, 1126-1148.

Friesner, R., Banks, J., Murphy, R., Halgren, T., Klicic, J., Mainz, D., Repasky, M., Knoll, E., Shelley, M., Perry, J., Shaw, D., Francis, P., & Shenkin, P. (2004). Glide: A New Approach for Rapid, Accurate Docking and Scoring. 1. Method and Assessment of Docking Accuracy. *Journal of medicinal chemistry*, **47**, 1739-1749. https://doi.org/10.1021/jm0306430

Fry, D. W., Harvey, P. J., Keller, P. R., Elliott, W. L., Meade, M., Trachet, E., Albassam, M., Zheng, X., Leopold, W. R., & Pryer, N. K. (2004). Specific Inhibition of Cyclin-Dependent Kinase 4/6 by Pd 0332991 and Associated Antitumor Activity in Human Tumor Xenografts. *Molecular cancer therapeutics*, **3(11)**, 1427-1438.

Genheden, S., & Ryde, U. (2015). The Mm/Pbsa and Mm/Gbsa Methods to Estimate Ligand-Binding Affinities. *Expert Opinion on Drug Discovery*, **10(5)**, 449-461. https://doi.org/10.1517/17460441.2015.1032936

Gillett, J., Ientile, C., Hiscock, J., Plank, A., & Martin, J. (2012). Complementary and Alternative Medicine Use in Radiotherapy: What Are Patients Using? *Journal of alternative and complementary medicine* (New York, N.Y.), **18**. https://doi.org/10.1089/acm.2011.0334

Gkretsi, V., & Stylianopoulos, T. (2018). Cell Adhesion and Matrix Stiffness: Coordinating Cancer Cell Invasion and Metastasis. *Frontiers in Oncology*, **8**, 145-145. https://doi.org/10.3389/fonc.2018.00145

Goodman, L. S., Wintrobe, M. M., & et al. (1946). Nitrogen Mustard Therapy; Use of Methyl-Bis (Beta-Chloroethyl) Amine Hydrochloride and Tris (Beta-Chloroethyl) Amine Hydrochloride for Hodgkin's Disease, Lymphosarcoma, Leukemia and Certain Allied and Miscellaneous Disorders. *Journal of the American Medical Association*, **132**, 126-132.

Gulzar, M., Ali, S., Khan, F. I., Khan, P., Taneja, P., & Hassan, M. I. (2019). Binding Mechanism of Caffeic Acid and Simvastatin to the Integrin Linked Kinase for Therapeutic Implications: A Comparative Docking and Md Simulation Studies. *Journal of Biomolecular Structure and Dynamics*, **37(16)**, 4327-4337. https://doi.org/10.1080/07391102.2018.1546621

Gulzar, M., Syed, S. B., Khan, F. I., Khan, P., Ali, S., Hasan, G. M., Taneja, P., & Hassan, M. I. (2019). Elucidation of Interaction Mechanism of Ellagic Acid to the Integrin Linked Kinase. *International Journal of Biological Macromolecules*, **122**, 1297-1304. https://doi.org/https://doi.org/10.1016/j.ijbiomac.2018.09.089

Hall, M., & Peters, G. (1996). Genetic Alterations of Cyclins, Cyclin-Dependent Kinases, and Cdk Inhibitors in Human Cancer. *In Advances in Cancer Research* , **68**, 67-108). Elsevier.

Hanahan, D., & Weinberg, R. A. (2000). The Hallmarks of Cancer. *Cell*, **100(1)**, 57-70. https://doi.org/10.1016/S0092-8674(00)81683-9

Hanahan, D., & Weinberg, Robert A. (2011). Hallmarks of Cancer: The Next Generation. *Cell*, **144(5)**, 646-674. https://doi.org/10.1016/j.cell.2011.02.013

Hannigan, G., Troussard, A. A., & Dedhar, S. (2005). Integrin-Linked Kinase: A Cancer Therapeutic Target Unique among Its Ilk. Nature Reviews Cancer, 5(1), 51-63. https://doi.org/10.1038/nrc1524

Hanwell, M. D., Curtis, D. E., Lonie, D. C., Vandermeersch, T., Zurek, E., & Hutchison, G. R. (2012). Avogadro: An Advanced Semantic Chemical Editor, Visualization, and Analysis Platform. *Journal of cheminformatics*, **4(1)**, 17.

Hess, U., Blairy, S., & Kleck, R. (1997). The Intensity of Emotional Facial Expressions and Decoding Accuracy. Journal of Nonverbal Behavior, 21, 241-257. https://doi.org/10.1023/A:1024952730333

Hinchliffe, A. (2011). Molecular Modeling for Beginners. In.

Hirsch, J. (2006). An Anniversary for Cancer Chemotherapy. *JAMA*, **296(12)**, 1518-1520.

Hitchings, G. H., & Elion, G. B. (1954). The Chemistry and Biochemistry of Purine Analogs. NYAS Annals of the New York *Academy of Sciences*, **60(2)**, 195-199.

Holt, L. J., Tuch, B. B., Villén, J., Johnson, A. D., Gygi, S. P., & Morgan, D. O. (2009). Global Analysis of Cdk1 Substrate Phosphorylation Sites Provides Insights into Evolution. *Science*, **325(5948)**, 1682-1686.

Honarparvar, B., Govender, T., Maguire, G. E. M., Soliman, M. E. S., & Kruger, H. G. (2014). Integrated Approach to Structure-Based Enzymatic Drug Design: Molecular Modeling, Spectroscopy, and Experimental Bioactivity. *Chemical Reviews*, **114(1)**, 493-537. https://doi.org/10.1021/cr300314q

Huebner, J., Micke, O., Mücke, R., Buentzel, J., Prott, F., Kleeberg, U., Senf, B., & Münstedt, K. (2014). User Rate of Complementary and Alternative Medicine (Cam) of Patients Visiting a Counseling Facility for Cam of a German Comprehensive Cancer Center. *Anticancer research*, **34**, 943-948.

Institute, N. C. (2018, April 5). Laetrile/Amygdalin (Pdq®)–Patient Version. https://www.cancer.gov/about-cancer/treatment/cam/patient/laetrile-pdq

Jain, A. (2003). Surflex: Fully Automatic Flexible Molecular Docking Using a Molecular Similarity-Based Search Engine. *Journal of medicinal chemistry*, **46**, 499-511. https://doi.org/10.1021/jm020406h

Jan, R. (2019). Understanding Apoptosis and Apoptotic Pathways Targeted Cancer Therapeutics. *Advanced pharmaceutical bulletin*, **9(2)**, 205.

Jean, C., Chen, X. L., Nam, J.-O., Tancioni, I., Uryu, S., Lawson, C., Ward, K. K., Walsh, C. T., Miller, N. L. G., Ghassemian, M., Turowski, P., Dejana, E., Weis, S., Cheresh, D. A., & Schlaepfer, D. D. (2014). Inhibition of Endothelial Fak Activity Prevents Tumor Metastasis by Enhancing Barrier Function. *The Journal of Cell Biology*, **204(2)**, 247. https://doi.org/10.1083/jcb.201307067

Jensen, F. (1989). An Introduction to Computational Chemistry. 2.

Johnson, I. S., Armstrong, J. G., Gorman, M., & Burnett, J. P., Jr. (1963). The Vinca Alkaloids: A New Class of Oncolytic Agents. *Cancer Research*, **23**, 1390-1427.

Jones, G., Willett, P., Glen, R., Leach, A., & Taylor, R. (1997). Development and Validation of a Genetic Algorithm for Flexible Docking. *Journal of molecular biology*, **267**, 727-748. https://doi.org/10.1006/jmbi.1996.0897

Juengel, E., Thomas, A., Rutz, J., Makarevic, J., Tsaur, I., Nelson, K., Haferkamp, A., & Blaheta, R. A. (2016). Amygdalin Inhibits the Growth of Renal Cell Carcinoma Cells in Vitro. *International journal of molecular medicine*, **37(2)**, 526-532. https://doi.org/10.3892/ijmm.2015.2439

Kamerlin, S. C., Haranczyk, M., & Warshel, A. (2009). Progress in Ab Initio Qm/Mm Free-Energy Simulations of Electrostatic Energies in Proteins: Accelerated Qm/Mm Studies of P K a, Redox Reactions and Solvation Free Energies. *The Journal of Physical Chemistry B*, **113(5)**, 1253-1272.

Khan, M. T. H. (2009). Molecular Interactions of Cholinesterases Inhibitors Using in Silico Methods: Current Status and Future Prospects. *New biotechnology*, **25**, 331-346. https://doi.org/10.1016/j.nbt.2009.03.008

Kim, S., Thiessen, P. A., Bolton, E. E., Chen, J., Fu, G., Gindulyte, A., Han, L., He, J., He, S., Shoemaker, B. A., Wang, J., Yu, B., Zhang, J., & Bryant, S. H. (2015). Pubchem Substance and Compound Databases. *Nucleic acids research*, **44(D1)**, D1202-D1213. https://doi.org/10.1093/nar/gkv951

Knockaert, M., Greengard, P., & Meijer, L. (2002). Pharmacological Inhibitors of Cyclin-Dependent Kinases. *Trends in pharmacological sciences*, **23(9)**, 417-425.

Kollman, P. (1993). Free Energy Calculations: Applications to Chemical and Biochemical Phenomena. *Chemical Reviews*, **93(7)**, 2395-2417.

Konstantinidis, A. K., Radhakrishnan, R., Gu, F., Rao, R. N., & Yeh, W.-K. (1998). Purification, Characterization, and Kinetic Mechanism of Cyclin D1· Cdk4, a Major Target for Cell Cycle Regulation. *Journal of Biological Chemistry*, **273(41)**, 26506-26515.

Kumar, S. (1995). Ice-Like Proteases in Apoptosis. *Trends in biochemical sciences*, **20(5)**, 198-202.

Kumari, R., Kumar, R., Open Source Drug Discovery, C., & Lynn, A. (2014). G_Mmpbsa--a Gromacs Tool for High-Throughput Mm-Pbsa Calculations. *Journal of chemical information and modeling*, **54(7)**, 1951-1962. https://doi.org/10.1021/ci500020m

Kumari, R., & Lynn, A. (2011). Application of Mm/Pbsa in the Prediction of Relative Binding Free Energy: Re-Scoring of Docking Hit-List [Article]. *Journal of Natural Science, Biology and Medicine*, **2(3)**, 92-92. http://www.jnsbm.org/article.asp?issn=0976-9668;year=2011;volume=2;issue=3;spage=92;epage=92;aulast=Kumari

Lapenna, S., & Giordano, A. (2009). Cell Cycle Kinases as Therapeutic Targets for Cancer. *Nature reviews Drug discovery*, **8(7)**, 547.

Lee, H. M., & Moon, A. (2016). Amygdalin Regulates Apoptosis and Adhesion in Hs578t Triple-Negative Breast Cancer Cells. *Biomolecules & therapeutics*, **24(1)**, 62.

Legate, K. R., Montañez, E., Kudlacek, O., & Füssler, R. (2006). Ilk, Pinch and Parvin: The Tipp of Integrin Signalling. *Nature Reviews Molecular Cell Biology*, **7(1)**, 20-31. https://doi.org/10.1038/nrm1789

Li, D., Zhang, Y., Zhang, H., Zhan, C., Li, X., Ba, T., Qiu, Z., E, F., Lv, G., Zou, C., Wang, C., Si, L., Zou, C., Li, Q., & Gao, X. (2018). Cadm2, as a New Target of Mir-10b, Promotes Tumor Metastasis through Fak/Akt Pathway in Hepatocellular Carcinoma. *Journal of experimental & clinical cancer research : CR*, **37(1)**, 46-46. https://doi.org/10.1186/s13046-018-0699-1

Lim, S., & Kaldis, P. (2013). Cdks, Cyclins and Ckis: Roles Beyond Cell Cycle Regulation. *Development*, **140(15)**, 3079-3093.

Liu, H., Radisky, D. C., Nelson, C. M., Zhang, H., Fata, J. E., Roth, R. A., & Bissell, M. J. (2006). Mechanism of Akt1 Inhibition of Breast Cancer Cell Invasion Reveals a Protumorigenic Role for Tsc2. *Proceedings of the National Academy of Sciences of the United States of America*, **103(11)**, 4134. https://doi.org/10.1073/pnas.0511342103

Liu, X., Zou, H., Slaughter, C., & Wang, X. (1997). Dff, a Heterodimeric Protein That Functions Downstream of Caspase-3 to Trigger DNA Fragmentation During Apoptosis. *Cell*, **89(2)**, 175-184.

Lord, C. J., & Ashworth, A. (2010). Biology-Driven Cancer Drug Development: Back to the Future. *BMC Biol BMC Biology*, **8(1)**, 1-12.

Makarević, J., Rutz, J., Juengel, E., Kaulfuss, S., Reiter, M., Tsaur, I., Bartsch, G., Haferkamp, A., & Blaheta, R. A. (2014). Amygdalin Blocks Bladder Cancer Cell Growth in Vitro by Diminishing Cyclin a and Cdk2. *PloS one*, **9(8)**, e105590. https://doi.org/10.1371/journal.pone.0105590

Makarević, J., Rutz, J., Juengel, E., Kaulfuss, S., Tsaur, I., Nelson, K., Pfitzenmaier, J., Haferkamp, A., & Blaheta, R. A. (2014). Amygdalin Influences Bladder Cancer Cell Adhesion and Invasion in Vitro. *PloS one*, **9(10)**, e110244.

Malumbres, M., & Barbacid, M. (2005). Mammalian Cyclin-Dependent Kinases. *Trends in biochemical sciences*, **30(11)**, 630-641.

Malumbres, M., & Barbacid, M. (2009). Cell Cycle, Cdks and Cancer: A Changing Paradigm. *Nature reviews cancer*, **9(3)**, 153.

Manning, G., Whyte, D. B., Martinez, R., Hunter, T., & Sudarsanam, S. (2002). The Protein Kinase Complement of the Human Genome. *Science*, **298(5600**), 1912-1934.

McDonald, P. C., Fielding, A. B., & Dedhar, S. (2008). Integrin-Linked Kinase – Essential Roles in Physiology and Cancer Biology. *Journal of Cell Science*, **121(19)**, 3121. https://doi.org/10.1242/jcs.017996

Meiselbach, H., Horn, A. H., Harrer, T., & Sticht, H. (2007). Insights into Amprenavir Resistance in E35d Hiv-1 Protease Mutation from Molecular Dynamics and Binding Free-Energy Calculations. *Journal of Molecular Modeling*, **13(2)**, 297-304.

Merlo, L. M. F., Pepper, J. W., Reid, B. J., & Maley, C. C. (2006). Cancer as an Evolutionary and Ecological Process. *Nature Reviews Cancer*, **6(12)**, 924-935. https://doi.org/10.1038/nrc2013

Milazzo, S., Lejeune, S., & Ernst, E. (2007). Laetrile for Cancer: A Systematic Review of the Clinical Evidence. *Supportive care in cancer : official journal of the Multinational Association of Supportive Care in Cancer*, **15**, 583-595. https://doi.org/10.1007/s00520-006-0168-9

Mitra, A., Biswas, R., Bagchi, A., & Ghosh, R. (2019). Insight into the Binding of a Synthetic Nitro-Flavone Derivative with Human Poly-Adp Ribose Polymerase 1. *International Journal of Biological Macromolecules*.

Mohammad, R. M., Muqbil, I., Lowe, L., Yedjou, C., Hsu, H.-Y., Lin, L.-T., Siegelin, M. D., Fimognari, C., Kumar, N. B., & Dou, Q. P. (2015). Broad Targeting of Resistance to Apoptosis in Cancer. *Seminars in cancer biology*,

Morgan, D. O. (1997). Cyclin-Dependent Kinases: Engines, Clocks, and Microprocessors. *Annual review of cell and developmental biology*, **13(1)**, 261-291.

Morris, G. (1998). Automated Docking Using a Lamarckian Genetic Algorithm and Empirical Binding Free Energy Function. *J. Comput. Chem.*, **19**.

https://doi.org/10.1002/(SICI)1096-987X(19981115)19:14<1639::AID-JCC10>3.0.CO;2-B

Morris, G., & Huey, R. (2009). Autodock4 and Autodocktools4: Automated Docking with Selective Receptor Flexibility. *J. Comput. Chem*., **48**, 443-453.

Moss, R. W. (2005). Patient Perspectives: Tijuana Cancer Clinics in the Post-Nafta Era. *Integrative Cancer Therapies*, **4(1)**, 65-86. https://doi.org/10.1177/1534735404273918

Mukherjee, S., Balius, T., & Rizzo, R. (2010). Docking Validation Resources: Protein Family and Ligand Flexibility Experiments. *Journal of chemical information and modeling*, **50,** 1986-2000. https://doi.org/10.1021/ci1001982

Newmark, J., Brady, R., Grimley, P., Gal, A., Waller, S., & Thistlethwaite, J. (1981). Amygdalin (Laetrile) and Prunasin Beta-Glucosidases: Distribution in Germ-Free Rat and in Human Tumor Tissue. *Proceedings of the National Academy of Sciences of the United States of America*, **78**, 6513-6516. https://doi.org/10.1073/pnas.78.10.6513

Nitulescu, G. M., Van De Venter, M., Nitulescu, G., Ungurianu, A., Juzenas, P., Peng, Q., Olaru, O. T., Grădinaru, D., Tsatsakis, A., Tsoukalas, D., Spandidos, D. A., & Margina, D. (2018). The Akt Pathway in Oncology Therapy and Beyond (Review). *International journal of oncology*, **53(6)**, 2319-2331. https://doi.org/10.3892/ijo.2018.4597

Obaya, A., & Sedivy, J. M. (2002). Regulation of Cyclin-Cdk Activity in Mammalian Cells. *Cellular and Molecular Life Sciences CMLS*, **59(1)**, 126-142.

Olson, A. J., & Goodsell, D. (1998). Automated Docking and the Search for Hiv Protease Inhibitors. *SAR and QSAR in environmental research*, **8**, 273-285. https://doi.org/10.1080/10629369808039144

Owens, L., Lh, X., Craven, R., Dent, G., Weiner, T., Kornberg, L., Liu, E., & Cance, W. (1995). Overexpression of the Focal Adhesion Kinase (P125fak) in Invasive Human Tumors. *Cancer Research*, **55**, 2752-2755.

Pandey, R. K., Kumbhar, B. V., Sundar, S., Kunwar, A., & Prajapati, V. K. (2017). Structure-Based Virtual Screening, Molecular Docking, Admet and Molecular Simulations to Develop Benzoxaborole Analogs as Potential Inhibitor against Leishmania Donovani Trypanothione Reductase. *Journal of receptors and signal transduction*, **37(1)**, 60-70.

Park, H.-J., Yoon, S.-H., Han, L.-S., Zheng, L.-T., Jung, K.-H., Uhm, Y.-K., Lee, J.-H., Jeong, J.-S., Joo, W.-S., & Yim, S.-V. (2005). Amygdalin Inhibits Genes Related to Cell Cycle in Snu-C4 Human Colon Cancer Cells. *World journal of gastroenterology: WJG*, **11(33)**, 5156.

Parker, P., Urbauer, D., Fisch, M., Fellman, B., Hough, H., Miller, J., Lanzotti, V., Whisnant, M., Weiss, M., Fellenz, L., Bury, M., Kokx, P., Finn, K., Daily, M., & Cohen, L. (2013). A Multisite, Community Oncology-Based Randomized Trial of a Brief Educational Intervention to Increase Communication Regarding Complementary and Alternative Medicine. *Cancer*, **119**. https://doi.org/10.1002/cncr.28240

Parrill, A. L., & Lipkowitz, K. B. (2016). Reviews in Computational Chemistry. https://doi.org/10.1002/9781119148739

Parrinello, M., & Rahman, A. (1981). Polymorphic Transitions in Single Crystals: A New Molecular Dynamics Method. *Journal of Applied physics*, **52(12)**, 7182-7190.

Persad, S., & Dedhar, S. (2003). The Role of Integrin-Linked Kinase (Ilk) in Cancer Progression. *Cancer and Metastasis Reviews*, **22(4)**, 375-384. https://doi.org/10.1023/A:1023777013659

Peters, J.-M. (2006). The Anaphase Promoting Complex/Cyclosome: A Machine Designed to Destroy. *Nature reviews Molecular cell biology*, **7(9)**, 644.

Petersen, J., & Markle, G. (1984). The Laetrile Controversy. In (pp. 175-196).

Pfeffer, C., & Singh, A. (2018). Apoptosis: A Target for Anticancer Therapy. *International Journal of Molecular Sciences*, **19(2)**, 448.

Pines, J., & Hunter, T. (1989). Isolation of a Human Cyclin Cdna: Evidence for Cyclin Mrna and Protein Regulation in the Cell Cycle and for Interaction with P34cdc2. *Cell*, **58(5)**, 833-846.

Pinto, M., Perez, J. J., & Rubio-Martinez, J. (2004). Molecular Dynamics Study of Peptide Segments of the Bh3 Domain of the Proapoptotic Proteins Bak, Bax, Bid and Hrk Bound to the Bcl-X L and Bcl-2 Proteins. *Journal of computer-aided molecular design*, **18(1)**, 13-22.

Plewczynski, D., Lazniewski, M., Augustyniak, R., & Ginalski, K. (2011). Can We Trust Docking Results? Evaluation of Seven Commonly Used Programs on Pdbbind Database. *Journal of computational chemistry*, **32**, 742-755. https://doi.org/10.1002/jcc.21643

Qian, L., Xie, B., Wang, Y., & Qian, J. (2015). Amygdalin-Mediated Inhibition of Non-Small Cell Lung Cancer Cell Invasion in Vitro. *International journal of clinical and experimental pathology*, **8(5)**, 5363.

Rarey, M., Kramer, B., Lengauer, T., & Klebe, G. (1996). A Fast Flexible Docking Method Using an Incremental Construction Algorithm. *Journal of molecular biology*, **261**, 470-489. https://doi.org/10.1006/jmbi.1996.0477

Ravindranath, P. A., Forli, S., Goodsell, D. S., Olson, A. J., & Sanner, M. F. (2015). Autodockfr: Advances in Protein-Ligand Docking with Explicitly Specified Binding Site Flexibility. *PLoS computational biology*, **11(12)**, e1004586.

Rigiracciolo, D. C., Santolla, M. F., Lappano, R., Vivacqua, A., Cirillo, F., Galli, G. R., Talia, M., Muglia, L., Pellegrino, M., Nohata, N., Di Martino, M. T., & Maggiolini, M. (2019). Focal Adhesion Kinase (Fak) Activation by Estrogens Involves Gper in Triple-Negative Breast Cancer Cells. *Journal of Experimental & Clinical Cancer Research*, **38(1)**, 58. https://doi.org/10.1186/s13046-019-1056-8

Rogers, D. (1990). Computational Chemistry Using the Pc.

Rudnitskaya, A., Torok, B., & Torok, M. (2010). Molecular Docking of Enzyme Inhibitors: A Computational Tool for Structure-Based Drug Design. *Biochemistry and molecular biology education : a bimonthly publication of the International*

Union of Biochemistry and Molecular Biology, **38**, 261-265. https://doi.org/10.1002/bmb.20392

Saghatchian, M., Bihan, C., Chenailler, C., Mazouni, C., Dauchy, S., & Delaloge, S. (2014). Exploring Frontiers: Use of Complementary and Alternative Medicine among Patients with Early-Stage Breast Cancer. *The Breast*, **23**. https://doi.org/10.1016/j.breast.2014.01.009

Samuel, S., Tumilasci, V. F., Oliere, S., Nguyên, T. L.-A., Shamy, A., Bell, J., & Hiscott, J. (2010). Vsv Oncolysis in Combination with the Bcl-2 Inhibitor Obatoclax Overcomes Apoptosis Resistance in Chronic Lymphocytic Leukemia. *Molecular Therapy*, **18(12)**, 2094-2103.

Sansom, C., & Smith, C. (2010). Computer Applications in the Biomolecular Sciences. Part 1: Molecular Modelling. *Biochemical Education*, **26**, 103-110. https://doi.org/10.1016/S0307-4412(97)00155-6

Sathishkumar, N., Sathiyamoorthy, S., Ramya, M., Yang, D.-U., Lee, H. N., & Yang, D.-C. (2012). Molecular Docking Studies of Anti-Apoptotic Bcl-2, Bcl-Xl, and Mcl-1 Proteins with Ginsenosides from Panax Ginseng. *Journal of enzyme inhibition and medicinal chemistry*, **27(5)**, 685-692.

Satyanarayana, A., & Kaldis, P. (2009). Mammalian Cell-Cycle Regulation: Several Cdks, Numerous Cyclins and Diverse Compensatory Mechanisms. *Oncogene*, **28(33)**, 2925.

Schlick, T. (2010). Biomolecular Structure and Modeling: Historical Perspective. 21. https://doi.org/10.1007/978-1-4419-6351-2_1

Senderowicz, A. M. (2003). Small-Molecule Cyclin-Dependent Kinase Modulators. *Oncogene*, **22(42)**, 6609.

Sharma, P. (2011). An Assessment of the Conformational Profile of Bombesin and Its Mammalian Analogues Using Computational Chemistry Methods

Soldani, C., & Scovassi, A. (2002). Poly (Adp-Ribose) Polymerase-1 Cleavage During Apoptosis: An Update. *Apoptosis*, **7(4)**, 321-328.

Soliman, M. E. S. (2009). *Computational Modelling of Glycosidase Mechanisms University* Library].

Song, Z., & Xu, X. (2014). Advanced Research on Anti-Tumor Effects of Amygdalin. *Journal of cancer research and therapeutics*, **10(5)**, 3.

Strebhardt, K., & Ullrich, A. (2008). Paul Ehrlich's Magic Bullet Concept: 100 Years of Progress. *NATURE REVIEWS CANCER*, **8(6)**, 473-480.

Taliaferro-Smith, L., Oberlick, E., Liu, T., McGlothen, T., Alcaide, T., Tobin, R., Donnelly, S., Commander, R., Kline, E., Nagaraju, G. P., Havel, L., Marcus, A., Nahta, R., & O'Regan, R. (2015). Fak Activation Is Required for Igf1r-Mediated Regulation of Emt, Migration, and Invasion in Mesenchymal Triple Negative Breast Cancer Cells. *Oncotarget*, **6(7)**, 4757-4772. https://doi.org/10.18632/oncotarget.3023

Taylor, R. D., Jewsbury, P. J., & Essex, J. W. (2002). A Review of Protein-Small Molecule Docking Methods. *Journal of computer-aided molecular design*, **16(3)**, 151-166.

Teodoro, M., Phillips, G., & Kavraki, L. (2002). Molecular Docking: A Problem with Thousands of Degrees of Freedom. Proceedings - *IEEE International Conference on Robotics and Automation*, 1. https://doi.org/10.1109/ROBOT.2001.932674

Thamilselvan, V., Craig, D. H., & Basson, M. D. (2007). Fak Association with Multiple Signal Proteins Mediates Pressure-Induced Colon Cancer Cell Adhesion Via a Src-Dependent Pi3k/Akt Pathway. *The FASEB Journal*, **21(8)**, 1730-1741. https://doi.org/10.1096/fj.06-6545com

Thornberry, N. A., Rano, T. A., Peterson, E. P., Rasper, D. M., Timkey, T., Garcia-Calvo, M., Houtzager, V. M., Nordstrom, P. A., Roy, S., & Vaillancourt, J. P. (1997). A Combinatorial Approach Defines Specificities of Members of the Caspase Family and Granzyme B Functional Relationships Established for Key Mediators of Apoptosis. *Journal of Biological Chemistry*, **272(29)**, 17907-17911.

Vanamala, J., Radhakrishnan, S., Reddivari, L., Bhat, V. B., & Ptitsyn, A. (2011). Resveratrol Suppresses Human Colon Cancer Cell Proliferation and Induces

Apoptosis Via Targeting the Pentose Phosphate and the Talin-Fak Signaling Pathways-a Proteomic Approach. *Proteome science*, **9(1)**, 49-49. https://doi.org/10.1186/1477-5956-9-49

Vasanthakumari, D., Vadakkethil Lalithabhai, P., & Kanthimathi Bahuleyan, M. (2019). An in Silico Approach to Discover the Best Molecular Modeling Strategy for Designing Novel Cdk4 Inhibitors. *Chemical Biology & Drug Design*, **93(4)**, 556-569. https://doi.org/10.1111/cbdd.13452

Verma, S., Singh, A., & Mishra, A. (2015). Complex Disruption Effect of Natural Polyphenols on Bcl-2-Bax: Molecular Dynamics Simulation and Essential Dynamics Study. *Journal of Biomolecular Structure and Dynamics*, **33(5)**, 1094-1106.

Virág, L., & Szabó, C. (2002). The Therapeutic Potential of Poly (Adp-Ribose) Polymerase Inhibitors. *Pharmacological reviews*, **54(3)**, 375-429.

Walters, J., Pop, C., Scott, F. L., Drag, M., Swartz, P., Mattos, C., Salvesen, G. S., & Clark, A. C. (2009). A Constitutively Active and Uninhibitable Caspase-3 Zymogen Efficiently Induces Apoptosis. *Biochemical Journal*, **424(3)**, 335-345.

Wang, W., Donini, O., Reyes, C., & Kollman, P. (2001). Biomolecular Simulations: Recent Developments in Force Fields, Simulations of Enzyme Catalysis, Protein-Ligand, Protein-Protein, and Protein-Nucleic Acid Noncovalent Interactions. *Annual review of biophysics and biomolecular structure*, **30**, 211-243. https://doi.org/10.1146/annurev.biophys.30.1.211

Weiner, S., Kollman, P., Case, D., Singh, U., Ghio, C., Alagona, G., Profeta Jr, S., & Weiner, P. (1983). A New Force Field for Molecular Mechanical Simulation of Nucleic Acids and Proteins. *Journal of the American Chemical Society*, **106**, 765-784. https://doi.org/10.1021/ja00315a051

Węsierska- Gądek, J., Gueorguieva, M., Wojciechowski, J., & Tudzarova-Trajkovska, S. (2004). In Vivo Activated Caspase- 3 Cleaves Parp- 1 in Rat Liver after Administration of the Hepatocarcinogen N- Nitrosomorpholine (Nnm) Generating the 85 Kda Fragment. *Journal of cellular biochemistry*, **93(4)**, 774-787.

White, D. E., Cardiff, R. D., Dedhar, S., & Muller, W. J. (2001). Mammary Epithelial-Specific Expression of the Integrin Linked Kinase (Ilk) Results in the Induction of Mammary Gland Hyperplasias and Tumors in Transgenic Mice. *Oncogene*, **20(48)**, 7064-7072. https://doi.org/10.1038/sj.onc.1204910

Wittekind, C., & Neid, M. (2005). Cancer Invasion and Metastasis. *Oncology*, *69(suppl 1)*(Suppl. 1), 14-16. https://doi.org/10.1159/000086626

Xu, Z., Ma, D.-z., Wang, L.-y., Su, J.-m., & Zha, X.-l. (2003). Transforming Growth Factor-B1 Stimulated Protein Kinase B Serine-473 and Focal Adhesion Kinase Tyrosine Phosphorylation Dependent on Cell Adhesion in Human Hepatocellular Carcinoma Smmc-7721 Cells. *Biochemical and Biophysical Research Communications*, **312(2)**, 388-396. https://doi.org/https://doi.org/10.1016/j.bbrc.2003.10.130

Yang, Y., Shen, Y., Liu, H., & Yao, X. (2011). Molecular Dynamics Simulation and Free Energy Calculation Studies of the Binding Mechanism of Allosteric Inhibitors with P38α Map Kinase. *Journal of chemical information and modeling*, **51(12)**, 3235-3246.

Yoon, H., Choi, Y.-L., Song, J.-Y., Do, I., Kang, S. Y., Ko, Y.-H., Song, S., & Kim, B.-G. (2014). Targeted Inhibition of Fak, Pyk2 and Bcl-Xl Synergistically Enhances Apoptosis in Ovarian Clear Cell Carcinoma Cell Lines. *Plos One*, **9(2)**, e88587. https://doi.org/10.1371/journal.pone.0088587

Zhan, J.-Y., Zhang, J.-L., Wang, Y., Li, Y., Zhang, H.-X., & Zheng, Q.-C. (2015). Exploring the Interaction between Human Focal Adhesion Kinase and Inhibitors: A Molecular Dynamic Simulation and Free Energy Calculations. *Journal of Biomolecular Structure and Dynamics*, **34**, 1-56. https://doi.org/10.1080/07391102.2015.1115780

Zhang, L.-L., Liu, J., Lei, S., Zhang, J., Zhou, W., & Yu, H.-G. (2014). Pten Inhibits the Invasion and Metastasis of Gastric Cancer Via Downregulation of Fak Expression. *Cellular Signalling*, **26(5)**, 1011-1020. https://doi.org/https://doi.org/10.1016/j.cellsig.2014.01.025

Zhang, X., Jiang, G., Sun, M., Zhou, H., Miao, Y., Liang, M., Wang, E., & Zhang, Y. (2017). Cytosolic Thumpd1 Promotes Breast Cancer Cells Invasion and Metastasis Via the Akt-Gsk3-Snail Pathway. Oncotarget, 8(8), 13357-13366. https://doi.org/10.18632/oncotarget.14528

Zugazagoitia, J., Guedes, C., Ponce, S., Ferrer, I., Molina-Pinelo, S., & Paz-Ares, L. (2016). Current Challenges in Cancer Treatment. *Clinical Therapeutics*, **38(7)**, 1551-1566. https://doi.org/10.1016/j.clinthera.2016.03.026

APPENDICE

APPENDIX A

Table A. 1 The generated poses of amygdalin inside the binding sites of below listed targeted proteins.

Target	**Rank**	**Estimated Free Energy of Binding (kcal/mol)**	**Estimated Inhibition Constant, Ki (nM)**	**vdW + Hbond + desolv Energy (kcal/mol)**	**Electrostatic Energy (kcal/mol)**	**RMSD (A^0)**
Bcl-2/BAX	1	-8.69	423.98	-10.03	-1.05	2.12
	2	-7.97	1430	-9.49	-0.87	1.793
	3	-7.28	4620	-8.24	-1.43	2.513
	4	-7.2	5230	-9.16	-0.43	2.495
	5	-6.98	7690	-8.08	-1.28	4.121
	6	-6.66	13050	-9	-0.05	4.299
	7	-6.46	18490	-7.39	-1.45	4.074
	8	-6.24	26550	-7.06	-1.57	3.165
	9	-5.99	40700	-7.44	-0.94	3.947
Caspase-3	1	-10.4	23.74	-8.64	-5.94	1.932
	2	-8.91	293.45	-8.71	-4.38	3.961
	3	-8.38	723.85	-7.27	-5.28	3.339
	4	-8.27	871.8	-6.97	-5.47	3.196
	5	-8.27	873.39	-7.82	-4.62	4.481
	6	-8.04	1270	-7.47	-4.75	4.204
	7	-7.62	2600	-6.83	-4.97	3.11
	8	-7.47	3350	-8.07	-3.57	4.358
	9	-7.34	4190	-8.29	-3.23	2.005

Continued on next page

	10	-7.21	5190	-6.19	-5.2	4.379
PARP-1	1	-9.84	61.08	-11.12	-1.11	2.764
	2	-9.43	121.87	-10.98	-0.84	2.781
	3	-9.24	168.49	-10.88	-0.74	0.649
	4	-8.96	269.84	-10.23	-1.12	3.581
	5	-8.92	287.39	-10.01	-1.3	2.5
	6	-8.61	489.68	-9.97	-1.02	3.016
	7	-8	1360	-9.72	-0.67	2.903
	8	-7.88	1690	-10.06	-0.2	2.35
CDK1	1	-9.24	168.62	-10.33	-0.11	0.778
	2	-8.6	494.37	-9.69	-0.1	2.419
CDK2	1	-9.19	183.68	-10.72	-0.86	3.48
	2	-8.56	531.86	-10.33	-0.61	3.977
	3	-8.1	1150	-10.12	-0.37	2.758
	4	-8.04	1280	-10.49	0.06	4.096
	5	-7.71	2240	-9.92	-0.17	2.829
	6	-7.7	2250	-9.96	-0.13	2.493
	7	-7.16	5680	-9.19	-0.35	2.889
CDK4	1	-9.37	136.09	-11.28	-9.37	136.09
	2	-9.31	149.13	-10.85	-9.31	149.13
	3	-8.82	339.96	-10.13	-8.82	339.96
	4	-8.72	403.83	-10.99	-8.72	403.83
	5	-8.4	697.99	-9.3	-8.4	697.99
	6	-8.23	923.84	-9.47	-8.23	923.84
	7	-8.06	1230	-10.52	-8.06	1230
	8	-7.5	3190	-8.69	-7.5	3190
	9	-6.91	8630	-8.59	-6.91	8630
AKT1	1	-8.930	285.780	-9.050	-2.270	3.822
	2	-8.660	448.830	-9.400	-1.640	3.968
	3	-8.230	928.120	-8.720	-1.900	3.763
	4	-8.200	978.610	-9.010	-1.570	4.889

Continued on next page

	5	-8.240	915.970	-9.820	-0.800	2.797
	6	-8.100	1160.000	-10.330	-0.150	2.862
	7	-8.080	1200.000	-9.390	-1.070	1.944
	8	-8.070	1220.000	-10.750	0.290	2.242
	9	-7.820	1850.000	-10.050	-0.148	4.910
	10	-7.420	3640.000	-9.800	-0.010	3.797
ILK	1	-6.340	22420.000	-9.410	-1.100	3.474
	2	-6.180	29570.000	-9.990	-0.088	1.747
	3	-5.820	54020.000	-9.170	-0.830	3.385
	4	-5.810	55350.000	-9.390	-0.600	4.930
	5	-5.800	55760.000	-9.890	-0.090	2.413
	6	-5.720	63870.000	-9.520	-0.380	3.465
	7	-5.560	84400.000	-8.870	-0.870	4.034
	8	-5.500	93150.000	-9.220	-0.450	4.267
	9	-5.490	93840.000	-9.200	-0.470	3.925

APPENDIX B

Energy terms generated from g_mmpbsa (more details are presented in Appendix F and G)

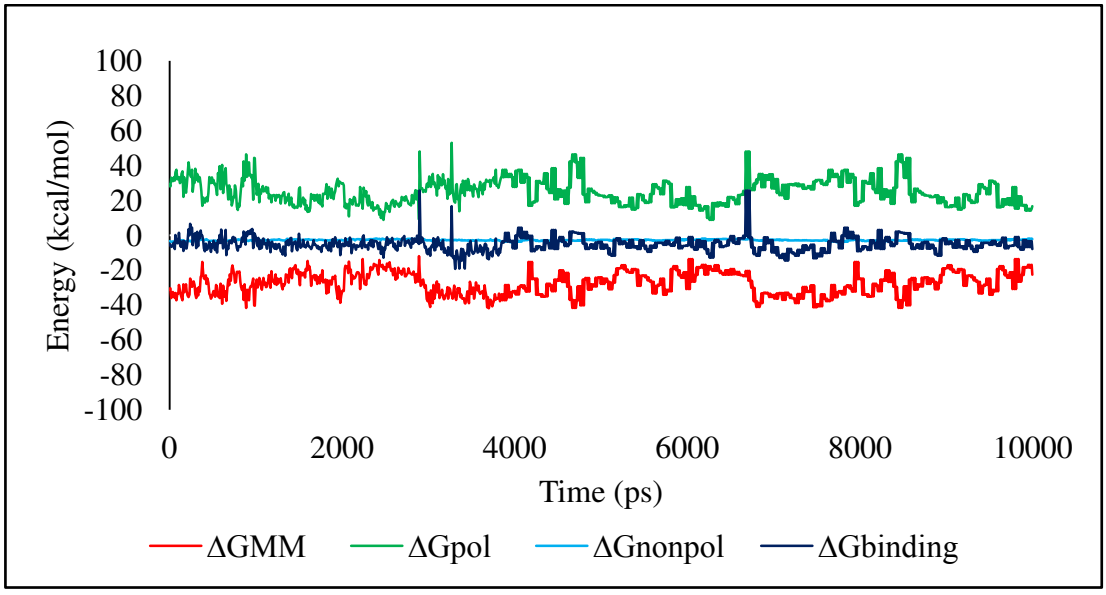

Figure B.1 Energy terms for the binding of amygdalin with Bcl-2.

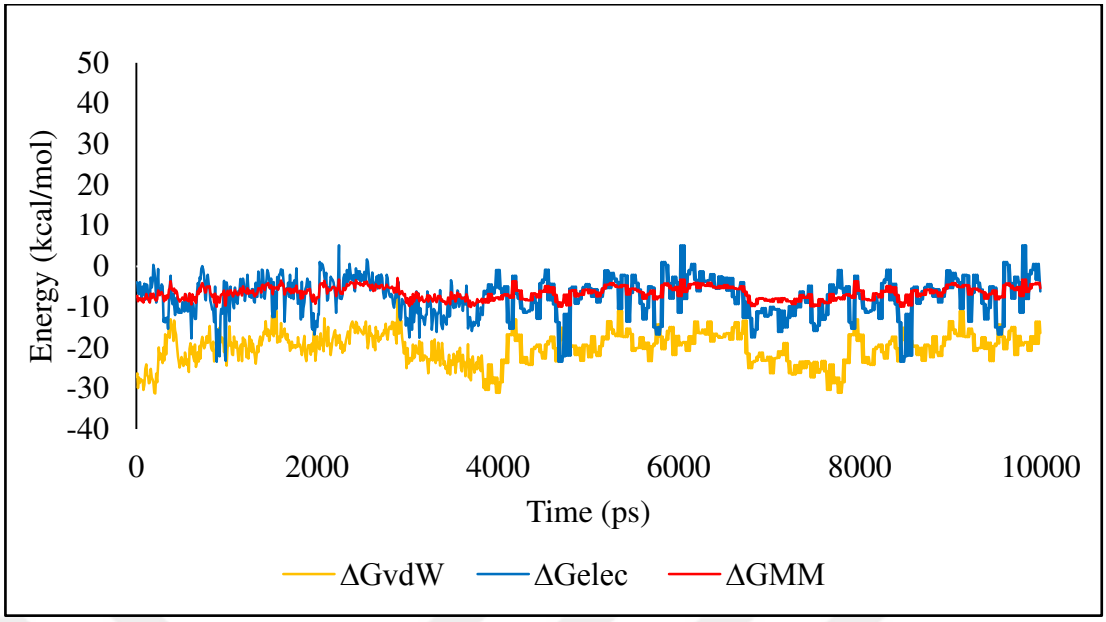

Figure B.2 Decomposition of molecular mechanics energy into electrostatic interaction energy and Vander Waals interaction energy of amygdalin inside the binding site of Bcl-2.

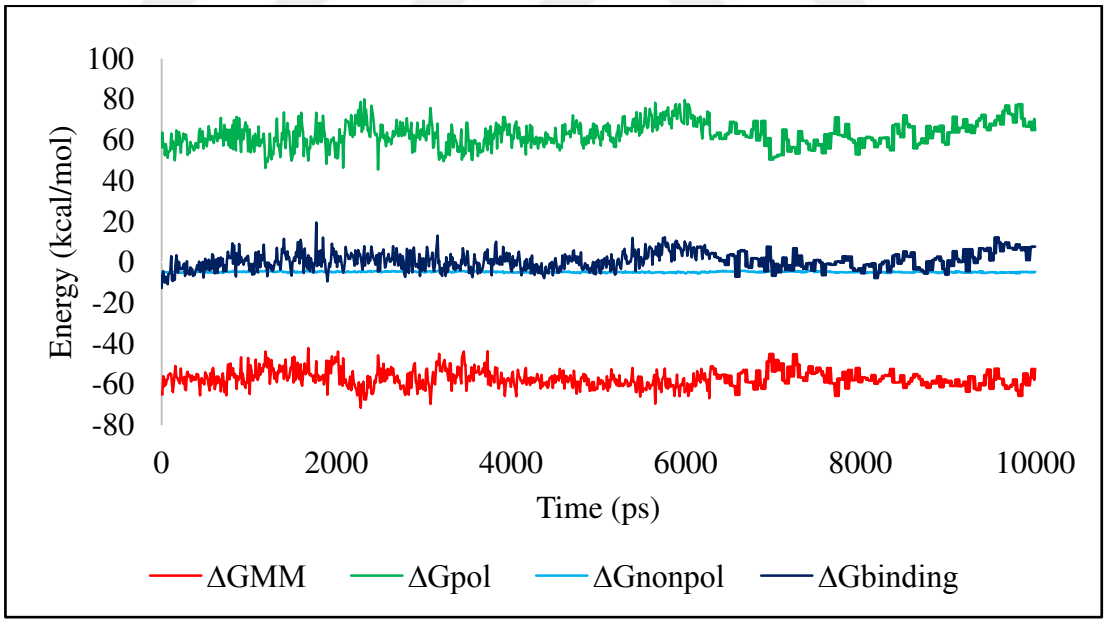

Figure B. 3 Energy terms for the binding of amygdalin with PARP-1.

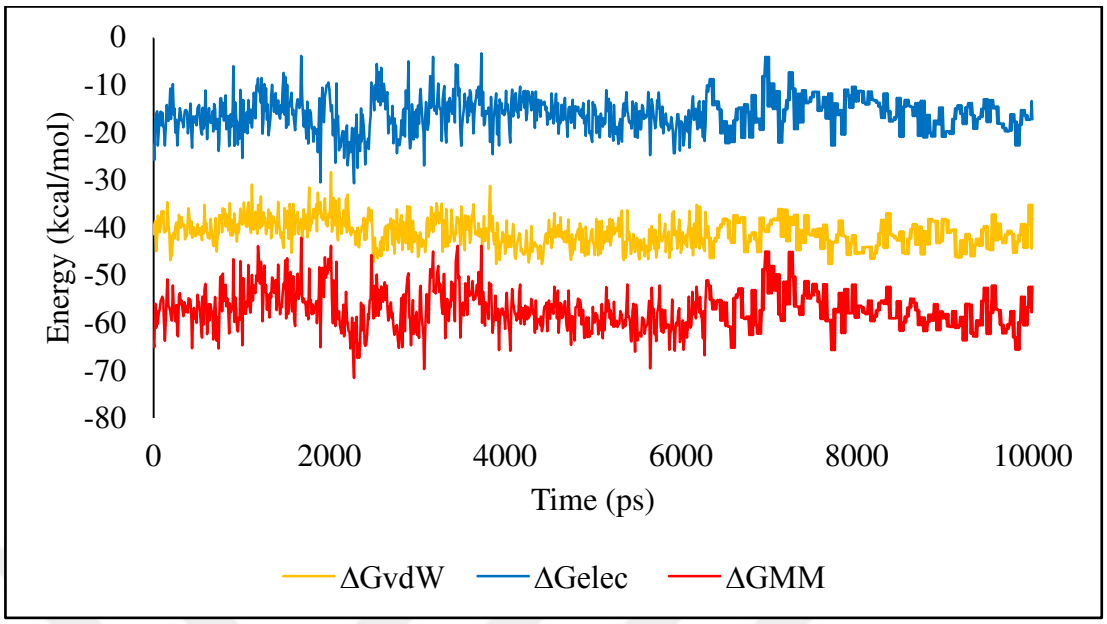

Figure B.4 Decomposition of molecular mechanics energy into electrostatic interaction energy and Vander Waals interaction energy of amygdalin inside the binding site of PARP-1.

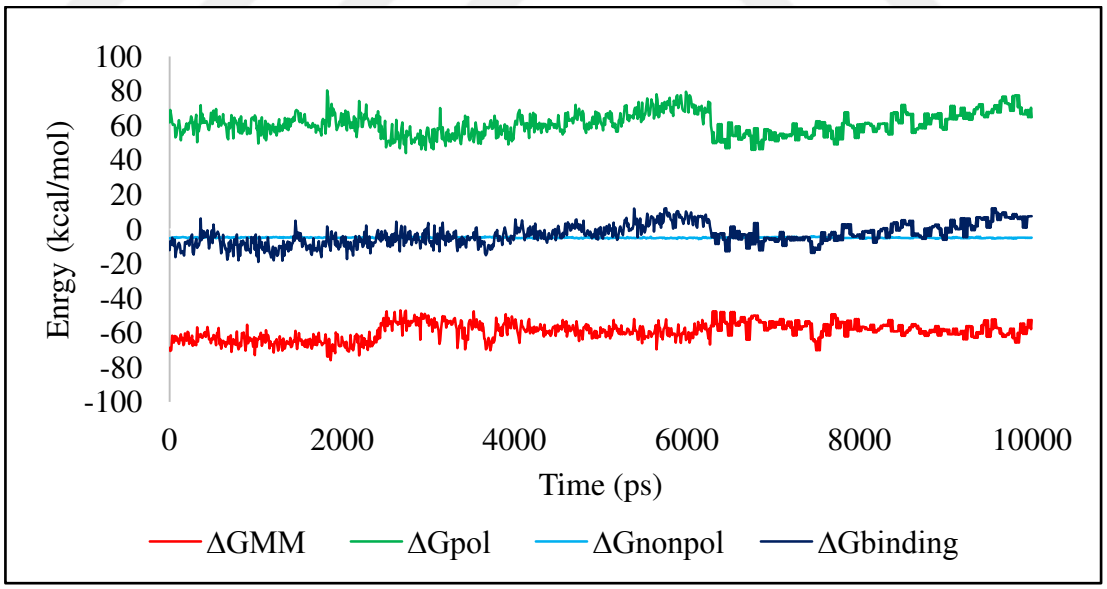

Figure B. 5 Energy terms for the binding of amygdalin with CDK1.

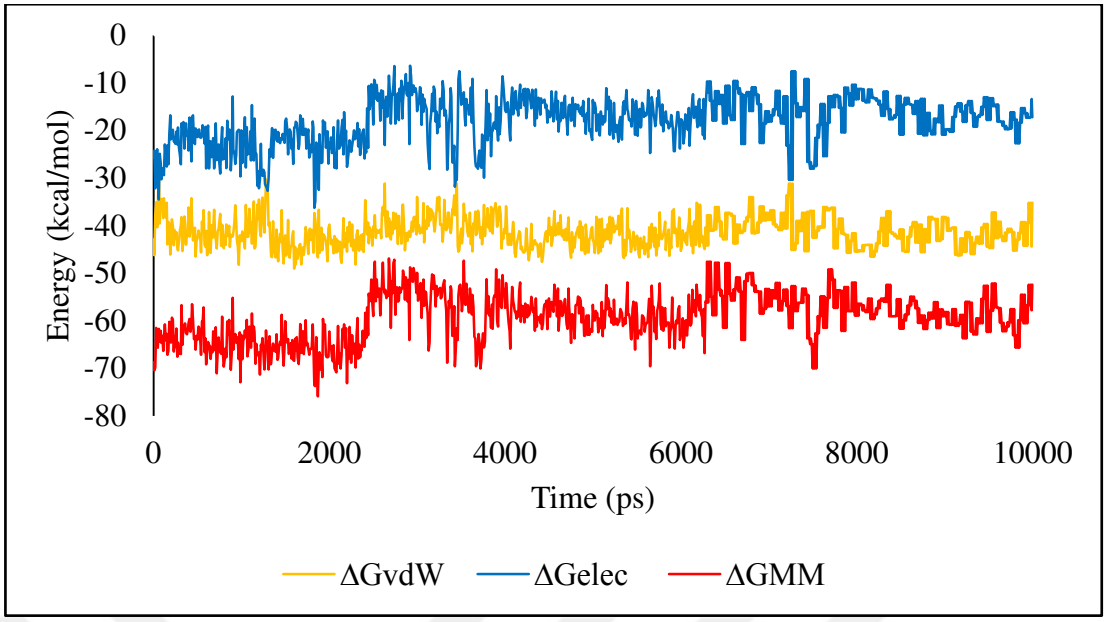

Figure B.6 Decomposition of molecular mechanics energy into electrostatic interaction energy and Vander Waals interaction energy of amygdalin inside the binding site of CDK1.

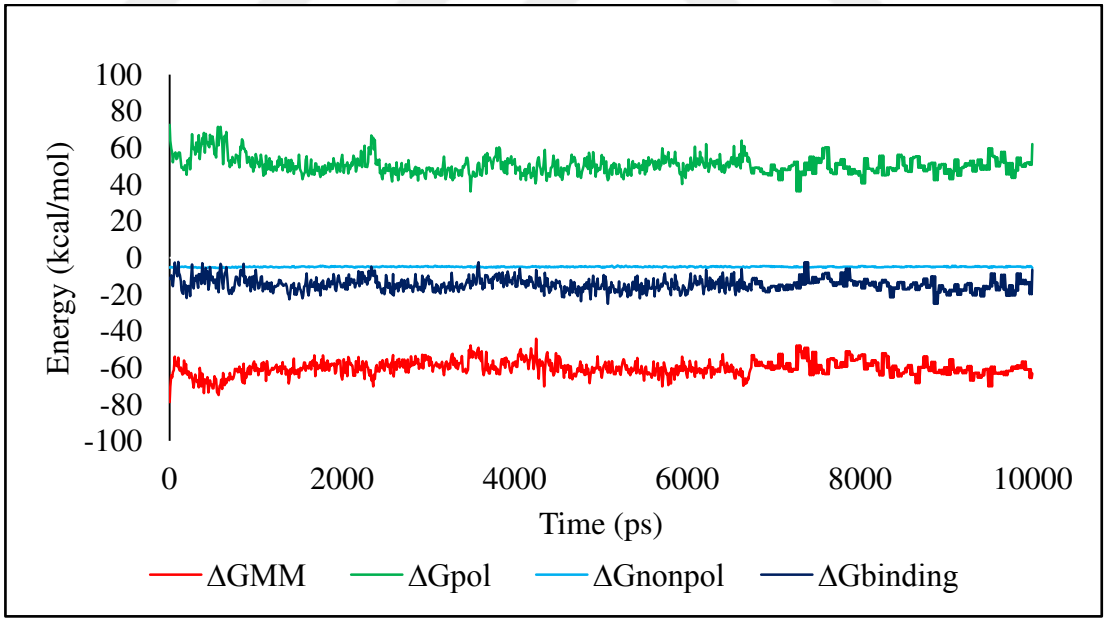

Figure B. 7 Energy terms for the binding of amygdalin with CDK2.

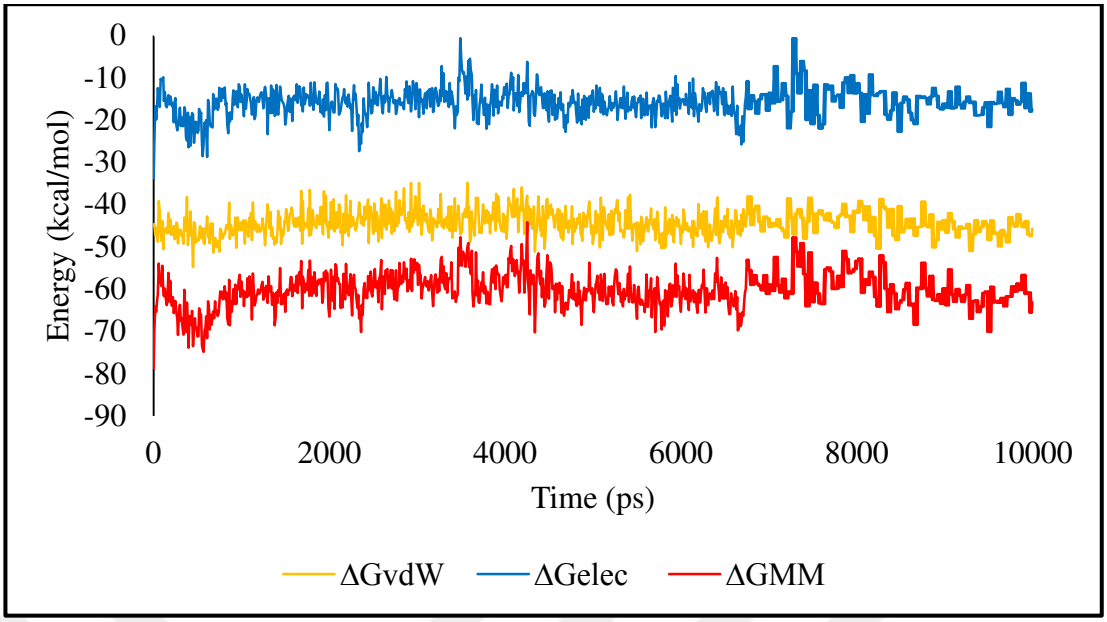

Figure B.8 Decomposition of molecular mechanics energy into electrostatic interaction energy and Vander Waals interaction energy of amygdalin inside the binding site of CDK2.

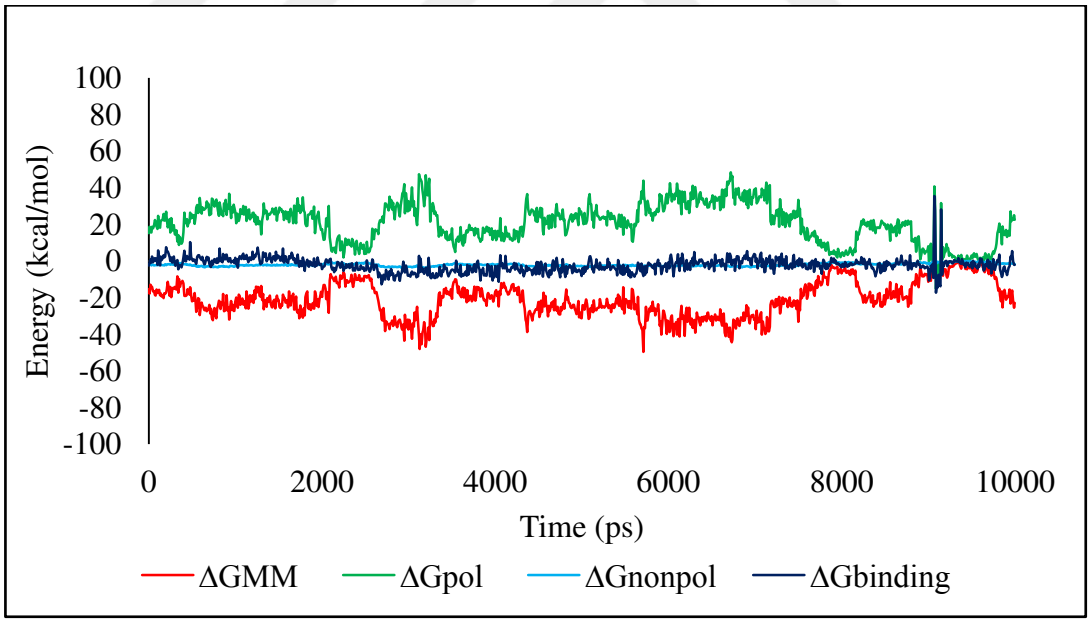

Figure B.9 Energy terms for the binding of amygdalin with CDK4.

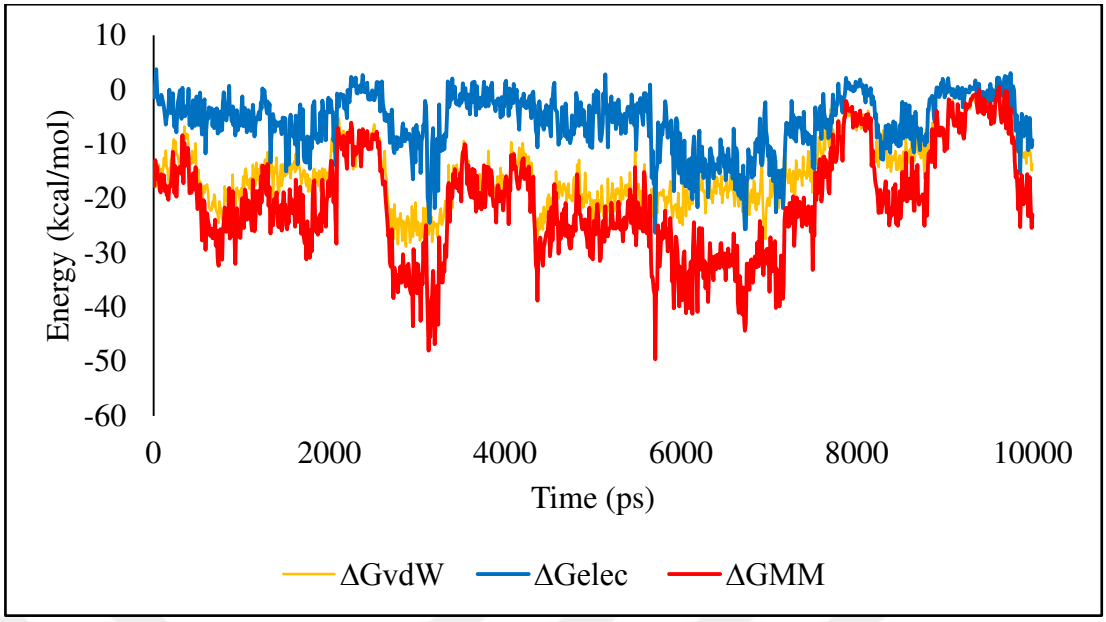

Figure B.10 Decomposition of molecular mechanics energy into electrostatic interaction energy and Vander Waals interaction energy of amygdalin inside the binding site of CDK4.

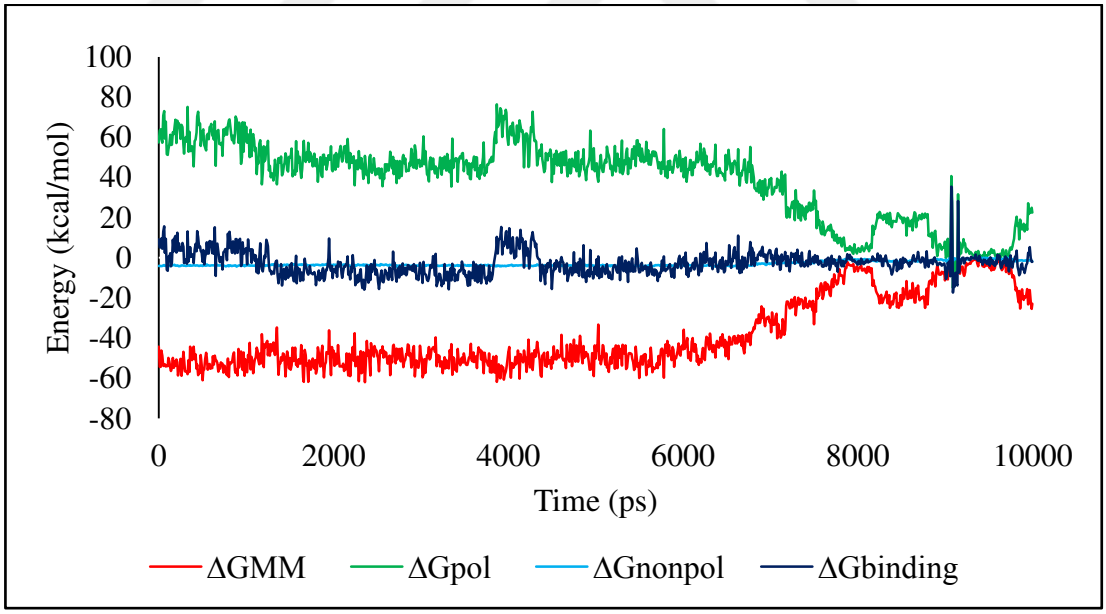

Figure B.11 Energy terms for the binding of amygdalin with AKT1.

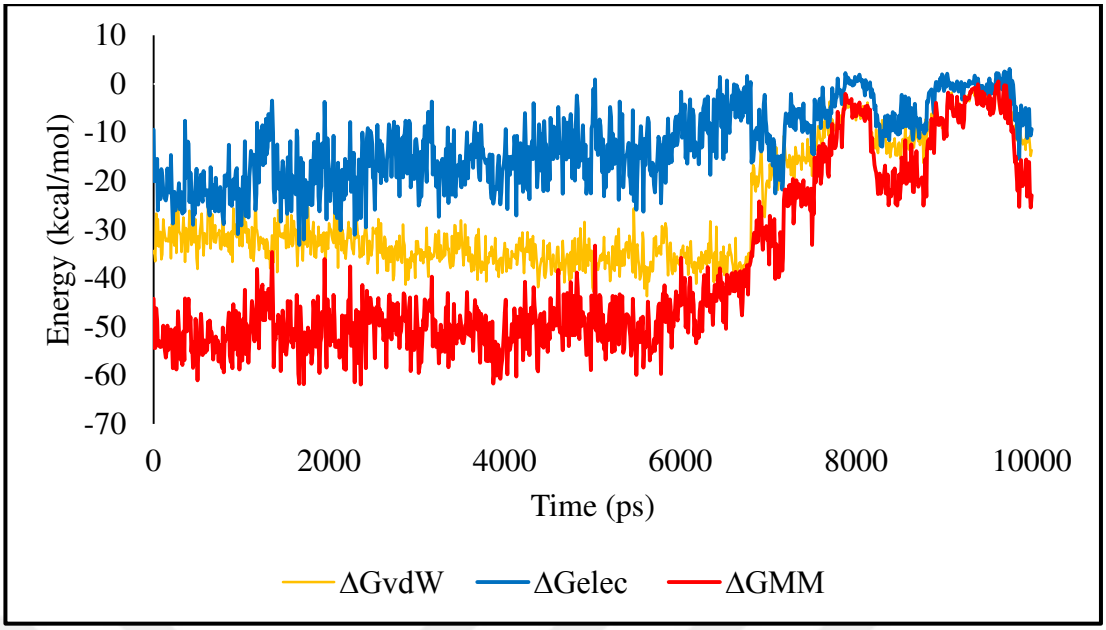

Figure B.12 Decomposition of molecular mechanics energy into electrostatic interaction energy and Vander Waals interaction energy of amygdalin inside the binding site of AKT1.

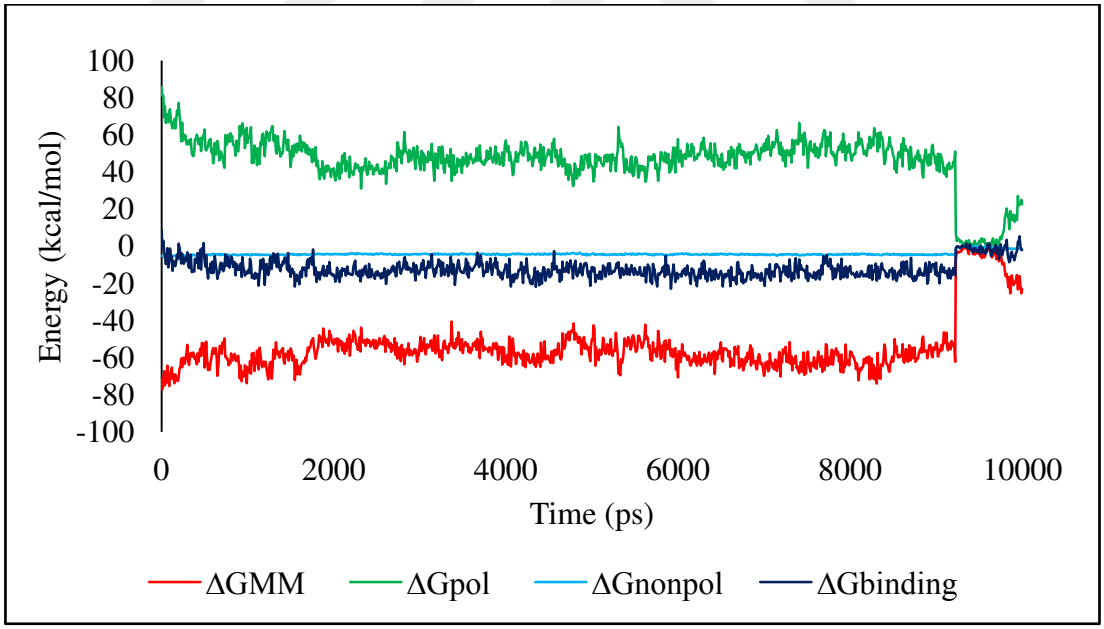

Figure B.13 Energy terms for the binding of amygdalin with FAK1.

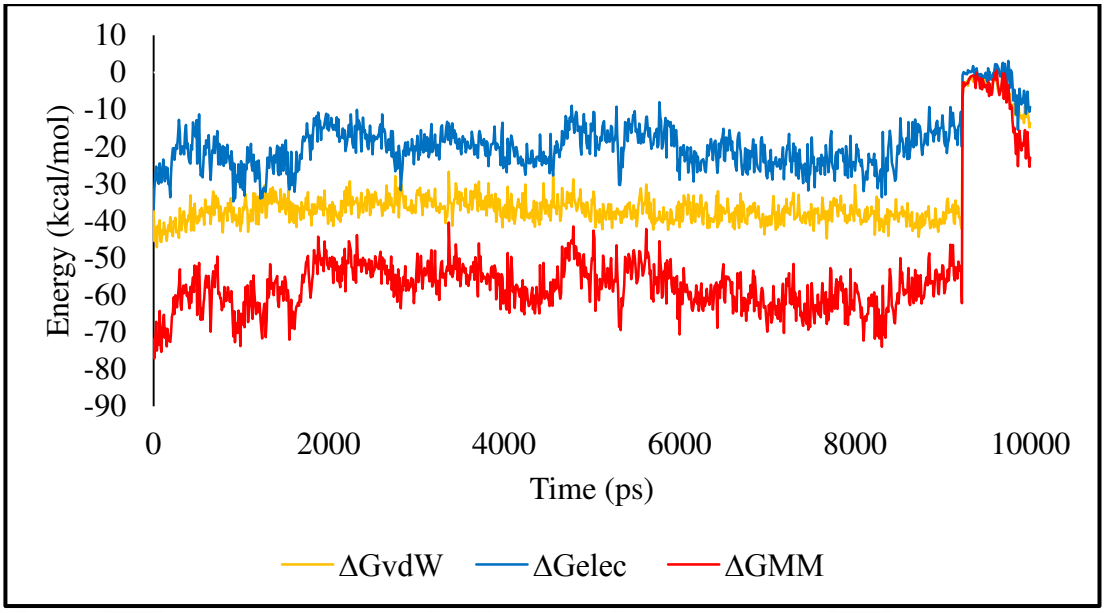

Figure B. 14 Decomposition of molecular mechanics energy into electrostatic interaction energy and Vander Waals interaction energy of amygdalin inside the binding site of FAK1.

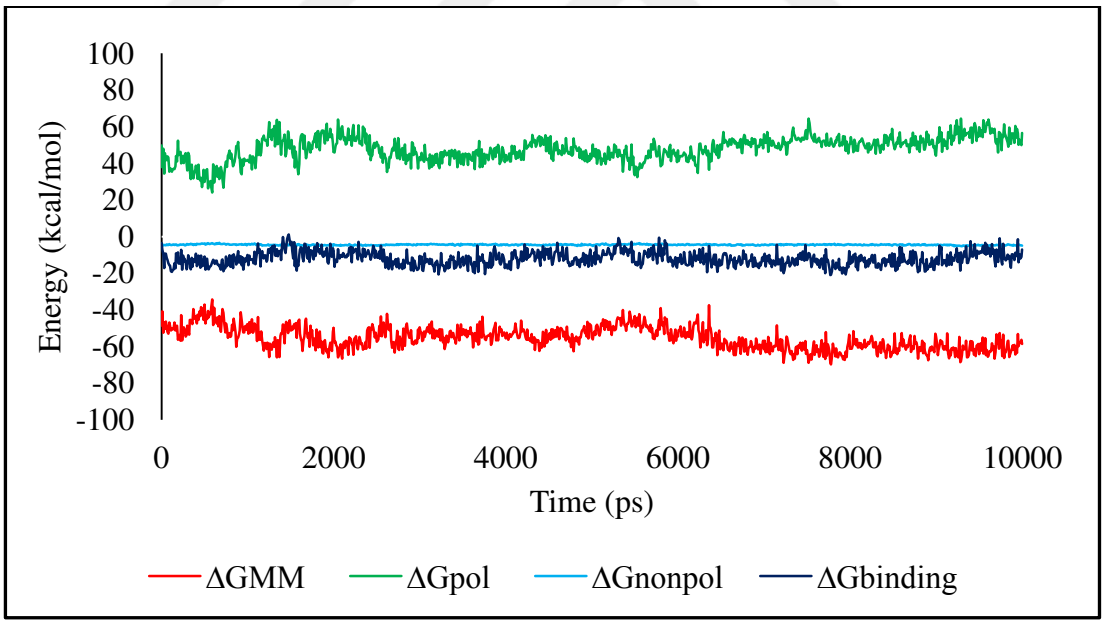

Figure B. 15 Energy terms for the binding of amygdalin with ILK.

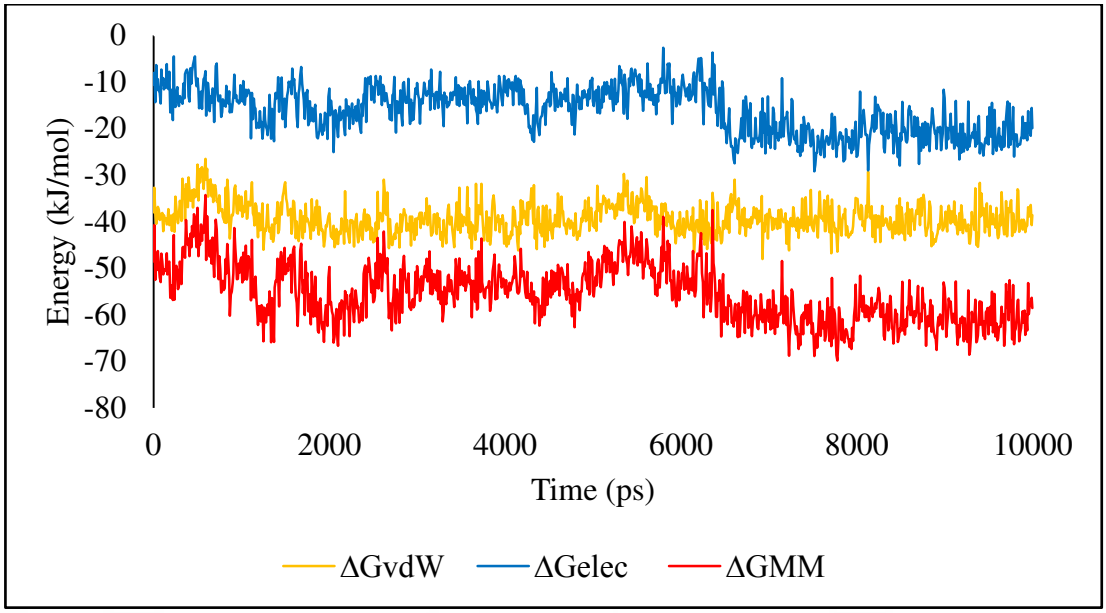

Figure B.16 Decomposition of molecular mechanics energy into electrostatic interaction energy and Vander Waals interaction energy of amygdalin inside the binding site of ILK.

APPENDIX C

Central Gromacs Files

To run a Gromacs simulation, we require three types of files; structure, topology and parameter files. These files can be either located online in larger databases or produced by the user itself (Hanwell et al., 2012).

Structure Files

The structure file (*.gro) or geometry file, summarizes the velocities and positions of the atoms inside the system. As well as, the file consists of the entire number of atoms and the volume of the box in nanometers.

Parameter Files

The user can set in the parameter file (*.mdp) a range of parameters for their system. The file includes information about temperature pressure coupling, period long of simulation, time constant for coupling, time steps (Δt) and so on. The parameter file provides Gromacs the needed data to know what to do with the starting structure.

Topology Files

The topology file (*.top) involves details of constant properties for every atom applied in the system. The file encompasses instruction on which parameters that requires to be implemented for other functions. It also collects information about which atoms, or mix of these, that contributes to the potential energy functions. The molecule topology file (*.itp) provides instruction about how the atoms are connected in a molecule, and is included in the system topology file. The force field employed for the simulation is too added in the topology file.

APPENDIX D

Gromacs Programs

Table D.1 The employed Gromacs programs in MD simulations.

Gromacs program	**Description**	**input**	**output**
gmx pdb2gmx	reads some database files and generates coordinates in GROMACS and a topology in GROMACS format	pdb.pdb	coordinate.gro and Topology.top
gmx editconf	Used to rescale the box dimensions of a system.	coordinate.gro	coordinate.gro
gmx solvate	Solvates a solute configuration.	coordinate.gro	Solvate.gro
gmx grompp	Reads the topology file, checks the validity of the file, expands (add atom descriptions to the topology) the topology from a molecular description to an atomic description.	solv.gro, Topology.top	ions.tpr and Topology.top
		solv_ions.gro, Topology.top	em.tpr and Topology.top
		em.gro, Topology.to	nvt.tpr and Topology.top

		p	
		nvt.tpr, Topology.top	npt.tpr and Topology.top
		npt.tpr, Topology.top	md_0_10.tpr and Topology.top
gmx genion	randomly replaces solvent molecules with monoatomic ions.	ions.tpr, Topology.top	solv_ions.gro
gmx mdrun	Gromacs main computational chemistry engine. Conducts MD simulations, like an energy minimization or an equilibration run of a system under isothermal-isobaric conditions.	em.tpr	em.gro and em.trr
		nvt.tpr	nvt.gro and nvt.trr
		npt.tpr	npt.gro and npt.trr
		md.tpr	md.gro and md.trr
gmx rms	compares two structures by computing the root mean square deviation (RMSD)	md.tpr and md.trr	rmsd.xvg
gmx rmsf	computes the root mean square fluctuation (RMSF, i.e. standard deviation) of atomic positions in the trajectory	md.tpr and md.trr	rmsf.xvg
gmx covar	calculates and diagonalizes the (mass-weighted) covariance matrix.	md.tpr and md.trr	eigenval.xvg
gmx anaeig	analyzes eigenvectors. The eigenvectors can be of a covariance matrix (gmx covar) or of a Normal Modes analysis	md.tpr and md.trr	2dproj.xvg (PCA)

gmx sham	Makes multi-dimensional free-energy, enthalpy and entropy plots. gmx sham reads one or more.	md.tpr and md.trr	gibbs.xpm (FEL)
gmx make_ndx	Index groups are necessary for almost every GROMACS program. All these programs can generate default index groups. You ONLY have to use gmx make_ndx when you need SPECIAL index groups	lig.gro	index_lig.ndx

APPENDIX E

Gromacs Parameter Files

E.1 Energy minimization

```
; minim.mdp - used as input into grompp to generate em.tpr
integrator = steep         ; Algorithm (steep = steepest
descent minimization)
emtol      = 1000.0; Stop minimization when the maximum force
< 1000.0 kJ/mol/nm
emstep      = 0.01; Energy step size
nsteps          = 50000; Maximum number of (minimization)
steps to perform

; Parameters describing how to find the neighbors of each atom
and how to calculate the interactions
nstlist             = 1; Frequency to update the neighbor
list and long-range forces
cutoff-scheme   = Verlet
ns_type             = grid; Method to determine neighbor list
(simple, grid)
coulombtype         = PME; Treatment of long-range
electrostatic interactions
rcoulomb       = 1.0; Short-range electrostatic cut-off
rvdw           = 1.0; Short-range Van der Waals cut-off
pbc                = xyz         ; Periodic Boundary
Conditions (yes/no)
```

E.2 NVT equilibration

```
title                    = Protein-ligand complex NVT
equilibration
define                   = -DPOSRES; position restrain the
protein and ligand
; Run parameters
integrator               = md; leap-frog integrator
nsteps                   = 50000; 2 * 50000 = 100 ps
dt                       = 0.002; 2 fs
; Output control
nstenergy                = 500; save energies every 1.0 ps
nstlog                   = 500; update log file every 1.0 ps
nstxout-compressed       = 500; save coordinates every 1.0 ps
; Bond parameters
continuation             = no; first dynamics run
constraint_algorithm     = lincs; holonomic constraints
constraints              = h-bonds; bonds to H are constrained
lincs_iter               = 1; accuracy of LINCS
lincs_order              = 4; also related to accuracy
; Neighbor searching and vdW
cutoff-scheme            = Verlet
ns_type                  = grid; search neighboring grid cells
nstlist                  = 20; largely irrelevant with Verlet
rlist                    = 1.2
vdwtype                  = cutoff
vdw-modifier             = force-switch
rvdw-switch              = 1.0
rvdw                     = 1.2; short-range van der Waals
cutoff (in nm)
; Electrostatics
coulombtype              = PME; Particle Mesh Ewald for long-
range electrostatics
rcoulomb                 = 1.2; short-range electrostatic
cutoff (in nm)
pme_order                = 4; cubic interpolation
fourierspacing           = 0.16; grid spacing for FFT
; Temperature coupling
tcoupl                   = V-rescale; modified Berendsen
thermostat
tc-grps                  = Protein LIG SOL CL NA; two coupling
groups - more accurate
tau_t                    = 0.1 0.1 0.1 0.1 0.1; time constant,
in ps
ref_t                    = 300 300 300 300 300; reference
temperature, one for each group, in K
; Pressure coupling
pcoupl                   = no; no pressure coupling in NVT
; Periodic boundary conditions
pbc                      = xyz; 3-D PBC
; Dispersion correction is not used for proteins with the C36
additive FF
DispCorr                 = no
; Velocity generation
```

```
gen_vel                 = yes; assign velocities from Maxwell
distribution
gen_temp                = 300; temperature for Maxwell
distribution
gen_seed                = -1; generate a random seed
```

E.3 NPT equilibration

```
title                   = Protein-ligand complex NPT
equilibration
define                  = -DPOSRES; position restrain the
protein and ligand
; Run parameters
integrator              = md; leap-frog integrator
nsteps                  = 50000; 2 * 50000 = 100 ps
dt                      = 0.002; 2 fs
; Output control
nstenergy               = 500; save energies every 1.0 ps
nstlog                  = 500; update log file every 1.0 ps
nstxout-compressed      = 500; save coordinates every 1.0 ps
; Bond parameters
continuation            = yes; continuing from NVT
constraint_algorithm    = lincs; holonomic constraints
constraints             = h-bonds; bonds to H are constrained
lincs_iter              = 1; accuracy of LINCS
lincs_order             = 4; also related to accuracy
; Neighbor searching and vdW
cutoff-scheme           = Verlet
ns_type                 = grid; search neighboring grid cells
nstlist                 = 20; largely irrelevant with Verlet
rlist                   = 1.2
vdwtype                 = cutoff
vdw-modifier            = force-switch
rvdw-switch             = 1.0
rvdw                    = 1.2; short-range van der Waals
cutoff (in nm)
; Electrostatics
coulombtype             = PME; Particle Mesh Ewald for long-
range electrostatics
rcoulomb                = 1.2
pme_order               = 4; cubic interpolation
fourierspacing          = 0.16; grid spacing for FFT
; Temperature coupling
tcoupl                  = V-rescale; modified Berendsen
thermostat
tc-grps                 = Protein LIG SOL CL NA; two coupling
groups - more accurate
tau_t                   = 0.1 0.1 0.1 0.1 0.1; time constant,
in ps
ref_t                   = 300 300 300 300 300; reference
temperature, one for each group, in K
; Pressure coupling
pcoupl                  = Berendsen; pressure coupling is on
for NPT
```

```
pcoupltype              = isotropic; uniform scaling of box
vectors
tau_p                   = 2.0 ; time constant, in ps
ref_p                   = 1.0; reference pressure, in bar
compressibility         = 4.5e-5; isothermal compressibility
of water, bar^-1
refcoord_scaling        = com
; Periodic boundary conditions
pbc                     = xyz; 3-D PBC
; Dispersion correction is not used for proteins with the C36
additive FF
DispCorr                = no
; Velocity generation
gen_vel                 = no; velocity generation off after
NVT
```

E.4 MD simulation production

```
title                   = Protein-ligand complex MD simulation
; Run parameters
integrator              = md; leap-frog integrator
nsteps                  = 5000000; 2 * 5000000 = 10000 ps (10
ns)
dt                      = 0.002; 2 fs
; Output control
nstenergy               = 5000; save energies every 10.0 ps
nstlog                  = 5000; update log file every 10.0 ps
nstxout-compressed      = 5000; save coordinates every 10.0 ps
; Bond parameters
continuation            = yes; continuing from NPT
constraint_algorithm    = lincs; holonomic constraints
constraints             = h-bonds; bonds to H are constrained
lincs_iter              = 1; accuracy of LINCS
lincs_order             = 4; also related to accuracy
; Neighbor searching and vdW
cutoff-scheme           = Verlet
ns_type                 = grid; search neighboring grid cells
nstlist                 = 20; largely irrelevant with Verlet
rlist                   = 1.2
vdwtype                 = cutoff
vdw-modifier            = force-switch
rvdw-switch             = 1.0
rvdw                    = 1.2; short-range van der Waals
cutoff (in nm)
; Electrostatics
coulombtype             = PME; Particle Mesh Ewald for long-
range electrostatics
rcoulomb                = 1.2
pme_order               = 4; cubic interpolation
fourierspacing          = 0.16; grid spacing for FFT
; Temperature coupling
tcoupl                  = V-rescale; modified Berendsen
thermostat
```

```
tc-grps                  = Protein LIG SOL CL NA; two coupling
groups - more accurate
tau_t                    = 0.1 0.1 0.1 0.1 0.1
; time constant, in ps
ref_t                    = 300 300 300 300 300; reference
temperature, one for each group, in K
; Pressure coupling
pcoupl                   = Parrinello-Rahman; pressure coupling
is on for NPT
pcoupltype               = isotropic; uniform scaling of box
vectors
tau_p                    = 2.0; time constant, in ps
ref_p                    = 1.0; reference pressure, in bar
compressibility          = 4.5e-5; isothermal compressibility
of water, bar^-1
; Periodic boundary conditions
pbc                      = xyz; 3-D PBC
; Dispersion correction is not used for proteins with the C36
additive FF
DispCorr                 = no
; Velocity generation
gen_vel                  = no; continuing from NPT
equilibration
```

APPENDIX F

g_mmpbsa Program

Table F.1 The employed g_MMPBSA Program in binding energy calculations in MD trajectories.

Gromacs program	Description	input	output
g_mmpbsa	calculates binding energy of biomolecular associations like protein-protein, protein-ligand protein-DNA etc using MM-PBSA.	md.tpr, md.trr, index.ndx	energy_MM.xvg, polar.xvg, apolar.xvg, contrib_MM.dat, contrib_pol.dat, contrib_apol.dat

APPENDIX G

g_MMPBSA parameter file

G.1 MMPBSA

```
MMPBSA
;Polar calculation: "yes" or "no"
polar      = yes

;=============
;PSIZE options
;=============
;Factor by which to expand molecular dimensions to get
coarsegrid dimensions.
cfac       = 1.5

;The desired fine mesh spacing (in A)
gridspace  = 0.5

:Amount (in A) to add to molecular dimensions to get fine grid
dimensions.
fadd       = 5

;Maximum memory (in MB) available per-processor for a
calculation.
gmemceil   = 4000

;============================================
;APBS kwywords for polar solvation calculation
;============================================
;Charge of positive ions
pcharge    = 1

;Radius of positive charged ions
prad       = 0.95

;Concentration of positive charged ions
pconc           = 0.150

;Charge of negative ions
ncharge    = -1

;Radius of negative charged ions
nrad       = 1.81

;Concentration of negative charged ions
nconc           = 0.150

;Solute dielectric constant
pdie       = 2

;Solvent dielectric constant
sdie       = 80

;Reference or vacuum dielectric constant
```

```
vdie       = 1

;Solvent probe radius
srad       = 1.4

;Method used to map biomolecular charges on grid. chgm = spl0
or spl2 or spl4
chgm           = spl4

;Model used to construct dielectric and ionic boundary. srfm =
smol or spl2 or spl4
srfm           = smol

;Value for cubic spline window. Only used in case of srfm =
spl2 or spl4.
swin       = 0.30

;Numebr of grid point per A^2. Not used when (srad = 0.0) or
(srfm = spl2 or spl4)
sdens          = 10

;Temperature in K
temp       = 300

;Type of boundary condition to solve PB equation. bcfl = zero
or sdh or mdh or focus or map
bcfl       = mdh

;Non-linear (npbe) or linear (lpbe) PB equation to solve
PBsolver   = lpbe


;============================================================
;APBS kwywords for Apolar/Non-polar solvation calculation
;============================================================
;Non-polar solvation calculation: "yes" or "no"
apolar         = no

;Repulsive contribution to Non-polar
;===SASA model ====

;Gamma (Surface Tension) kJ/(mol A^2)
gamma          = 0.0226778

;Probe radius for SASA (A)
sasrad         = 1.4

;Offset (c) kJ/mol
sasaconst      = 3.84928

;===SAV model===
;Pressure kJ/(mol A^3)
press          = 0

;Probe radius for SAV (A)
savrad         = 0
```

```
;Offset (c) kJ/mol
savconst        = 0

;Attractive contribution to Non-polar
;===WCA model ====
;using WCA method: "yes" or "no"
WCA             = no

;Probe radius for WCA
wcarad          = 1.20

;bulk solvent density in A^3
bconc      = 0.033428

;displacment in A for surface area derivative calculation
dpos       = 0.05

;Quadrature grid points per A for molecular surface or solvent
accessible surface
APsdens         = 20

;Quadrature grid spacing in A for volume integral calculations
grid            = 0.45 0.45 0.45

;Parameter to construct solvent related surface or volume
APsrfm          = sacc

;Cubic spline window in A for spline based surface definitions
APswin          = 0.3

;Temperature in K
APtemp          = 300
```

A CIRRICULUM VITAE (CV)

Personal Information:

Name Family name : Khattab Al-KHAFAJI

Languages : English: Advanced (Toefl IBT 84)
Turkish: very good (TOMER B2)
Arabic: mother Tongue.

Marital Status : single

Citizenship : Iraqi

Place of Birth : Baghdad/Iraq

Educational History and Achievements

From year	To year	Name & Address of Institution	Course Studies
2002	2005	AEMAM AL-SADEQ	Secondary school certificate/ scientific
2005	2010	College of Science, University of Baghdad	Bachelor degree in Chemistry
2010	2013	College of Science, Al-Nahrain University	Master degree in Chemistry

Published researches and conferences

Al-Khafaji, K, & Salman, T. A. (2013). ThermodynamicProperties of Nicotinicacid in Dilute HCl and inaqueous NaCl solutions at (293.15, 298.15, 303.15 and 308.15) K. Baghdad Science Journal, 10(2), 432-441.

Akın-Balı, D. F., **Al-Khafaji, K**., Aktas, S. H., & Taskin-Tok, T. (2020). Bioinformatic and computational analysis for predominant mutations of the Nrf2/Keap1 complex in pediatric leukemia. Journal of Biomolecular Structure and Dynamics, 1-14. Retrieved from https://doi.org/10.1080/07391102.2020.1775702. doi:10.1080/07391102.2020.1775702

Al-Khafaji, K., Al-Duhaidahawi, D., & Taskin Tok, T. (2020). Using integrated computational approaches to identify safe and rapid treatment for SARS-CoV-2. Journal of Biomolecular Structure and Dynamics, 1-9. Retrieved from https://doi.org/10.1080/07391102.2020.1764392. doi:10.1080/07391102.2020.1764392

Al-Khafaji, K., & Taskin Tok, T. (2020a). Amygdalin as multi-target anticancer drug against targets of cell division cycle: double docking and molecular dynamics simulation. Journal of Biomolecular Structure and Dynamics, 1-10. Retrieved from https://doi.org/10.1080/07391102.2020.1742792. doi:10.1080/07391102.2020.1742792

Al-Khafaji, K., & Taskin Tok, T. (2020b). Molecular dynamics simulation, free energy landscape and binding free energy computations in exploration the anti-invasive activity of amygdalin against metastasis. Computer Methods and Programs in Biomedicine, 195, 105660. Retrieved from http://www.sciencedirect.com/science/article/pii/S0169260720314930. doi:https://doi.org/10.1016/j.cmpb.2020.105660

Al-Khafaji, K., & Taskin Tok, T. (2020c). Understanding the mechanism of Amygdalin's multifunctional anti-cancer action using computational approach. Journal of Biomolecular Structure and Dynamics, 1-14. Retrieved from https://doi.org/10.1080/07391102.2020.1736159. doi:10.1080/07391102.2020.1736159

Aldahham, B. J. M., **Al-Khafaji, K.**, Saleh, M. Y., Abdelhakem, A. M., Alanazi, A. M., & Islam, M. A. (2020). Identification of naphthyridine and quinoline derivatives as potential Nsp16-Nsp10 inhibitors: a pharmacoinformatics study. Journal of Biomolecular Structure and Dynamics, 1-8. Retrieved from https://doi.org/10.1080/07391102.2020.1851305. doi:10.1080/07391102.2020.1851305

Rafi, M. O., **Al-Khafaji, K.**, Tok, T. T., & Rahman, M. S. (2020). Computer-based identification of potential compounds from Salviae miltiorrhizae against Neirisaral adhesion A regulatory protein. Journal of Biomolecular Structure and Dynamics, 1-

13. Retrieved from https://doi.org/10.1080/07391102.2020.1856189. doi:10.1080/07391102.2020.1856189

Rafi, M. O., Bhattacharje, G., **Al-Khafaji, K.**, Taskin-Tok, T., Alfasane, M. A., Das, A. K., . . . Rahman, M. S. (2020). Combination of QSAR, molecular docking, molecular dynamic simulation and MM-PBSA: analogues of lopinavir and favipiravir as potential drug candidates against COVID-19. Journal of Biomolecular Structure and Dynamics, 1-20. Retrieved from https://doi.org/10.1080/07391102.2020.1850355. doi:10.1080/07391102.2020.1850355

Türker, F., Noma, S. A. A., Aktaş, A., **Al-Khafaji, K.**, Taşkın Tok, T., Ateş, B., & Gök, Y. (2020). The (NHC)PdBr2(2-aminopyridine) complexes: synthesis, characterization, molecular docking study, and inhibitor effects on the human serum carbonic anhydrase and serum bovine xanthine oxidase. Monatshefte für Chemie - Chemical Monthly, 151(10), 1557-1567. Retrieved from https://doi.org/10.1007/s00706-020-02687-2. doi:10.1007/s00706-020-02687-2

Yagiz, G., Abbas Ali Noma, S., Altundas, A., **Al-khafaji, K.**, Taskin-Tok, T., & Ates, B. (2021). Synthesis, Inhibition Studies Against Xanthine Oxidase and Molecular Docking Studies of Dimethyl N-benzyl-1H-1,2,3-triazole-4,5-dicarboxylate and (N-Benzyl-1H-1,2,3-triazole-4,5-diyl)dimethanol Derivatives. Bioorganic Chemistry, 104654. Retrieved from http://www.sciencedirect.com/science/article/pii/S0045206821000304. doi:https://doi.org/10.1016/j.bioorg.2021.104654

PUBLICATIONS

1. **Khattab Al-Khafaji**, Tugba Taskin Tok (2020). "Amygdalin as multi-target anticancer drug against targets of cell division cycle: double docking and molecular dynamics simulation." Journal of Biomolecular Structure and Dynamics: 1-10.
2. **Khattab Al-Khafaji**, Tugba Taskin Tok (2020). "Molecular dynamics simulation, free energy landscape and binding free energy computations in exploration the anti-invasive activity of amygdalin against metastasis." Computer Methods and Programs in Biomedicine 195: 105660.
3. **Khattab Al-Khafaji**, Tugba Taskin Tok (2020). "Understanding the mechanism of amygdalin's multifunctional anti-cancer action using computational approach."